S. P. Dunfield,* L. Bliss, F. Zhang, J. M. Luther, K. Zhu, M. F. A. M. van Hest, M. O. Reese,* J. J. Berry*..... 1904054

From Defects to Degradation: A Mechanistic Understanding of Degradation in Perovskite Solar Cell Devices and Modules

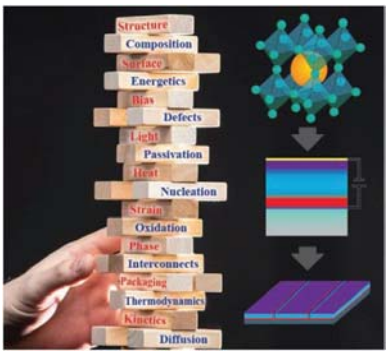

This article aims to present an in-depth review of the current understanding of metal halide perovskite device and module stability by outlining how basic material intrinsic and extrinsic degradation mechanisms as well as additional complications from the presence of other layers and nonequilibrium conditions impact device and module performance over time.

UNCORRECTED PROOF

Pursuant to the DOE Public Access Plan, this document represents the authors' peer-reviewed, accepted manuscript. The published version of the article is available from the relevant publisher.

ADVANCED ENERGY MATERIALS
www.advenergymat.de

From Defects to Degradation: A Mechanistic Understanding of Degradation in Perovskite Solar Cell Devices and Modules

Sean P. Dunfield,* Lyle Bliss, Fei Zhang, Joseph M. Luther, Kai Zhu, Maikel F. A. M. van Hest, Matthew O. Reese,* and Joseph J. Berry*

Metal halide perovskite solar cells (PSCs) have risen in efficiency from just 3.81% in 2009 to over 25.2% today. While metal halide perovskites have excelled in efficiency, advances in stability are significantly more complex and have progressed more slowly. The advance of efficiency, which is readily measured, over stability, which can require literally thousands of hours to demonstrate, is to be expected given the rapid rate of innovation in the field. In the face of changing absorber composition, synthetic approaches, and device stack components there is a premium in understanding basic material properties to rationalize how to enable stability in devices. In this article the aim is to present an in-depth review of the current understanding of metal halide perovskite device and module stability by focusing on what is known retarding intrinsic and extrinsic degradation mechanisms at the material, device, and module level. Once these considerations are presented the discussion then moves to connecting different degradation mechanisms to stresses anticipated in operation and how they can impact efficiency of cells and ultimately modules over time.

1. Introduction

Perovskite solar cells (PSCs) have excelled from just 3.81% in 2009[1] to over 25.2% today (**Figure 1**).[2] When coupled with their physical properties, which create unique opportunities for deployment, this affords them the ability to be a disruptive technology.[3] However, while perovskites have excelled in power conversion efficiency (PCE), their advances in stability are significantly more complex and have progressed more slowly.[4] In large, this is expected. The evolution of efficiency has always outpaced stability as rapid innovations in efficiency inherently require longer duration validation to ensure that they do not introduce new degradation pathways; this is especially true for emerging technologies. However, progress has been further hindered by the lack of standard protocols, such as the International Summit on Organic Photovoltaic Stability (ISOS) protocols established to standardize organic photovoltaic (OPV) stability measurements.[5] This has resulted in stability being measured in a variety of ways. This variability, while justifiable on a technical basis, makes directly comparing stability results difficult. Despite this, many trends and observations can be made. Here, we aim to present an in-depth review of the current understanding of perovskite device and module stability by discussing known intrinsic and extrinsic degradation mechanisms at the material, device, and module level, and their connection as demonstrated in state-of-the-art results.

S. P. Dunfield, L. Bliss, F. Zhang, J. M. Luther, K. Zhu, M. F. A. M. van Hest, M. O. Reese, J. J. Berry
National Renewable Energy Laboratory
Golden, CO 80401, USA
E-mail: sean.dunfield@nrel.go; Matthew.Reese@nrel.gov; joe.berry@nrel.gov
S. P. Dunfield, J. J. Berry
Renewable and Sustainable Energy Institute
University of Colorado Boulder
Boulder, CO 80309, USA
S. P. Dunfield
Materials Science & Engineering Program
University of Colorado Boulder
Boulder, CO 80309, USA
L. Bliss
Department of Chemical & Biological Engineering
University of Colorado Boulder
Boulder, CO 80309, USA
J. J. Berry
Department of Physics
University of Colorado Boulder
Boulder, CO 80309, USA
The ORCID identification number(s) for the author(s) of this article can be found under https://doi.org/10.1002/aenm.201904054.

DOI: 10.1002/aenm.201904054

2. Perovskite Intrinsic Stability

2.1. Structural Stability

The term perovskite refers to a broad set of materials with ABX_3 crystal structure, where A is a large monovalent cation, B is a much smaller divalent cation, and X is an anion that bonds to both the A and B cations. The ability of elements A, B, and X to form a perovskite structure can be predicted by the Goldschmidt tolerance factor, t[6]

$$t = \frac{R_A + R_X}{\sqrt{2}(R_X + R_B)} \quad (1)$$

where R_A is the atomic radius of the A cation, R_X is the atomic radius of the X anion, and R_B is the atomic radius of the B cation. Theoretically, tolerance factors greater than 1 produce hexagonal or tetragonal structures, between 0.9 and 1 produce cubic structures, between 0.71 and 0.9 produce orthorhombic

© 2020 WILEY-VCH Verlag GmbH & Co. KGaA, Weinheim

Pursuant to the DOE Public Access Plan, this document represents the authors' peer-reviewed, accepted manuscript. The published version of the article is available from the relevant publisher.

or rhombohedral structures, and less than 0.71 do not form perovskites. The A and B cations then provide one and two electrons, respectively, to charge balance three positive X anions. This forms a bandgap between the unoccupied B cation's p-orbital and occupied X anion's p-orbital.[7]

While the tolerance factor is a good 0th order approximation, it has been shown to mispredict 26% of structures tested.[8] Due to this, Bartel et al. proposed a modified tolerance factor, τ[8]

$$\tau = \frac{R_X}{R_B} - n_A\left(n_A - \frac{R_A/R_B}{\ln\left(R_A/R_B\right)}\right) \quad (2)$$

where R_A, R_B, and R_X have the same definitions, n_A is the oxidation state of the A cation, and $\tau < 4.18$ indicates perovskite formation with increasing probability. While the new modified tolerance factor does not predict alternate structures, it predicts perovskite structures much more accurately (8% incorrect) and provides a likelihood of formation. As a result, using a combination of the two, a functional estimate of structural stability can be made for neat compositions.

Given the wide variety of formulations possible, we will limit our discussion to a subclass of perovskites that better resemble those studied in 2009 by Kojima et al. than the classical "perovskite" ($CaTiO_3$) discovered by Lev Perovski in 1839. This subclass of metal-halide perovskites has relevant photovoltaic properties such as a band gap in the visible light regime. To achieve this, they utilize tin (Sn) or lead (Pb) at the B-site and iodide (I), bromine (Br), and/or chlorine (Cl) at the X-site. Given the B- and X-site components, appropriate A-sites such as methylammonium (MA), formamidinium (FA), and cesium (Cs) can then be chosen to obtain suitable tolerance factor.

A-sites that successfully form a perovskite structure come in three flavors: too small, too large, and just right. A-sites too small fail to properly separate B-site cations, leading to edge sharing octahedra. On the other hand, A-sites too large force the perovskite to form lower dimensional face sharing octahedra structures. While these compositions may not be directly photovoltaically relevant due to their wider bandgaps, lower carrier mobility, and higher exciton binding energies, they have recently been incorporated to aid with stability, as will be discussed later. Finally, A-sites just right perfectly space B-site cations, resulting in a symmetrical 3D cubic lattice.

However, as temperature changes so do preferred phases. For example, methylammonium lead halides undergo phase transitions from orthorhombic to tetragonal and then to cubic as temperature is increased whereas cesium lead halides undergo phase transitions from orthorhombic to cubic. These phase transition temperatures are highly dependent on composition—several examples are shown in **Table 1**.

It is noteworthy that these changes can have a drastic effect on the optoelectronic properties of perovskites; many noncubic phases are photovoltaically inactive, such as room temperature structures for $FAPbI_3$ and $CsPbI_3$. As such, these neat compositions are considered "phase unstable" using this evaluation and would not be expected to make stable solar cells. However, it has been shown that alloys can be used to improve phase stability.

Sean P. Dunfield is a Graduate student pursuing his Ph.D. in Materials Science and Engineering at University of Colorado Boulder while conducting research on perovskites at the National Renewable Energy Laboratory (NREL). He received his B.S. in Physics and B.A. in Applied Mathematics from Syracuse University in 2014. His research interests focus on surface science, degradation mechanisms, and understanding the effects processing, composition, and additives have on material properties. To compare the myriad of device architectures utilized at NREL, he has spent significant time improving and standardizing stability measurement capabilities and analysis.

Matthew O. Reese is a senior scientist at the National Renewable Energy Laboratory. He received his B.S. from Caltech and Ph.D. from Yale. He has expertise in the fabrication and characterization of a variety of thin-film material sets including CdTe, organic PV, and perovskites. His interests include nano- and microstructured materials for energy applications, understanding interfacial roles and morphology in thin-film devices, lightweight/flexible packaging solutions, water vapor transmission measurement, and reliability mechanisms that can be addressed with a material and/or cell level understanding. To aid these efforts, he also has a keen interest in developing new measurement tools and methods.

Joseph J. Berry is a senior scientist at the National Renewable Energy Laboratory working on halide perovskite solar cells. His Ph.D. for work was on spin transport and physics in semiconductor heterostructures from Penn State University. His efforts at NREL emphasize relating basic interfacial properties to technologically relevant device level behaviors in traditional and novel semiconductor heterostructures including oxides, organics, and most recently hybrid semiconducting materials. He also leads the DOE SETO "De-risking Halide Perovskite Solar Cells" project with Laura T. Schelhas.

© 2020 WILEY-VCH Verlag GmbH & Co. KGaA, Weinheim

Pursuant to the DOE Public Access Plan, this document represents the authors' peer-reviewed, accepted manuscript. The published version of the article is available from the relevant publisher.

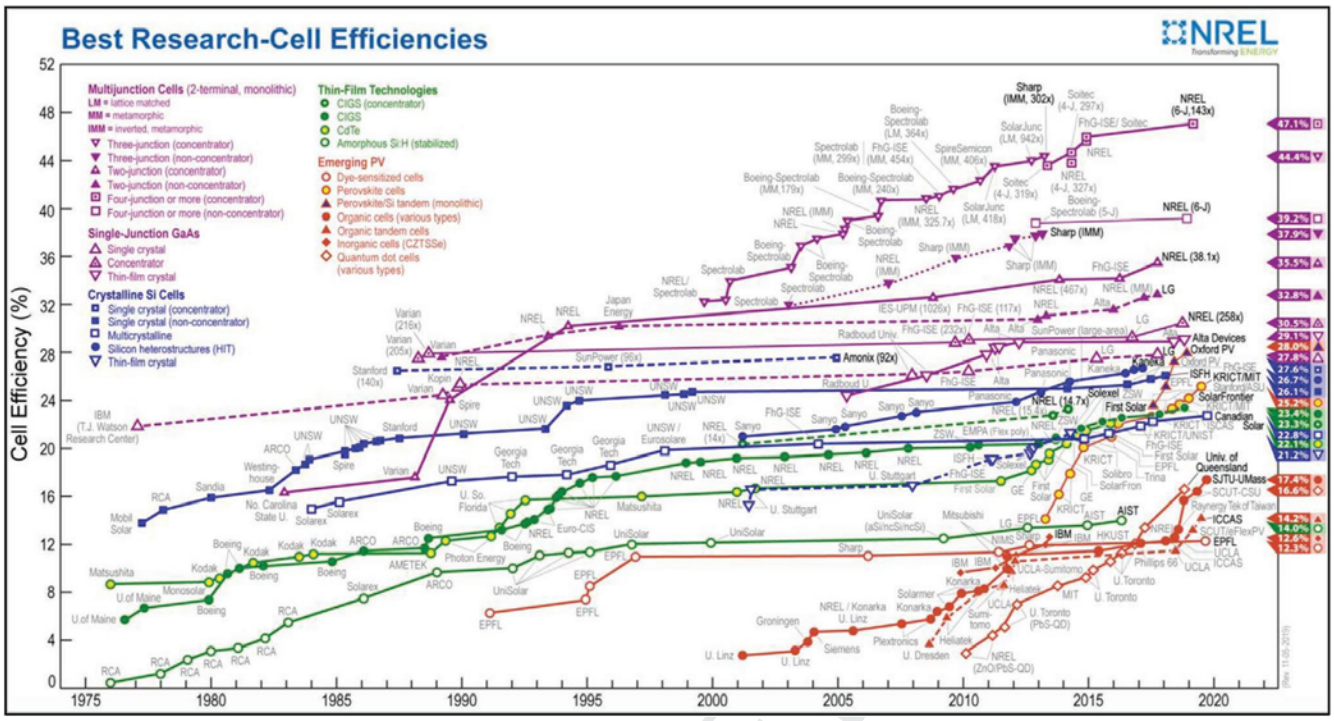

Figure 1. Record certified power conversion efficiencies (PCEs) for a range of photovoltaic technologies. This plot is courtesy of the National Renewable Energy Laboratory, Golden, CO.[2]

2.2. Phase Stability

An alloyed perovskite can be approximated as a linear combination of the two neat perovskites. Thus, solving structural stability has been boiled down to what one may naively consider a simple two-step process:

Step 1. Select the correct Sn/Pb and I/Br ratios to obtain the desired bandgap.
Step 2. Select an appropriately sized mixture of A-site cations to obtain suitable tolerance factor, as shown in **Figure 2** for $FA_xCs_{1-x}PbI_3$.

Indeed, this line of thinking has been responsible for many formulations, leading to compositions that have a highly alloyed A-site and either a mixed Sn:Pb B-site to lower the bandgap or mixed I:Br A-site to raise the bandgap.[19,20] However, it has become clear that many of the more advanced compositions are prone to phase segregate due to extremely small differences in the formation energy of available phases.

Table 1. Phase stability for various perovskite compositions.

Structure	Phase transition to cubic/pseudocubic phase [K]
$MAPbI_3$	327[9–11]
$FAPbI_3$	350[12,13]
$CsPbI_3$	583[14,15]
$MAPbBr_3$	237[9,11]
$FAPbBr_3$	275[16]
$MASnI_3$	275[17,18]
$FASnI_3$	250[16]

At the A-site, this has shown to be governed by the Gibbs free energy of mixing (ΔG_{mix}) at constant pressure and volume[21]

$$\Delta G_{mix} = \Delta H_{mix} - T\Delta S_{mix} \quad (3)$$

where ΔH_{mix} is the enthalpy of mixing calculated by taking the difference between the total energy of the mixed state with respect to the constituent states, and $T\Delta S_{mix}$ is the entropy of mixing. Compositions with $\Delta G_{mix} < 0$ have components which are energetically favored to mix, causing them to form a shared single phase. Compositions with $\Delta G_{mix} > 0$, on the other hand, are prone to phase segregate. Note that this applies to extremely small length scales and is temperature dependent. As such, local structural inhomogeneity can create a driving force sufficiently large to propagate phase segregation.

While calculating ΔG_{mix} for complex compositions is computationally demanding, two design rules for preventing phase segregation at the A-site were identified by Schelhas et al. in binary systems of the form $A^1A^2PbI_3$ that should persist in more complicated cases (**Figure 3**):

1. To make films homogenous at the time of fabrication, initial components and annealing temperatures should be chosen such that the pure and end point compositions have the same structural phase (i.e., >600 K should be used to process $FA_xCs_{1-x}PbI_3$ because $FAPbI_3$ takes on the cubic phase at >300 K and $CsPbI_3$ at >600 K).
2. To make films which stay homogenous during device operation, the mixed phase must be energetically favorable

UNCORRECTED

© 2020 WILEY-VCH Verlag GmbH & Co. KGaA, Weinheim

Pursuant to the DOE Public Access Plan, this document represents the authors' peer-reviewed, accepted manuscript.
The published version of the article is available from the relevant publisher.

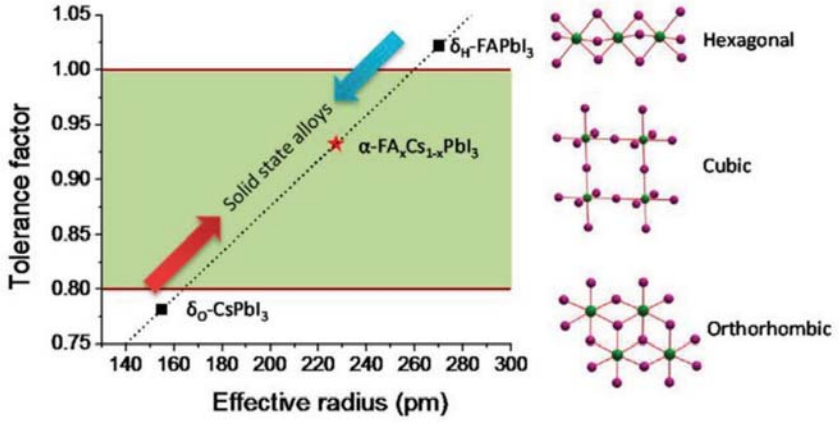

Figure 2. Correlation between tolerance factor, FA-to-Cs A-site composition, and crystal structure. Reproduced with permission.[6] Copyright 2016, American Chemical Society.

($\Delta G_{mix} < 0$) all other phases in their low temperature structures (i.e., cubic $FA_{1-x}Cs_xPbI_3$ must be favorable to orthorhombic $CsPbI_3$, cubic $FAPbI_3$, and hexagonal $FAPbI_3$. This is the case for $0.5 < x < 1.0$).

In addition to the A-site, phase segregation has been shown to take place at the X-site. This effect was first observed by Hoke et al.[22] in $MAPb(I_xBr_{1-x})_3$ and later explained by Bischak et al.[23] In short, naturally occurring variations in composition prior to illumination yield I-rich regions with reduced bandgap. When illuminated, electron–hole pairs created quickly disassociate, and carriers move to lower-gap iodine-rich regions before recombining. While there, the large concentration of carriers interacts with the highly ionic perovskite structure, deforming the surrounding lattice through electron–phonon coupling, as shown schematically in **Figure 4**. This strain increases the enthalpy of mixing enough to create a second minima in the free energy versus bromine content diagram, driving the perovskite to form I-rich/Br-rich phases (Figure 4).

When light continues to be shined onto the perovskite, most photoexcited charges rush to iodine-rich low-gap areas of the film where they are extracted before recombining. Due to the lower gap, these carriers generate less voltage than if they had come from a stoichiometric mixed-halide region. However, when light is removed the perovskite's free energy diagram returns to its preillumination state, reestablishing a driving force for a single phase. Thus, in contrast to the A-site, this phase segregation is normally reversible. Nonetheless, given its impact on device performance, namely the reduction of open circuit voltage (V_{oc}), it is best to avoid. Theoretical simulations suggest that this can be achieved by keeping iodine-to-bromine ratios within certain levels (<20–30% Br), reducing ionic mobility, reducing electron–phonon coupling, and/or reducing the lifetime/mobility of free carriers.[23] While the latter can have other negative impacts on performance, the middle two have been accomplished by improving film quality and partially replacing the polar MA^+ cation with less polar cations.[24]

It is noteworthy that so far, no phase segregation at the B-site has been documented. Thus, using the methods outlined above, one should be able to provide a good approximation

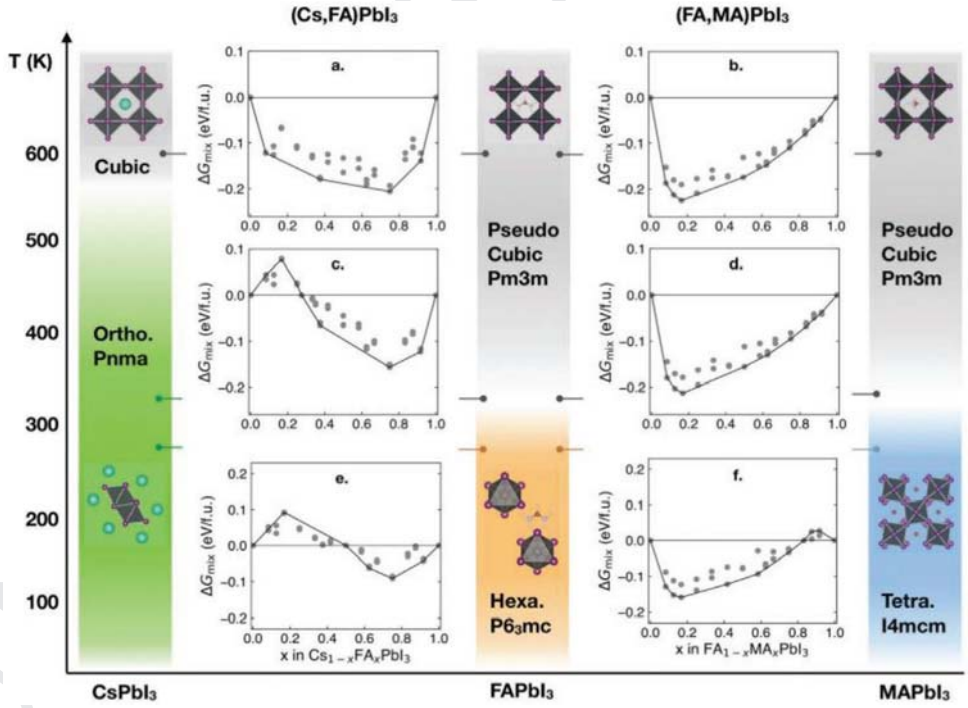

Figure 3. Density functional theory (DFT) calculated Gibbs free energy of mixing for $Cs_{1-x}FA_xPbI_3$ and $FA_{1-x}MA_xPbI_3$ as a function of A-site composition and temperature. Reproduced with permission.[21] Copyright 2019, The Royal Society of Chemistry.

© 2020 WILEY-VCH Verlag GmbH & Co. KGaA, Weinheim

Pursuant to the DOE Public Access Plan, this document represents the authors' peer-reviewed, accepted manuscript. The published version of the article is available from the relevant publisher.

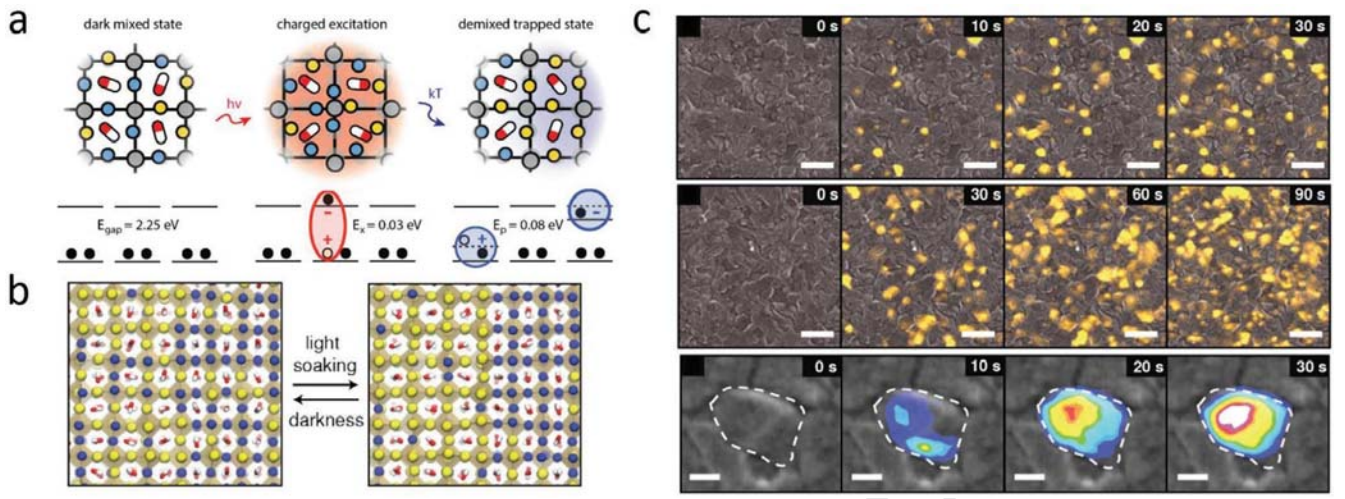

Figure 4. Photoinduced phase segregation in $MAPb(I_xBr_{1-x})_3$ films. a) Schematic of photoinduced polaron trapping and associated energy levels. Yellow and blue spheres represent I^- and Br^-, respectively. b) Schematic of macroscale phase segregation with same color key. c) Cathodoluminescence imaging showing phase segregation of iodide (yellow) under various light soaking durations. Reproduced with permission.[23] Copyright 2017, American Chemical Society.

of structural/phase stability in inert environments. However, due to the low formation energy of these materials, the ratios of components measured in the film often deviate from solution. Moreover, when perovskites are exposed to other elements such as water, reactions can result in phase transitions. These transitions are composition/element specific, and besides those governed by humidity which will be discussed in Section 3, are poorly understood.

2.3. Defect Tolerance

The rules dictating the structural stability of perovskite materials directly couple to the primary consideration of any semiconductor, namely the electronic band structure. To cover this, we will first discuss the electronic structure of $MAPbI_3$ and its origins, which are fairly well understood, and then move on to cover how understanding of this system generalizes to other compositions with alternate or mixed A-, B-, and X-sites.

The bulk of $MAPbI_3$ is well known to be defect tolerant. While similar levels of intrinsic defects are known to destroy the efficiencies of most other photovoltaic semiconductor materials, $MAPbI_3$ films riddled with vacancies can be incorporated into relatively efficient devices. The first theoretical assessment of this defect tolerance was conducted by Yin et al.[7] In said manuscript, the formation enthalpy of $MAPbI_3$ and the chemical potential of each component were analyzed to determine the range of growth conditions required to synthesize single-phase cubic $MAPbI_3$. Density functional theory (DFT) calculations were then performed for three representative points within this region (iodine-rich/lead-poor, neutral, and lead-rich/iodine-poor) to determine defect transition energy levels and associated formation energies. The model used considered all possible point defects: three vacancies (V_{MA}, V_{Pb}, V_I), three interstitials (MA_i, Pb_i, I_i), two cation substitutions (MA_{Pb}, Pb_{MA}), and four antisite substitutions (MA_I, Pb_I, I_{MA}, I_{Pb}). Results are shown in **Figure 5**.

As can be seen, altering growth conditions can drastically alter defects formation energy, and thus concentration. Under I-rich/Pb-poor conditions, defect structures are dominated by low-energy V_{Pb} acceptor defects, causing the Fermi level to reside near the valence band, as shown by the vertical

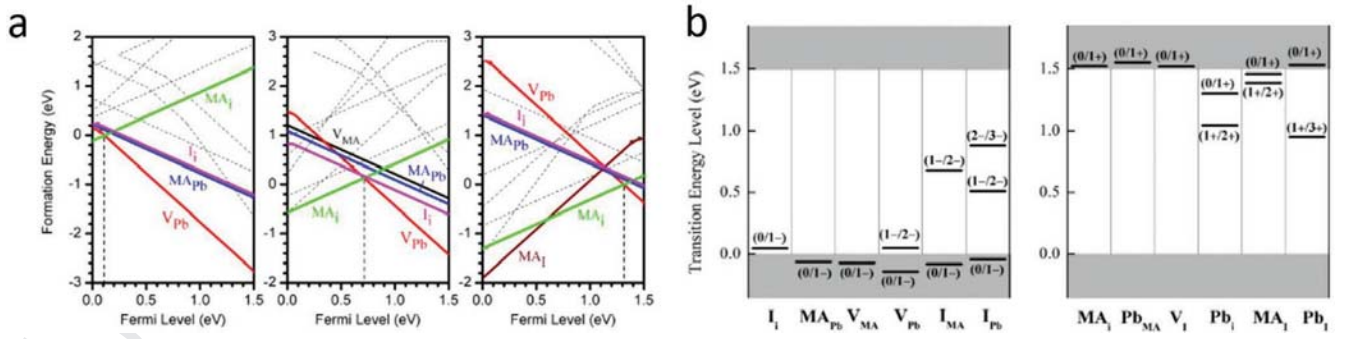

Figure 5. Defect tolerance of $MAPbI_3$. a) Formation energy of intrinsic point-defects for I-rich/Pb-poor (left), neutral (middle), and Pb-rich/I-poor (right) growth conditions. b) Transition energy levels for intrinsic acceptor (left) and donor (right) point-defects. Reproduced with permission.[7] Copyright 2014, AIP Publishing.

© 2020 WILEY-VCH Verlag GmbH & Co. KGaA, Weinheim

Pursuant to the DOE Public Access Plan, this document represents the authors' peer-reviewed, accepted manuscript. The published version of the article is available from the relevant publisher.

dotted line in Figure 5a. However, as the ratio of lead-to-iodide is increased, the energy required to form acceptor defects increases while the energy required to form donor defects decreases. This causes the lowest energy acceptor defect, V_{Pb}, and donor defect, MA_i, to have similar formation energies and therefore concentrations, setting the Fermi level near midgap as shown in Figure 5b. Finally, moving to lead-rich/iodine-poor conditions (Figure 5c), the above trend continues causing two donor defects, MA_i and MA_I, to dominate the defect structure and the sample to display n-type behavior. Thus, while growth conditions must be carefully controlled to form a stoichiometric and stable phase, they can also be tuned to control the concentration of donor and acceptor defects, allowing the material to display a range of carrier concentrations. Amazingly, despite the large difference in defects and formation energies in these three regions, detrimental defects have been found to be extremely rare for all three cases. Defects with low formation energies such as I_i, MA_{Pb}, V_{MA}, V_{Pb}, MA_i, Pb_{MA}, and V_I form trap states 0.05 eV within the conduction/valence band edge whereas deeper defect states such as I_{MA}, I_{Pb}, Pb_i, and Pb_I, have very high formation energies. These results suggest that the defects which readily form in high concentrations perturb the electronic structure by altering carrier concentrations, not forming midgap states that serve as centers for nonradiative recombination.

The proposed tolerance to methylammonium and iodide vacancies (V_{MA}, V_I) has been experimentally verified by Steirer et al.,[25] who mechanistically studied the relation between the composition and electronic structure of $MAPbI_3$ using X-ray photoemission spectroscopy (XPS) on $MAPbI_3/TiO_x$/fluorine doped tin oxide (FTO) films. As the samples were exposed to 350 W X-rays, $MAPbI_3$ decomposed by an initial off-gassing of methylamine (V_{MA}), as seen in C-1s and N-1s spectra, followed quickly by a loss in iodine (V_I). By comparing the ratio of I:Pb and the location of the valence band maximum relative to the Fermi level it is shown that from an I:Pb ratio of ≈3.0 to ≈2.5 the electronic structure remains relatively constant, but that once a ratio of 2.5 is reached, further reducing the ratio starts to negatively impact the electronic structure. As shown in **Figure 6**, this correlation between a decrease in the iodide-to-lead ratio and shift in the valence band occurs until roughly a 2:1 ratio is reached, at which point the film is predominately PbI_2.

It is noteworthy that this defect tolerance is dramatically different than most other well-known semiconductor systems, such as Silicon, whose photovoltaic performance can be destroyed by low defect concentrations. As a result, it is not surprising that its origins have been credited to the unique iconicity and band structure of $MAPbI_3$.[7] Specifically, the acceptor defects at the valence band maximum (V_{Pb} and MA_{Pb}) are believed to be shallow because of the Pb-5s I-5p antibond coupling afforded by the ABX_3 structure. Without this coupling the valence band maximum would be determined by the I-5p states and defect states would reside within the gap. However, this coupling creates a valence band above the energy level of the I-5p states that is decoupled from easily formed defects. This increase in the valence band level is enough to cause most acceptor defects to reside inside the band. On the other hand, the shallow donor defects at the conduction band minimum

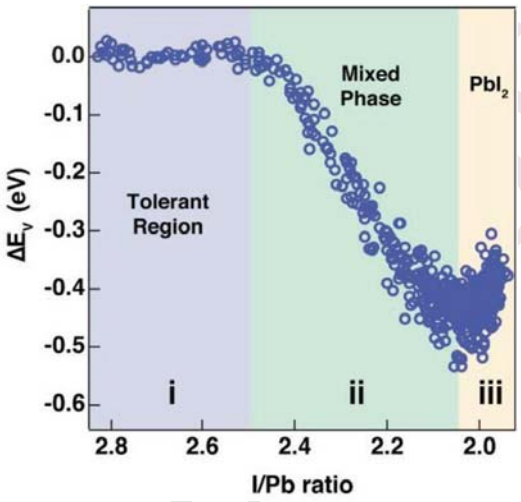

Figure 6. Correlation between valence band maximum and I/Pb ratio in $MAPbI_3$ film as measured by X-ray photoemission spectroscopy (XPS). Reproduced with permission.[25] Copyright 2016, American Chemical Society.

(MA_i and V_I) have been attributed to the MA^+ and Pb^{2+} cations donating their electrons to three I^- anions, which causes the conduction band to form from empty Pb-6p orbitals. These orbitals couple to each other, creating an energy level lower than the p-orbital of the Pb atom, similarly pushing donor defects out of the gap.

Since the discovery of $MAPbI_3$'s defect tolerance and tunability, numerous studies have explored the defect tolerance of other neat ABX_3 compositions. Each study has generated the set of chemical potentials required to generate the perovskite as well as the formation energy and transition energy level of defects for several points within the region. The results from these studies vary widely depending on composition; not all chemical compositions appear to possess the defect tolerance or carrier conductivity tunability seen in $MAPbI_3$. However, there appears to be a strong correlation between defect tolerance and structural stability, as dictated by the tolerance factor (t). Namely, compositions suggested to be defect tolerant in their lowest energy phase ($CsPbBr_3$,[26] $CsSnI_3$,[27] $MAPbI_3$,[7] $CsSnBr_3$,[28] $CsSnCl_3$,[28] $MAPbBr_3$[29]) all have tolerance factors grouped from roughly 0.82–0.85, whereas compositions which were not have tolerance factors outside this range ($CsPbI_3$,[30] $MASnI_3$,[31] $FAPbI_3$,[32] $FASnI_3$[31]). Given this observation, it appears that alloying the A-site to achieve appropriate tolerance factor should be a powerful strategy to mitigate defects. Although studies of this nature are limited due to their computationally demanding nature, this has been suggested to be the case for $FAPbI_3$. More specifically, it has been shown that the formation energy of deep-level defects (FA_I and I_{FA}) present in $FAPbI_3$ can be drastically increased by replacing roughly half of the FA cations with MA ($FA_{0.52}MA_{0.48}PbI_3$).[32] Doing so prevents them from forming, causing the material to become defect tolerant. However, we note that doing so also reduces the tolerance factor of the composition to roughly 0.84, a value just within the golden range of tolerance factors described above.

Thus, tuning A-sites to increase structural stability simultaneously appears to increase defect tolerance. As a result, it

© 2020 WILEY-VCH Verlag GmbH & Co. KGaA, Weinheim

Pursuant to the DOE Public Access Plan, this document represents the authors' peer-reviewed, accepted manuscript. The published version of the article is available from the relevant publisher.

seems reasonable to assume that most chemical compositions which readily form structurally stable perovskites with high device performance should possess this intrinsic bulk defect tolerance.[33] However, the surfaces of these materials have drastically different chemical potentials, and therefore defect structures, than the bulk. This is because, conceptually, the surfaces of these materials are defects—points at which the repeating unit cell is broken—resulting in perturbation of the electronic structure. Due to the large surface area-to-volume ratio and bulk defect tolerance, these defects have been suggested to be critical in material and device degradation, as will be discussed later.[34]

3. Perovskite Extrinsic Stability

Despite perovskites general robustness to internal defects, external factors such as light, oxygen, temperature, and humidity (water) have been shown to interact with the perovskite material. These interactions can induce general phase changes by altering the structure's tolerance factor, as discussed earlier, or induce chemical reactions that have the potential to cause irreversible degradation, as will be discussed in this section. Although the details of these mechanisms are not well known for most formulations, they have been studied most extensively for $MAPbI_3$ given its prevalence in literature. Thus, $MAPbI_3$ serves as a logical starting point for our discussion. Moreover, due to its appropriate tolerance factor and single A-, B-, and X-sites, $MAPbI_3$ offers a phase pure system where chemical reactions, rather than phase transitions, dominate material degradation. This has allowed the community to develop an unconvoluted mechanistic understanding of chemical degradation in $MAPbI_3$ that can be used to predict how and why altering a given lattice site alters degradation.

3.1. Light (Photostability)

Like other semiconductors, $MAPbI_3$ forms an excited state when it absorbs light. In this state, it has been shown to have increased ionic mobility due to the creation of iodide vacancies.[35–37] It has been theorized that this is due to the oxidation of iodide atoms by photogenerated holes.[36] This transformation from iodide to iodine causes a reduction in ionic size, allowing it to leave the lattice and form an interstitial and vacancy

$$I_I^x + h^+ \rightarrow I_i^x + V_I^+ \quad (5)$$

While it is unclear to what extent this reaction is reversible, the creation of charged iodide vacancies and free iodine could lower the activation energy for various degradation pathways, create new degradation mechanisms, and/or alter device behavior.

3.2. Oxygen (Photooxidative Stability)

As mentioned in the last subsection, light increases iodide vacancies and ionic mobility in the perovskite. When coupled with oxygen, this leads to irreversible degradation into PbI_2, as shown by the absorbance profiles and corresponding pictures of films in **Figure 7**. Several reports by Haque et al. investigated this reaction.[38–41] They suggest that molecular oxygen reversibly adsorbs and diffuses through iodide vacancies, where they create a state near the conduction band. If these states are present when the perovskite is excited, they trap a photoexcited electron, forming a highly reactive and charged O_2^- superoxide. To become neutral, this oxide initiates an acid–base reaction with the MA cation, deprotonating it to form water, iodine,

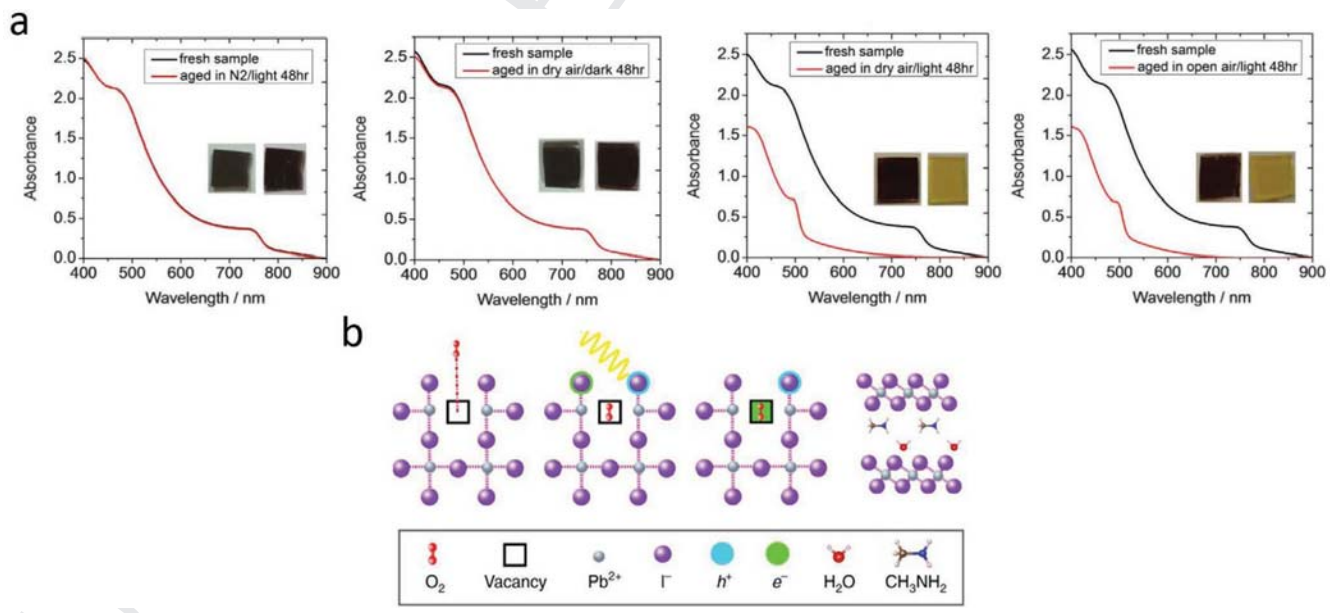

Figure 7. Oxygen induced degradation of perovskites. a) Absorbance profile and pictures of $MAPbI_3$ films before and after aging in stated conditions. Reproduced with permission.[41] Copyright 2016, The Royal Society of Chemistry, under a Creative Commons 3.0 License. b) Schematic of oxygen induced degradation. Reproduced under the terms of the Creative Commons 4.0 License.[38] Copyright 2017, Nature Publishing Group.

© 2020 WILEY-VCH Verlag GmbH & Co. KGaA, Weinheim

Pursuant to the DOE Public Access Plan, this document represents the authors' peer-reviewed, accepted manuscript. The published version of the article is available from the relevant publisher.

lead-iodide, and methylamine gas, as detailed below and schematically in Figure 7

$$CH_3NH_3PbI_3\,(s) \xrightarrow{\text{Light}} CH_3NH_3PbI_3^*\,(s) \quad (6)$$

$$O_2\,(g) \xrightarrow{MAPbI_3^*} O_2^{*-}\,(g) \quad (7)$$

$$CH_3NH_3PbI_3\,(s) + O_2^{*-}\,(g) \xrightarrow{\text{Deprotonation}} CH_3NH_2\,(g) + PbI_2\,(s) + \frac{1}{2}I_2\,(s) + H_2O\,(l) \quad (8)$$

Although the deprotonation process is afforded by the methylammonium cation, the general process of photooxidation, where an excited electron in the conduction band is oxidized by molecular oxygen, is common among most neat photovoltaic absorbers due to the prevalence of long-lived carriers in the excited state. However, when these materials are incorporated into a solar cell, the density of electrons in the conduction band is drastically reduced as they are quickly extracted by the electron transport layer (ETL). Consequently, the degree to which the perovskite oxidizes is highly dependent on the relative rates of oxidation and electron charge transfer to another material and will be much smaller for a perovskite incorporated into a device or on an ETL.[40]

3.3. Temperature (Thermochemical Stability)

In addition to oxygen and light, $MAPbI_3$ has been shown to be sensitive to temperature, degrading into PbI_2 in inert environments at temperatures as low as 85 °C, as can be seen by the conductive atomic force microscopy (C-AFM) images in **Figure 8**.[42] Studies using thermogravimetric analysis (TGA) agree that this occurs through an initial sublimation of the organic halide components, followed by decomposition of the metal halide at much higher temperatures. However, the community disagrees on the required temperatures and whether the products are hydroiodic acid and deprotonated methylammonium,[43–45] ammonia and methyl iodide,[46–48] or both[49,50]

$$CH_3NH_3PbI_3\,(s) \rightleftharpoons CH_3NH_2\,(g) + HI\,(g) + PbI_2\,(s) \quad (9)$$

$$CH_3NH_3PbI_3\,(s) \rightarrow CH_3I\,(g) + NH_3\,(g) + PbI_2\,(s) \quad (10)$$

It is noteworthy that the products of the first reaction have been demonstrated to form perovskite when used as precursors,[51,52] while the products in the second have been demonstrated to form nonprimary ammonium salts,[46] denoted by the reversible and irreversible arrows. However, lamination studies using a combination of temperature and pressure show improvements in material properties when temperatures sufficient for thermal degradation are utilized and mass transport is prevented.[53,54] As such, both reactions are likely reversible in systems where constituents are not prone to evaporate away or be consumed by other reactions.

3.4. Water (Hygroscopic Stability)

Finally, water and other polar solvents/vapors have been demonstrated to affect the perovskite due to their ability to form solvated phases. Although degradation from polar solvents can be avoided by controlling processing environments and using orthogonal solvents to deposit sequential layers, completed devices will necessarily be exposed to humid environments when fielded. As such, significant effort has been made understanding interactions between water vapor and $MAPbI_3$. In general, it has been shown that water molecules initially hydrate the perovskite crystal structure, forming a monohydrate phase in single crystals[55,56]

$$CH_3NH_3PbI_3\,(s) + H_2O\,(g) \rightleftharpoons CH_3NH_3PbI_3 \cdot H_2O\,(s) \quad (11)$$

Or both a monohydrate and dihydrate phase in thin films[56]

$$4\,(CH_3NH_3)\,PbI_3 + 4H_2O \rightleftharpoons 4\,[CH_3NH_3PbI_3 \cdot H_2O] \quad (12)$$

$$4\,[CH_3NH_3PbI_3 \cdot H_2O] \rightleftharpoons (CH_3NH_3)_4\,PbI_6 \cdot 2H_2O + 3PbI_2 + 2H_2O \quad (13)$$

In both cases, these reactions are reversible. As such, mono- and dihydrated perovskites stored in inert environments with

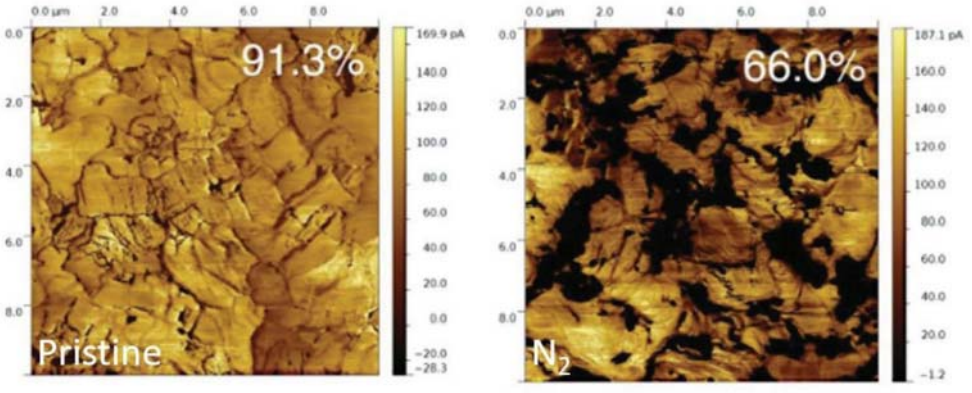

Figure 8. Conductive atomic force microscopy (C-AFM) images of pristine $MAPbI_3$ films (left) and $MAPbI_3$ films subjected to 85 °C for 24 h in N_2 (right). Percentages represent the fraction of area that contributes to current. Reproduced with permission.[42] Copyright 2015, Wiley-VCH.

© 2020 WILEY-VCH Verlag GmbH & Co. KGaA, Weinheim

Pursuant to the DOE Public Access Plan, this document represents the authors' peer-reviewed, accepted manuscript. The published version of the article is available from the relevant publisher.

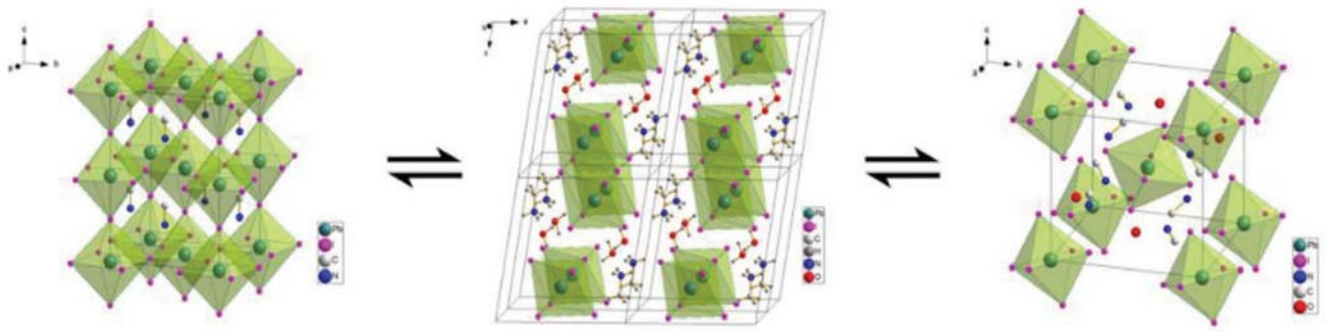

Figure 9. Structure of cubic $MAPbI_3$ (left), monohydrate $MAPbI_3{\cdot}H_2O$ (middle), and dihydrate $(MA)_4PbI_6{\cdot}2H_2O$ (right). Reproduced with permission.[56] Copyright 2015, American Chemical Society.

no external input kinetically revert to their dehydrated phase with some minor limitations due to phase separation of the products.[55,56] However, while incorporation of water does not initially cause permanent degradation, it does induce significant structural deformation by forcing the $[PbI_6]^{4-}$ octahedra to separate.[55,56] This separation causes the dehydrated structure to transform from a 3D network of octahedra to a 1D chain of octahedra for the monohydrate and a 0D framework of isolated octahedra for the dihydrate (**Figure 9**). In addition to destroying the photovoltaic properties of the material, this structural deformation weakens the bonds between the organic cation and the $[PbI_6]^{4-}$ octahedra, allowing for easier deprotonation of the cation and/or degradation of the film through external energy inputs such as heat and/or electrical bias.

This generally reversible hydration occurs until the perovskite structure has been saturated with water, at which point the organic component of the perovskite structure starts to dissolve, irreversibly creating lead iodide and aqueous methylammonium iodide. For the single crystal, this phase is suggested to evolve directly from the monohydrate phase[55,56]

$$CH_3NH_3PbI_3 \cdot H_2O(s) + H_2O(l) \rightarrow CH_3NH_3I(aq) + PbI_2(s) + 2H_2O(l) \quad (14)$$

On the other hand, for thin films it has been suggested to evolve from the dihydrate phase[56]

$$(CH_3NH_3)_4\,PbI_6 \cdot 2H_2O + H_2O(l) \rightarrow 4CH_3NH_3I(aq) + PbI_2(s) + 2H_2O(l) \quad (15)$$

We note that that the discrepancies between these reactions are likely explainable by the differences between the defect structure of thin films and single crystals. Specifically, thin films have grain boundaries/a higher surface-area-to-bulk ratio and therefore possess more defects with different formation energies and transition levels than their single crystal counterparts. These defects may make the formation of the dihydrate phase energetically favorable to the irreversible dissolution of the organic component, causing it to form first.[57]

3.5. Beyond $MAPbI_3$

Once exposed to the elements, the above reactions suggest the coexistence of many compounds within the film including $CH_3NH_3PbI_3$, PbI_2, CH_3NH_3I, CH_3NH_2, HI, CH_3I, NH_3, I, and I_2. While the presence of small amounts of these may not be detrimental to $MAPbI_3$, they may further react with other available chemical species or each other. As such, limiting their existence is of utmost importance.

Given the numerous degradation mechanisms afforded by the methylammonium cation, partially or fully replacing it with less volatile cations is one of the most widely employed paths toward greater chemical stability. Additional insight as to why can be gained by understanding the reaction mechanisms involved in each decay pathway: photooxidative degradation is enabled by an acid–base reaction between the superoxide and the MA cation, thermal decomposition is enabled by the light and organic nature of the MA cation, and hygroscopic decomposition is enabled by the solubility of the MA cation in water. As a result, going from MA to FA, a less acidic, heavier, cation with a ten times lower dipole moment, drastically improves chemical stability, and going further to the inorganic Cs forces chemical decomposition to proceed through a different route.[58] However, TGA studies by Tan et al. have shown that $Cs_{0.05}(MA_{0.17}FA_{0.83})_{0.95}Pb(I_{0.83}Br_{0.17})_3$ perovskites thermally decay in two steps, with the first akin to that of MA-based perovskites and the second that of FACs (**Figure 10**).[59] Thus, alloying at the A-site appears to only kinetically limit thermal degradation. This creates a problem for any devices employing MA both during operation and annealing, as a correct balance between driving away excess solvent and decomposing the newly formed perovskite must be found. As a result, many groups have completely moved away from MA-based perovskites. However, given its favorable tolerance factor and associated defect tolerance, film and device level strategies have been developed to control these chemical instabilities that warrant additional investigation.[60–62]

Although FA- and Cs-based compositions have drastically improved chemical stability, they still suffer from phase stability issues when exposed to external factors: water, oxygen, and temperature can all induce phase transitions. While these phase transitions do not necessarily lead to irreversible changes, they can result in rapid loss of photovoltaic performance and therefore should be avoided. This appears to be most easily done by alloying to achieve appropriate tolerance factor, as described earlier in section 2. Thus, due to its lack of a role in determining the band structure, changes to the A-site can be made to increase the defect tolerance, chemical stability, and structural stability of the perovskite with little concern for

UNCORRECTED PROOF

 © 2020 WILEY-VCH Verlag GmbH & Co. KGaA, Weinheim

Pursuant to the DOE Public Access Plan, this document represents the authors' peer-reviewed, accepted manuscript. The published version of the article is available from the relevant publisher.

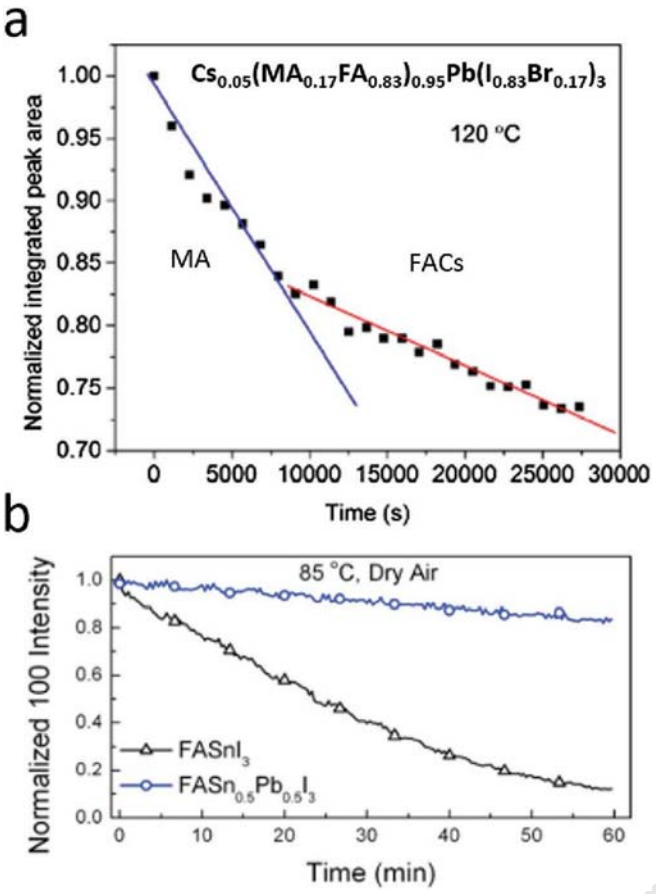

Figure 10. Effect of alloying to increase stability. a) Normalized X-ray diffraction (XRD) peak areas of $Cs_{0.5}(MA_{0.17}FA_{0.83})_{0.95}Pb(I_{0.83}Br_{0.17})_3$ films aged at 120 °C in N_2 showing two separate degradation steps—one akin to MA-based perovskites and the other to FACs. Reproduced with permission.[59] Copyright 2018, American Chemical Society. b) Normalized XRD peak areas of $FASnI_3$ and $FASn_{0.5}Pb_{0.5}I_3$ films aged at 85 °C in dry air showing just one rate of degradation. Reproduced with permission.[67] Copyright 2017, American Chemical Society.

harming its electronic properties. In contrast, changes to the B- and X-site significantly perturb electronic structure. As a result, these sites are normally altered to obtain desirable bandgap, not improve stability. Nonetheless, these changes result in variations to chemical stability and therefore warrant a discussion.

Changes at the X-site are primarily employed to increase the bandgap of the perovskite; alloying bromine into $MAPbI_3$ allows tuning of the bandgap from 1.6 to 2.3 eV.[63] In addition to bromine, chlorine can be used, although incorporation directly into the lattice in ambient conditions is challenging and it is more often used as an agent to control crystallization.[64] In relation to iodide, these halides are smaller and more electronegative. As a result, assuming the structure remains unchanged, they form stronger bonds with the A-site cations. This simultaneously 1) increases the stability of the perovskite structure by increasing the strength of A-to-BX bonds[65] and 2) increases the chance that the halide will deprotonate the A-site cation.[49] However, due to the different ionic radii of these elements, this effect can be secondary to those resulting from the change in lattice spacing.

On the other hand, alloying tin into the B-site of $FAPbI_3$ allows the bandgap to be decreased from 1.52 to 1.25 eV.[66] However, partially or fully replacing lead with tin also drastically reduces the chemical stability of the resulting perovskite, as tin prefers to oxidize from the +2 to +4 state. Using TGA, Leijtens et al. showed that compositions with high tin contents quickly decay via a mechanism involving adjacent Sn^{2+} ions, forming tin (IV) oxide and tin (IV) iodide through the following reaction:[67]

$$2ASnI_3(s) + O_2(g) \Rightarrow 2AI(s) + SnO_2(s) + SnI_4(g) \quad (16)$$

where A is any A-site cation. In this reaction, iodide ions bonded to the tin cation are transferred to an adjacent iodide-sharing tin cation, breaking just two bonds to form SnI_4 and SnO_2. On the other hand, compositions with a Pb:Sn ratio of 1:1 or greater must react through a different mechanism as Pb^{2+} does not easily oxidize to Pb^{4+}. As a result, I_2 must be generated, causing three times as many iodide bonds to be broken, as shown below[67]

$$2[APb_{0.5}Sn_{0.5}I_3](s) + O_2(g) \Rightarrow 2AI(s) + SnO_2(s) + PbI_2(s) + I_2(g) \quad (17)$$

Due to its less favorable reaction mechanics, this degradation pathway proceeds at a much slower rate, as shown in Figure 10. This is an interesting and unique result: while many studies have shown that alloying can be used to kinetically limit a degradation mode this shows that local chemistry can be used to force chemical degradation to proceed through a different mechanistic route. We note that this is akin to what has been seen when alloying to increase phase stability, but the opposite to what has been seen when alloying to increase thermal stability. Given this bifurcation, further exploration into the degradation mechanisms of perovskites with improved stability is warranted.

4. Alloying, Additives, and Adaptations

The last section covered the effect of changing chemical composition on material stability. While it is apparent that alloying is an effective means to reduce defects and increase both the structural and chemical stability of the bulk, changing the composition of the perovskite in a way that is restricted to ABX_3 compositions is unlikely to significantly improve the defect chemistry of the surface; regardless of what elements are chosen, the surface allows for the low-energy formation of deep-level trap states, such as undercoordinated halide or lead species, lead clusters, and Pb-I antisite defects (PbI_3^-), as well as the usual shallow-level traps such as iodide or methylammonium vacancies. As mentioned earlier, these surfaces/defects have been demonstrated to dominate material degradation: Aristidou et al. demonstrated that photooxidation starts at the surface and proceeds into the bulk through iodide vacancies;[38] Yun et al. demonstrated that hygroscopic decomposition initiates phase transitions at the grain boundaries that proceed toward the interior;[68] and Fan et al. demonstrated that the lowest thermal decomposition temperatures witnessed in

UNCORRECTED PROOF

© 2020 WILEY-VCH Verlag GmbH & Co. KGaA, Weinheim

Pursuant to the DOE Public Access Plan, this document represents the authors' peer-reviewed, accepted manuscript. The published version of the article is available from the relevant publisher.

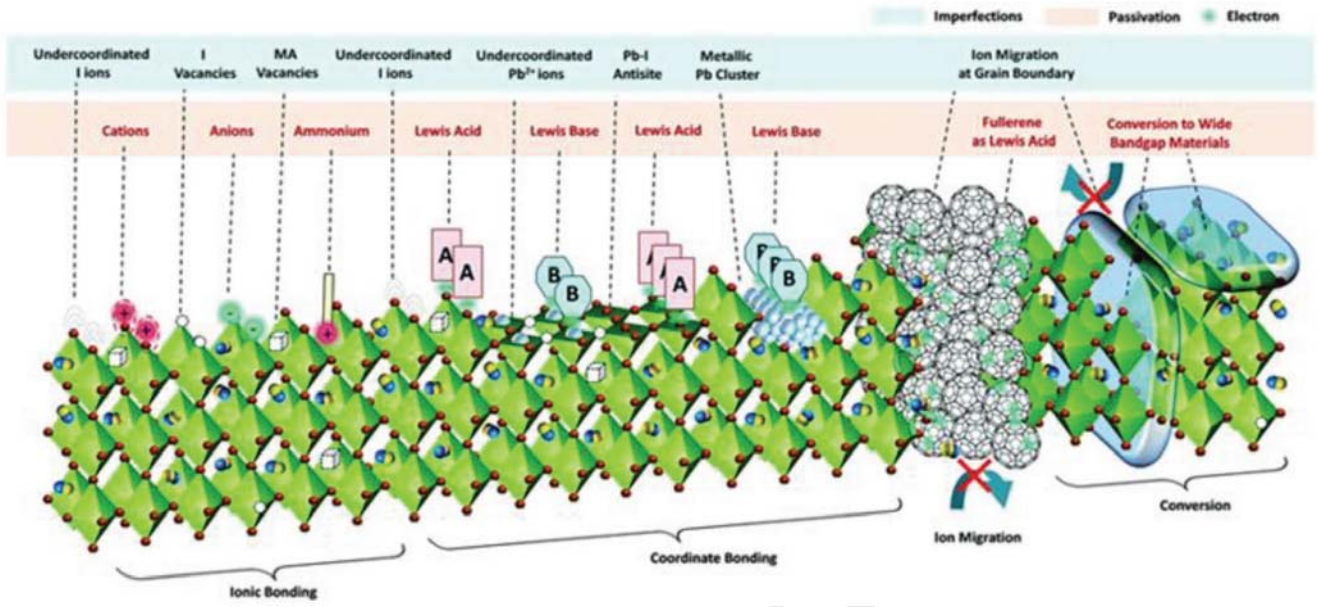

Figure 11. Common surface defects for perovskites and the effect of various additives. Reproduced with permission.[72] Copyright 2019, Royal Society of Chemistry.

$MAPbI_3$ are the result of a layer-by-layer decomposition process that initiates at the surface.[69] Thus, achieving the targeted 20+ year device lifespans desired for terrestrial grid scale deployment will require more than just material alloying. Specifically, these surface defects must be controlled in some way.

So far, this has been done by incorporating additives into the precursor solution, antisolvent, or post-treatment that form coordinate or ionic bonds with the charged defects of the perovskite. These passivating agents neutralize the charge of the defect site, reducing its ability to electronically perturb the ionic crystalline lattice and thus its effect on the band structure of the perovskite. Additives of this nature can be divided into a few categories: ammonium salts, Lewis acids, Lewis bases, lower dimensional perovskites, and ionic liquids. A schematic describing common defects at the surface and the effect of additives is shown in **Figure 11**. It is noteworthy that in addition to passivating surface defects, additives which are incorporated into the precursor solution or antisolvent can have a drastic impact on film formation, which can in turn alter the bulk defect concentration and terminating surfaces of the perovskite. In the section that follows, we will briefly touch on the effect of commonly used additives, but note that more in-depth articles have been recently written on the effect of additives by Zhang et al.[70] and the role of surfaces by Schulz et al.,[34] and highly recommend them and the most recent state of the art work by Yang et al.[62] and Min et al.[71] as further reads.

4.1. Ammonium Salts

As discussed above, most detrimental defects that must be passivated in perovskites exist at grain boundaries and surfaces. Due to the polycrystalline nature of the perovskite, these surfaces are predominately comprised of excess materials added to the precursor solution that do not incorporate into the bulk of the crystallite. As a result, it may be possible to tune the composition of the precursor solution to produce self-passivated surfaces. For example, Son et al. found that adding a small excess of MAI into the precursor solution of $MAPbI_3$ results in the accumulation of MAI at grain boundaries that suppresses nonradiative recombination.[73] Similarly, Yang et al. demonstrated that adding excess MAI and annealing at higher temperatures produces films with larger and more uniform grains.[74] In addition to MAI, a range of other ammonium salt derivative-based additives have proven to have similar effects, including organic halides (e.g., methylammonium chloride (MACl),[75–82] methylammonium bromide (MABr),[83] and ammonium chloride (NH4Cl)),[84–87] organic pseudohalides (e.g., methylammonium thiocyanate (MASCN),[88] guanidine thiocyanate (GuaSCN),[89,90] ammonium thiocyanate (NH4SCN)[91,92]), and organic nonhalides (e.g., methylammonium acetate (MAOAc)[93–95]). In fact, moving away from the prototypical MAI has generally demonstrated better results. For example, replacing iodide with chlorine has been shown to provide many of the same positive effects as MAI while simultaneously retarding crystallization due to chlorine incorporation, as shown by the pictures of films in **Figure 12**.[75] Similarly, further replacing MA^+ with NH_4^+ has been demonstrated to result in films with improved morphology and crystallinity to those with MACl[84] due to its ability to easily be removed in crystallization through the deprotonation of NH_4^+ by water, resulting in the formation of NH_3 and HI/HCl.[85] In addition to these more traditional molecules that mimic components of the perovskite, others have proven success with more complex molecules that do not. For example, Zhang et al. demonstrated that addition of quaternary ammonium halides (e.g., choline chloride—$(CH_3)_3NCH_2CH_2OH$) results in films with improved passivation, enabling devices with higher efficiency and stability against humidity and light.[96] Similarly, Li et al. have shown adding butyl phosphonic acid 4-ammonium chloride (4-ABPACl) into the $MAPbI_3$

UNCORRECTED

© 2020 WILEY-VCH Verlag GmbH & Co. KGaA, Weinheim

Pursuant to the DOE Public Access Plan, this document represents the authors' peer-reviewed, accepted manuscript. The published version of the article is available from the relevant publisher.

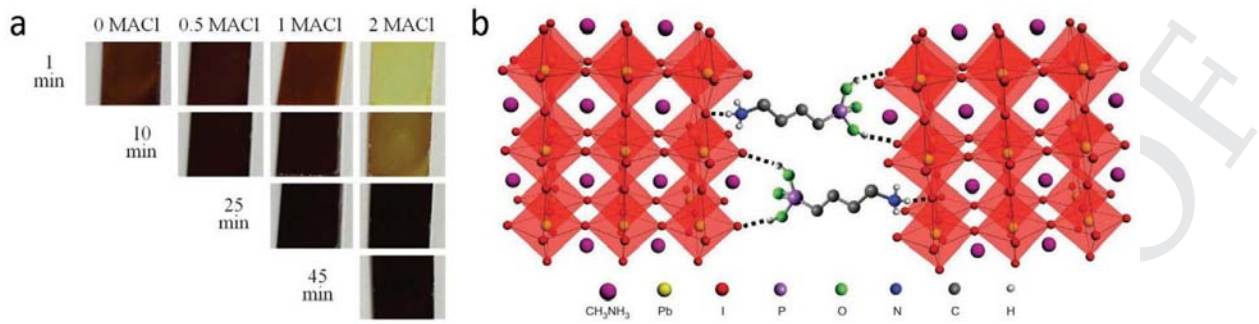

Figure 12. a) Images of $MAPbI_3$ films prepared with the stated amount of MACl annealed at 100 °C for stated duration. Reproduced with permission.[75] Copyright 2014, American Chemical Society. b) Schematic of cross-linked grains due to hydrogen-bonding interactions between the iodide of perovskite and $PO(OH)_2$ and $-NH_3^+$ terminating groups of 4-ABPACl. Reproduced with permission.[97] Copyright 2015, Nature Publishing Group.

precursor solution results in an almost a two-fold increase in PCE and stronger resistance to moisture due its $-PO(OH)_2$ and $-NH_3^+$ terminating groups ability to form strong hydrogen bonds with the perovskite surface and cross link adjacent grains. A schematic of this interaction is shown in Figure 12.[97]

4.2. Lewis Acids

The second class of additives, Lewis acids, are any material that has the capability of accepting a pair of nonbonding electrons. In perovskites, these materials form Lewis adducts with undercoordinated halides (I^-) and antisite defects (PbI_3^-), neutralizing the charge of the defect. While a broad range of materials are classifiable as Lewis acids, those that have proven to be successful fall into two main categories: metal cations (e.g., Pb^{2+}) and fullerene derivatives (e.g., $PC_{61}BM$).

Positively charged metal cations can impact the electronic structure of the perovskite in the vicinity of the band edges through ionic bonding and other electrostatic/dynamic interactions with negatively charged defects. Thus, as adding excess MAI can passivate defects, adding excess PbI_2 can as well. For example, Chen et al. and Kim et al. demonstrated that a small excess of PbI_2 in $MAPbI_3$ precursor solutions results in higher performing devices due to the PbI_2-based passivation of surface defects at interfaces and grain boundaries that limit charge carrier recombination.[98,99] Following this strategy, Ke et al. incorporated lead thiocyanate ($Pb(SCN)_2$) in the perovskite precursor, showing that it could serve a similar role due to the ability of the SCN^- anion to react with a MA^+ cation of $MAPbI_3$, forming HSCN and methylamine gasses that promote grain growth and leave PbI_2 at grain boundaries, as shown by the C-AFM in **Figure 13**.[100] However, while the addition of metal cations native to the perovskite film passivates defects, the use of other positively charged metal cations have been demonstrated to have improved passivation capabilities. For example, Abdi-Jalebi et al. have shown that addition of potassium iodide (KI) to a $Cs_{0.06}FA_{0.79}MA_{0.15}Pb(I_{0.85}Br_{0.15})_3$ precursor solution results in large boosts in PCE due to the accumulation of K^+ at interfaces that fills I-vacancies and bonds to uncoordinated halides, passivating nonradiative trap sites and reducing ionic mobility.[101] Similarly, Wang et al. demonstrated that addition of europium acetylacetonate to both MA- and MAFACs-based perovskite precursor solutions results in significantly more stable devices due to the formation of europium ion pairs (Eu^{3+}–Eu^{2+}) that serve as a "redox shuttle" to selectively oxidize metallic Pb (Pb^0) and reduce iodine (I^0) defects, as shown schematically in Figure 13.[102] In addition to these studies, a large range of other metal cations, including Li^{1+},[103] Na^{1+},[104–106] Ag^{1+},[104,106] Rb^{1+},[20,107,108] Cu^{1+},[104,106,109] Cu^{2+},[110,111] Zn^{2+},[112,113] Mg^{2+},[114] Ca^{2+},[115,116] Ni^{2+},[117] Sr^{2+},[118] Ba^{2+},[119,120] Fe^{2+},[102,121] and Bi^{3+},[122,123] have been shown to interact with the negativley charged defects of the perovskite.[124] However, there is a clear need for additional work to detail the mechanisms and associated opportunities for these other metals to improve stability while maintaining high PCE.

The second class of Lewis acids, fullerene derivatives, can passivate defects at the grain boundaries in much the same way as metal cations. However, while most metal cations must be stabilized with a corresponding anion to provide charge

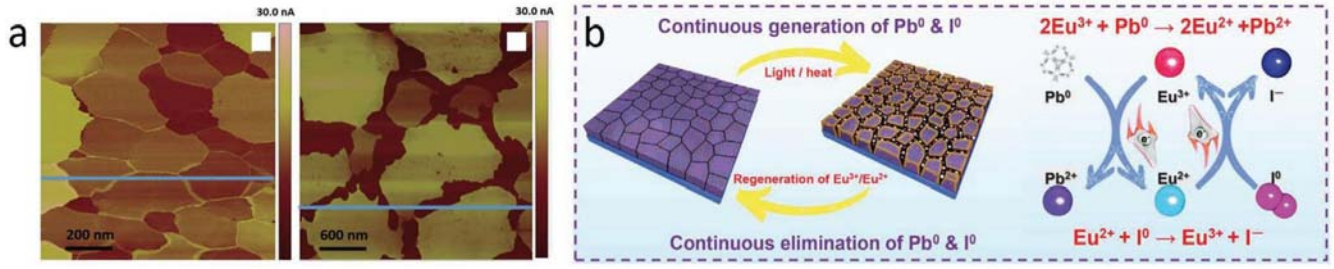

Figure 13. a) C-AFM images of perovskites prepared with (left) and without (right) 5% $Pb(SCN)_2$. Reproduced with permission.[100] Copyright 2016, Wiley-VCH. b) Schematic of Eu^{2+}–Eu^{3+} ion pairs ability to eliminate Pb^0 and I^0 defects. Reproduced with permission.[102] Copyright 2019, American Association for the Advancements of Science (AAAS).

© 2020 WILEY-VCH Verlag GmbH & Co. KGaA, Weinheim

Pursuant to the DOE Public Access Plan, this document represents the authors' peer-reviewed, accepted manuscript. The published version of the article is available from the relevant publisher.

neutrality, fullerenes are charge neutral and stabilize excess electronic charge resonantly. As a result, they are stable with and without interacting with defects on the perovskite surface. Due to their high electron affinity, small reorganization energy, and high electron mobility, this made them ideal as the ETL in devices. However, after noticing their effect on voltage, various groups began incorporating them into the perovskite where they coat surfaces and grain boundaries, creating an OPV like perovskite-fullerene bulk heterojunction that improves charge extraction and blocks intergrain ionic transport. For example, Liu et al. demonstrated that a C_{60}-$MAPb_{0.75}Sn_{0.25}I_3$ heterojunction improves device performance, hysteresis, and stability due to an improvement in bulk and surface recombination lifetimes afforded by a reduced number of trap states.[125] However, in addition to fullerenes, various fullerene-derivatives have been shown to provide similar defect passivation; for example, Xu et al. and Chiang et al. reported that phenyl-C61-butyric acid methyl ester ($PC_{61}BM$) results in improvements to hysteresis and device performance of both n–i–p[126] and p–i–n[127] devices due to enhanced crystallization and the passivation of Pb-I antisite defects at interfaces (**Figure 14**). Moreover, the functional group of these derivatives can be modified to provide other benefits. For example, Zhang et al. demonstrated that isomer—pure bis(1-[3-(methoxycarbonyl) propyl]-1-phenyl)-[6.6]C_{62} (α-bis-PCBM) can be mixed into the antisolvent to simultaneously prevent moisture-induced erosion, passivate voids and pinholes, enhance crystallization, and improve electron extraction, resulting in devices with improved performance and stability under heat and light soaking.[128] Similarly, Fu et al. have shown that fullerene end-capped polyethylene glycol (C_{60}-PEG) can be introduced into the antisolvent to enlarge grain size, passivate defects, improve carrier extraction, and provide hydrophobic coating to grains, once again resulting in devices with improved performance and stability.[129] Thus, tailoring fullerene derivatives with specific features to address the particular degradation modes associated with moisture, residual solvent complexes, or thermal degradation is a promising strategy to assist with stability while maintaining high PCE.

4.3. Lewis Bases

The third class of additives, Lewis bases, are the opposite of Lewis acids—namely, any material that has the capability of donating a pair of nonbonding electrons. In perovskites, these materials form Lewis adducts with undercoordinated metal sites (Pb^{2+}), neutralizing the charge of the defect. A good Lewis base for a given perovskite composition should have three properties: 1) an affinity for hydrogen bonds, 2) an accessible electron-donating atom, and 3) similar hardness to the Lewis acid.[130] While a broad set of materials are classifiable as Lewis bases, those that have proven to be successful in modulating perovskite defects fall into three categories: O-donors, S-donors, and N-donors.

O-donor Lewis bases have a lone pair of electrons on an oxygen molecule and, much like our previous additives, have been used in PSCs for a long time; most successful solvents for processing perovskites, including *N*,*N*-dimethylformamide (DMF), *N*,*N*-dimethyl sulfoxide (DMSO), and *N*-methyl-2-pyrrolidone (NMP), fall into this category. These solvent molecules aid crystallization by interacting with perovskite precursors in solution to form stable intermediate phases (e.g., $MAPbI_3 \cdot DMF$, $MAI \cdot PbI_2 \cdot DMSO$) that can be rapidly supersaturated by an antisolvent to form uniform and dense films, as shown in **Figure 15**.[131] While the effect of creating intermediate phases and supersaturating them through standard solvent systems is well known to community, recent research is starting to show that it can be heavily modified by other oxygen donating Lewis bases. For example, Bi et al. reported that poly(methyl methacrylate) (PMMA) can be added to the antisolvent to form an intermediate adduct with PbI_2 that slows down perovskite crystallization kinetics and allows for heterogenous nucleation.[132] In doing so, the randomly formed nuclei have time to adjust their orientation to minimize the total Gibbs free energy of the system and grow in their thermodynamically preferred orientation. This results in the formation of a dense, compact, and homogeneous films with fewer defects and larger grains that, when incorporated into a device, achieves improved PCE. Similarly, Wang et al. have shown that small molecules,

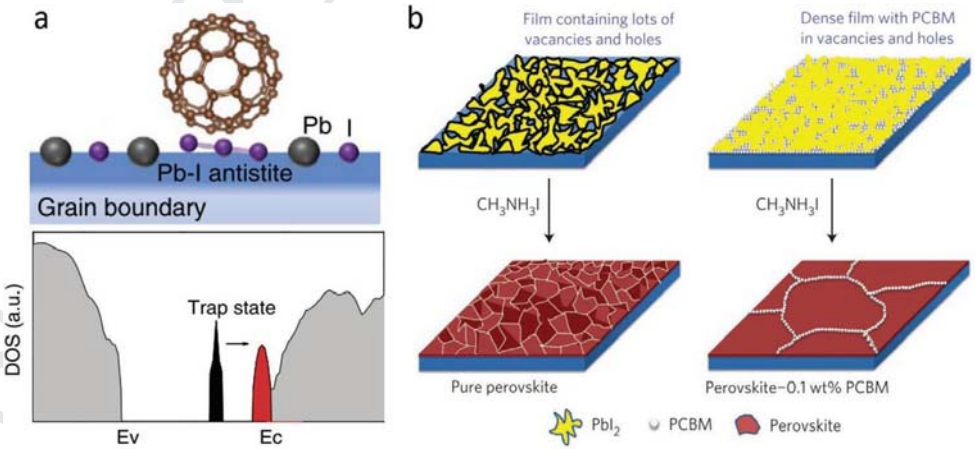

Figure 14. a) Schematic of PCBM-based passivation of Pb–I antisite defects and DFT calculations showing its ability to move the Pb–I antisite deep-level defect (black) to much shallower states (red). Reproduced with permission.[126] Copyright 2015, Nature Publishing Group, under a Creative Commons 4.0 License. b) Schematic of PCBM-enhanced grain growth. Reproduced with permission.[127] Copyright 2016, Nature Publishing Group.

© 2020 WILEY-VCH Verlag GmbH & Co. KGaA, Weinheim

Pursuant to the DOE Public Access Plan, this document represents the authors' peer-reviewed, accepted manuscript. The published version of the article is available from the relevant publisher.

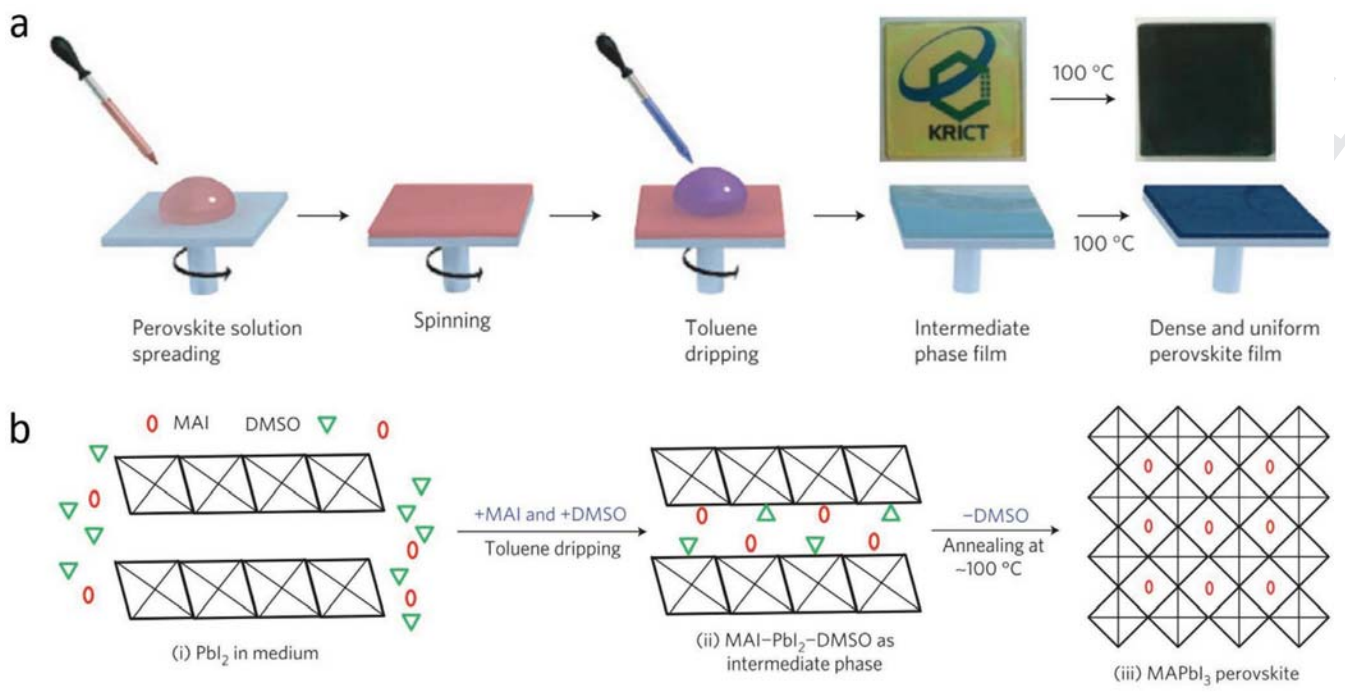

Figure 15. a) Schematic of supersaturating perovskite solution with antisolvent. b) The effect of rapid supersaturation and the resulting MAI–PbI_2–DMSO intermediary phase on film formation. Reproduced with permission.[131] Copyright 2014, Nature Publishing Group.

such as 1,3,7-trimethylxanthine (also known as caffeine), can be added to the precursor solution of a MA-based perovskite to control crystallization.[133] With its carboxyl groups, caffeine serves a similar role, complexing with Pb^{2+} to slow grain growth and allow orientation of the perovskite grains, resulting in higher PCE as well as improved thermal stability.

In addition to tailoring O-donors, S-donors—namely, Lewis bases with a lone pair of electrons on a sulfur molecule—can be used for a stronger effect.[134] The ability of these molecules to interact with undercoordinated Pb^{2+} atoms to passivate defects on the perovskite surface was first demonstrated for thiophene by Noel et al. (**Figure 16**).[135] However, since then, similar effects have been noted for a broad range of thiophene derivatives including 3-alkylthiophene,[136] polythiophene,[137] and poly[(thiophene)-alt-(6,7-difluoro-2-(2-hexyldecyloxy)quinoxaline)] (PTQ10).[138] Moreover, Fei et al. have shown that thiourea can be used to serve an analogous role while also incorporating two amino groups.[139] It has been theorized that this allows for multiple defects to be passivated simultaneously, as the amino acid groups can form hydrogen bonds with iodide while the sulfur-donor group can form Lewis acid–base adducts with undercoordinated Pb^{2+} sites or hydrogen bonds with NH_2 groups.[140,141] Like thiophene, several derivatives of thiourea have proven to be successful as well. For example, Wu et al. demonstrated that three organic D–π–A molecules with various phenyl units as the donor, a thiophene π-spacer, and a cyanoacetic acid acceptor can be used to passivate Pb^{2+} defects within $MAPbI_3$ due to large electron density on the carboxylate end group formed as a result of the strong electron-donating *N*,*N*-dibutylaminophenyl unit.[142] Additionally, Qin et al. found that the small molecule Th(3,9-bis(2-methylene-(3-(1,1-dicyanomethylene)-indanone))-5,5,11,11-tetrakis(5-hexylthienyl)-dithieno[2,3-d:2′,3′-d′]-s-indaceno[1,2-b:5,6-b′]dithiophene) (ITIC-Th) can be used to stabilize the perovskite precursor solution, suppressing the formation of the δ-phase in $FAPbI_3$ films as shown in Figure 16.[143]

Finally, a third class of Lewis bases with a nitrogen-bearing lone pair of electrons, dubbed N-donors, have recently started

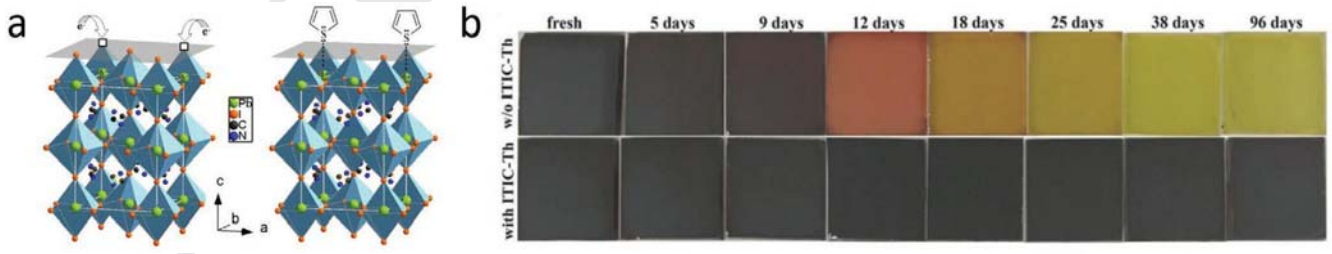

Figure 16. a) Schematic of thiophene-based passivation of undercoordinated Pb atoms at the perovskite surface. Reproduced with permission.[135] Copyright 2014, American Chemical Society. b) Photographs of films fabricated from $FAPbI_3$ precursor solutions with and without the ITIC-Th additive aged for the stated number of days. Reproduced with permission.[143] Copyright 2018, Wiley-VCH.

© 2020 WILEY-VCH Verlag GmbH & Co. KGaA, Weinheim

Pursuant to the DOE Public Access Plan, this document represents the authors' peer-reviewed, accepted manuscript. The published version of the article is available from the relevant publisher.

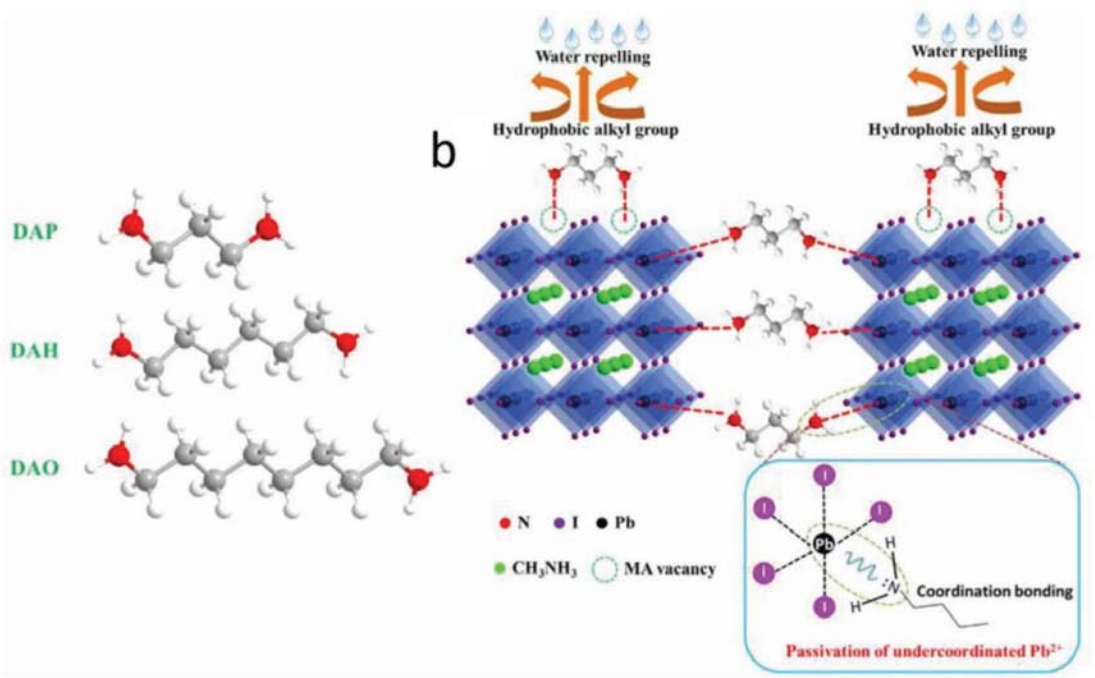

Figure 17. a) Various bilateral alkylamine additives. b) Their ability to passivate defects and repel water. Reproduced with permission.[146] Copyright 2017, American Association for the Advancements of Science (AAAS).

being used intentionally to achieve similar passivation. However, like many other additives, this class of donors have been used for a long time, as 4-*tert*-butylprydine, a N-donor Lewis base, has been commonly used to dope the top transport layer (i.e., Spiro-OMeTAD). Noticing its effect on device performance, Wu et al. tried introducing it into the antisolvent for a $MAPbI_3$ film.[144] In said study, they noted that enhancements in efficiency and stability could be achieved due to its ability to form an intermediary phase that suppressed nucleation, leading to high quality films. Following this discovery, several other groups have demonstrated that additional N-donating Lewis bases, primarily consisting of pyridine (C_5H_5N) and azanide (NH_2) derivatives, could be used to reap similar benefits. For example, Liu et al. reported that pyridine can be added to a precursor solution in small volumes to produce large-grain, pinhole free, compact perovskite films.[145] Similarly, Wu et al. demonstrated that addition of a small amount of bilateral alkylamine (BAA) (e.g., 1,3-diaminopropane (DAP), 1,6-diaminohexane (DAH), and 1,8-diaminooctane (DAO)) into the precursor solution results in passivated surfaces, improved film formation, and enhanced stability.[146] They attributed this improvement in material properties to the ability of the $-NH_2$ tails of the BAA atoms to coordinate with undercoordinated Pb^{2+} ions and fill A-site vacancies as well as the resulting orientation of the hydrophobic carbon chain normal to the surface. These molecules and their effect are shown in **Figure 17**.

4.4. Lower Dimensional Perovskites

The fourth class of additives, lower dimensional perovskites, have a perovskite like metal halide sublattice coupled with larger bulky cations that preclude the continuous 3D structure of canonical ABX_3 metal halide systems. While these types of low dimensional systems can make reasonable solar cells, they tend to be inferior to their 3D counterparts due to their larger bandgaps and anisotropic transport. However, it has been shown that when incorporated in the correct ratio and fashion, lower dimensional halide perovskites of the form $A'_2(A)_{n-1}BX_{3n+1}$ can orient themselves to the exterior of 3D grains where they replace the defect-ridden terminating groups of the 3D perovskite with their own that appear to be less detrimental, possibly due to their lower dimensionality, while serving multiple other functions afforded by their unique properties. First, due to their hydrophobic nature and anisotropic transport, incorporation of these materials can enhance chemical stability. One example of this type of strategy was employed by Tong et al. in which guanidinium thiocyanate (GuaSCN) was mixed into a Sn–Pb mixed metal halide precursor to produce low-bandgap (≈1.25 eV) perovskite thin films.[89] In this study, Tong et al. noted optoelectronic improvements when the GuaSCN additive was employed in a volume fraction that permitted formation of a 2D structure on surfaces and grain boundaries. The formation of such a 2D structure shelled the grains of the 3D perovskite, as shown in **Figure 18**, inhibiting its oxidation by simultaneously retarding reactions with oxygen at the grain boundaries and tin diffusion out the grains. In addition to improving the chemical stability of the perovskite absorber, these lower dimensional perovskites unique position within the film can induce strain into the 3D bulk, allowing them to control competing room temperature structural phases. For example Lee et al. demonstrated that the addition of small amounts (1.67 mol%) of 2D PEA_2PbI_4 into the precursor can suppress the yellow phase $FAPbI_3$ to produce an apparently phase-pure FA perovskite, as evidenced by the color

© 2020 WILEY-VCH Verlag GmbH & Co. KGaA, Weinheim

Pursuant to the DOE Public Access Plan, this document represents the authors' peer-reviewed, accepted manuscript. The published version of the article is available from the relevant publisher.

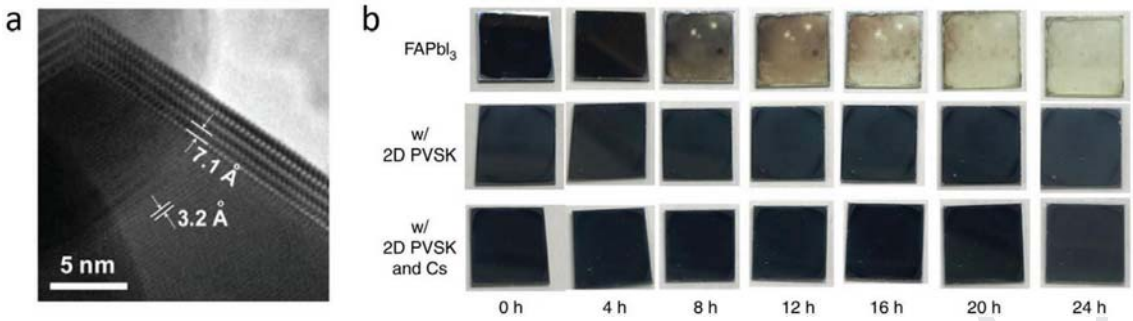

Figure 18. a) High resolution transmission electron microscopy images of the 2D Gua-based shell around the grain boundary of Sn-Pb-based perovskite obtained by adding 7% GuaSCN. Reproduced with permission.[89] Copyright 2019, American Association for the Advancements of Science (AAAS). b) Pictures of $FAPbI_3$, $FAPbI_3$ with 2D PEA additive, and $FA_{0.98}Cs_{0.02}PbI_3$ with 2D PEA additive exposed to 80% RH/20 °C for stated time. Reproduced under the terms of the Creative Commons 4.0 License.[147] Copyright 2018, American Association for the Advancements of Science (AAAS).

of resulting films (Figure 18), an order-of-magnitude enhancement in photoluminescence lifetime, and resulting device with improved PCE and operational stability.[147] Finally, due to wide-bandgap nature of these lower dimensional perovskites, they can create heterostructures at critical operational interfaces and grain boundaries that form electronic barriers, modulating charge transfer.[148] If properly controlled in thickness, these barriers can limit interfacial recombination while avoiding the losses in current that would result from over inhibition of carrier transport/extraction from the active layer. Thus, if used correctly, these additives provide a self-organized system that can passivate defects at the grain boundaries as well as modulate charge transfer, strain, and ionic transport.

4.5. Ionic Liquids

The final class of additives, Ionic liquids (ILs), are ionic salts comprised of large organic cations coupled with organic or inorganic anion counterparts. They have extremely low vapor pressure, low melting points (<100 °C), high ionic conductivity, and are capable of dissolving most organic and inorganic compounds—including perovskites. This allows them to simultaneously modify perovskite formation, passivate defects by ionically bonding to them and neutralizing their charge, and provide a hydrophobic coating to grain boundaries, resulting in similar effects to the previously described additives. For example, Shahiduzzaman et al. have shown that 1 wt% 1-hexyl-3-methylimidazolium chloride (HMImCl) could be added to a $MAPbI_3$/DMF solution to retard crystal formation and facilitate uniform nucleation to obtain high quality films and improved device performance.[149] Moreover, in a following publication, they demonstrated that the organic cation could be altered to reduce the viscosity of the IL to further improve morphology, crystallinity, and device performance.[150] On the other hand, Salado et al. demonstrated that by using 0.5 wt% of a hydrophobic IL additive, namely 1-methyl-3-(1*H*,1*H*,2*H*,2*H*-nonafluorohexyl) imidazolium iodide (FIm), the stability and performance of both MAFA- and MAFAC-based PSCs could be improved.[151,152] Similarly, Wang et al. have shown that triazolium ILs with an amino group and an varying alkyl side chains could be added into the precursor solution to achieve devices with improved performance and stability under humid conditions.[153] They contributed these improvements to the unique configuration of the IL, which allowed the lone pair of electrons on the amino group to interact with Pb^{2+} defects, passivating defects, retarding crystallization, and forming a self-assembled monolayer on the surface of the grains that kept the hydrophobic alkyl chains of the IL vertical to protect the perovskite (**Figure 19**). Finally, Bai et al. have shown that 1-butyl-3-methylimidazolium tetrafluoroborate ($BMIMBF_4$) could be mixed into MAFAC-based perovskites to enlarge grains, improve energetic alignment, and suppress ion migration, resulting in higher efficiency devices with remarkably enhanced stability.[154]

4.6. Future Approaches

Thus, each category of additive passivates defects by ionic or coordinate bonding with defects of the opposite charge, neutralizing their perturbation on the perovskite lattice and electronic structure. As a result, combining multiple approaches will likely

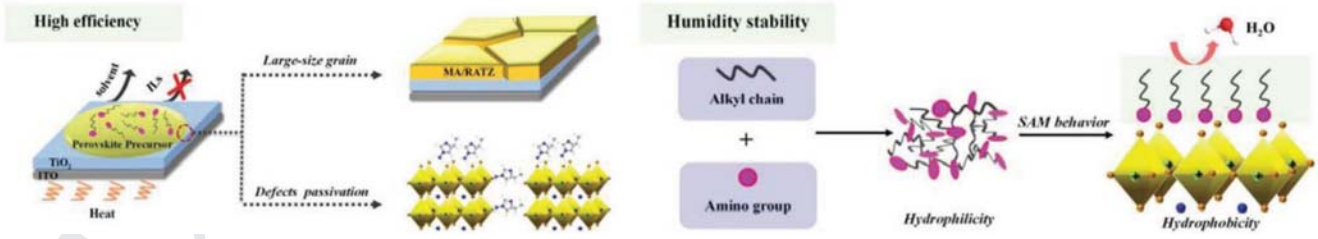

Figure 19. Schematic of triazoliums ability to enhance performance (left) and repel water (right). Reproduced with permission.[153] Copyright 2019, Wiley-VCH.

© 2020 WILEY-VCH Verlag GmbH & Co. KGaA, Weinheim

Pursuant to the DOE Public Access Plan, this document represents the authors' peer-reviewed, accepted manuscript. The published version of the article is available from the relevant publisher.

be required to passivate the variety of charged defects at perovskite surfaces. Some research has already been done on this front. For example, 2-pyridylthiourea has been shown to serve as both a N- and S-donor,[155] a combination of commercial bis-PCBM isomers in the antisolvent and *N*-(4-bromophenyl)thiourea (BrPh-ThR) in the perovskite precursor have been shown serve as both a N-donor and ammonia group,[156] NaF has been shown to simultaneously passivate both anion and cation vacancies,[157] and two thiadiazole derivatives (1,3,4-thiadiazolidine-2-thione and 1,3,4-thiadiazolidine- 2,5-dithione, TDZDT) have been shown to act as both S- and N-donors.[158] However, more work must be done on this front. To establish a directed guide to designing such additive combinations, additional characterization of not only the resulting films but also the details of materials formation will be critical. Moreover, additional work must be done in characterizing how these defect approaches interact with processing at scale.

5. Perovskite Device Stability

In the preceding sections, we have attempted to outline the field's current mechanistic understanding of perovskite material stability. In doing so, we stressed the role of film formation, composition, and additives in controlling defects, reviewed known degradation mechanisms afforded by the environment, and motivated that degradation can be altered by changing composition and defect concentration. In these sections, we hope to have conveyed that the material degradation of perovskites appears to be dominated by defects, particularly at the surfaces. Thus, while its rise to fame has been largely afforded by its intrinsic defect tolerance, its push to commercialization will likely require deeper understanding of surface defects, how they impact device performance, and how they ultimately precipitate specific degradation pathways. With a proper grasp of the perovskite material and the factors that affect its stability, we now move to the next level of complexity: device stability. Ideally, gauging stability at this level would be done by testing devices/modules in the field for over 20 years to prove their durability. However, optimization of device architectures through iterations on this process would take far too long and be debilitatingly expensive. As a result, we must develop protocols to accelerate degradation, being careful that we do not create additional mechanisms that are not present under standard operating conditions. To do this, we must understand not only which degradation mechanisms are present under standard operating conditions, but also the associated rate for each reaction, how to increase it (intensity, voltage, temperature, strain, etc.), and its impact on device performance.[5,159]

Building on the last few sections, we increase the complexity with additional layers, all of which can interact and cause degradation. Due to variations in perovskite composition, device architecture, processing conditions, initial efficiency, and degradation testing parameters, we will avoid quantitative comparisons between separate studies. Instead, we will focus on outlining the considerations that must be made when analyzing device degradation, reviewing known degradation mechanisms, and discussing state-of-the-art device stability results.

5.1. From Material to Device (Understanding Degradation Modes)

As previously discussed, continued optimization of the active layer through alloying and additives will be required to produce stable devices. However, in addition to this, incorporation of the perovskite into a device enables other degradation mechanisms due to the presence of new layers and nonequilibrium conditions that perturb the electronic and chemical structure of the device. These mechanisms are significantly more complex, architecture specific, and convoluted than those involving only the active layer. Thus, the effectiveness of device architectures is generally gauged by comparing the degradation modes of device parameters (e.g., V_{oc}, fill factor (FF), and short-circuit current density (J_{sc})). To hypothesize how changes in these parameters correlate with various degradation mechanisms, existing models for p–i–n and n–i–p photovoltaic technologies had to be modified to fit empirical device observations.

More specifically, previous models of most photovoltaic materials assumed that ions in the active layer are immobile. As a result, the ionization potential and electron affinity of the p- and n-type transport layers pin respective carrier densities at the active layer/transport layer interfaces. This results in a uniform drop in potential across the active layer that moves carriers to the interface where they can be extracted. In this case, changing the energetics of a contact impacts both the built-in voltage and location of carrier densities within the active layer. Although these changes should not affect bimolecular recombination in the device, which is determined by the product of carrier densities in the active layer rather than their location within the bandgap, it should alter the rate of monomolecular recombination as it is governed by a single carrier density. This will impact the V_{oc} of the device.

On the other hand, perovskites are theorized to have highly mobile halide vacancies that move to the perovskite/hole transport layer (HTL) interface when a potential gradient is formed across the active layer.[160,161] To obey charge neutrality, they leave behind an immobile anion-rich region near the ETL that grows wider as the vacancies drift toward the HTL. These charged defects shift the vacuum-level of the perovskite, causing band bending to occur over an extremely narrow region near the HTL and a larger region near the ETL. As a result, the location of carrier densities within the perovskite band remain relatively unaffected by the energetics of the ETL and HTL.[160,162] V_{oc} is then limited by the maximum Fermi level splitting of the active layer and decreases for every instance of nonradiative recombination (i.e., monomolecular recombination from trap sites at the surface). The model proposed[161] is summarized in **Figure 20** next to a standard p–n junction to elucidate similarities and differences.

If correct, this band diagram has several implications for enhancing performance. First, it implies that the best way achieve high voltages is not by choosing transport layers with ideal band offset to the perovskite, but rather those that increase its quasi Fermi level splitting through the passivation of defects at the HTL/ETL interface to limit surface recombination.[160,161] Below the perovskite, this can be done by enhancing nucleation, crystallization, and carrier concentration.[163] While it is still debated whether these changes are induced by electrical potential, terminating groups, or

UNCORRECTED PROOF

© 2020 WILEY-VCH Verlag GmbH & Co. KGaA, Weinheim

Pursuant to the DOE Public Access Plan, this document represents the authors' peer-reviewed, accepted manuscript.
The published version of the article is available from the relevant publisher.

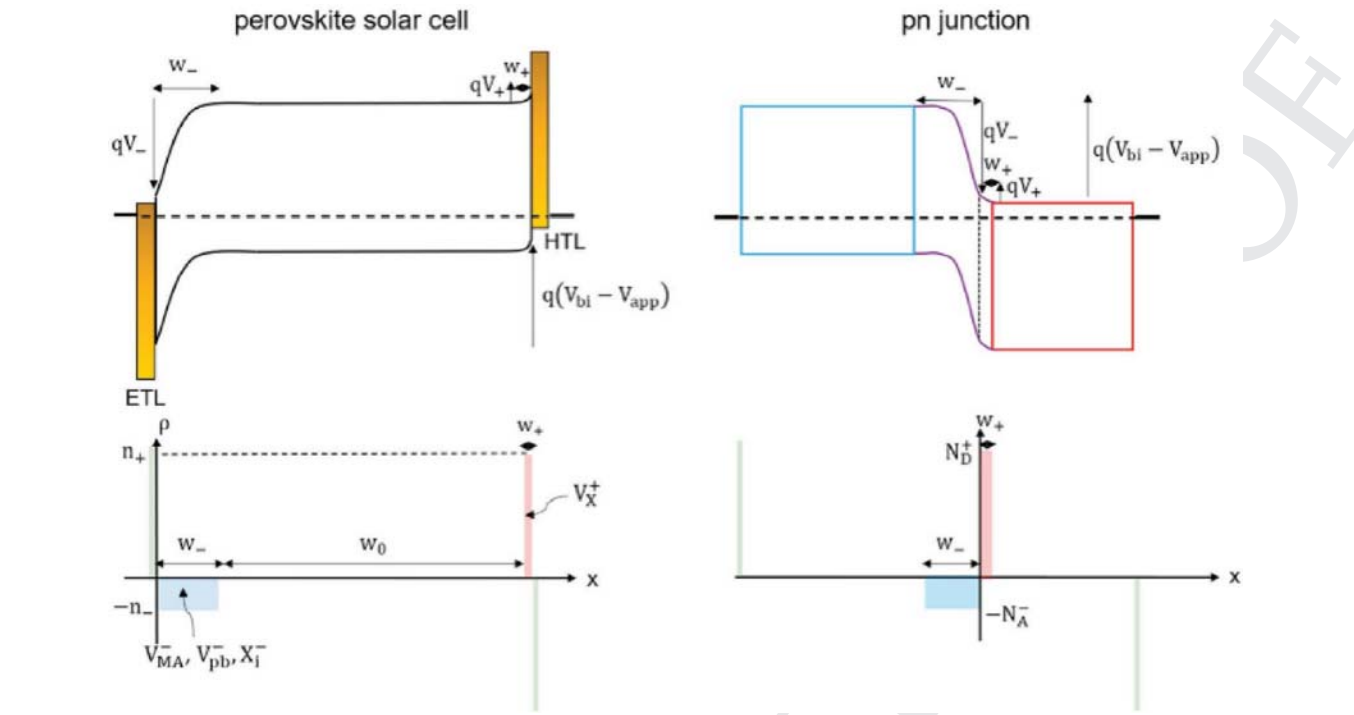

Figure 20. Band diagram (top) and charge distribution (bottom) for a perovskite solar cell (left) and standard p–n junction (right). Reproduced with permission.[161] Copyright 2019, Elsevier Publishing.

both, it has become clear they can have a large impact on the optoelectronic properties of the active layer: Miller et al. demonstrated that the Fermi level of the perovskite tends to correlate with that of the substrate,[164] Tirmzi et al. demonstrated that the microwave conductivity of the perovskite varies with the substrate,[165] and Du et al. demonstrated that a thin interlayer of PTAA can be inserted between nickel oxide and the perovskite to obtain a device with higher voltage.[166] On the other hand, transport layers above the perovskite can be chosen to dope or passivate defects on the surface. While reports of doing this intentionally are few and far between, it has become apparent that two of the most successful and widely used contacts have unknowingly done this. Namely, reports have shown that both C_{60},[70] the most commonly used ETL in p–i–n devices, and 4-*tert*-butylpyridine,[167] an additive used in the spiro-OMeTAD layer traditional to n–i–p devices, do just this. Second, it implies surface recombination is most detrimental near the HTL where the band bending from ionic species, and thus carrier selectivity, is smaller in magnitude and width than at the ETL interface. Thus, improvements to the HTL/perovskite interface will reap the largest benefits. Finally, it suggests that the negative effect of surface recombination can be mitigated by minimizing iodide vacancy concentrations such that they have insufficient charge to screen the entire built-in potential, allowing a small electric field to be formed over the bulk of the perovskite. We note that while this may help with current, extraction, charge disassociation, and limiting surface recombination, completely getting rid of mobile ionic species returns the band diagram to that of other semi-conductors. Thus, as perovskites improve in material quality and push toward theoretical efficiency limits, the energy levels of transport layers will have an increasing effect on device performance.

In addition to the above considerations for initial performance, the model has several implications for long-term stability as it suggests the distribution of defects within the active layer can be altered by the choice of selective contacts. More specifically, if halide vacancies move to the perovskite/HTL interface in order to counteract energetic offsets in band alignment, the number of defects required to screen the potential at a given interface should be related to its band offset; perovskites with a large offset at the HTL/perovskite interface should pull a high density of positively charged defects such as iodine vacancies to the interface, leaving behind a high density of negatively charged defects on the ETL side of the device. As a result, devices with a lower built-in voltage will have a lower interfacial concentration of defects when at equilibrium conditions, ceteris paribus. However, this distribution of defects is altered when the device is biased. Reverse biasing the device should increase the potential gradient across the perovskite and therefore the concentration of defects at the interface. Meanwhile, forward biasing the device should cause defects at the interface to be pushed toward the bulk of the perovskite until the applied voltage reaches the sum of the offsets at the two interfaces. At this point iodide vacancies should have entirely moved into the bulk and recombined, forming a spatially uniform material. Going past this point will then apply a voltage across the perovskite in the opposite direction of the built-in voltage, causing charged defects to move to the opposite interface. Combining these observations, the concentration of defects at perovskite interfaces should be dictated by the

© 2020 WILEY-VCH Verlag GmbH & Co. KGaA, Weinheim

Pursuant to the DOE Public Access Plan, this document represents the authors' peer-reviewed, accepted manuscript.
The published version of the article is available from the relevant publisher.

built-in voltage (V_{bi}) minus the applied voltage (V_{app}) and the type of defect by the sign of this voltage

$$D_{tot} \approx D(V_{tot}) \approx D(V_{bi} - V_{app}) \tag{18}$$

$$D_{tot} = \pm \frac{1}{4} \frac{\epsilon_0 \epsilon_r V_T}{L_D} \left[\left(1 + 16 \frac{V_{bi} - V_{app}}{V_T} \right)^{\frac{1}{2}} - 1 \right] \tag{19}$$

where ε_0 is permittivity of free space, ε_r is the relative permittivity of the perovskite, V_T is the thermal voltage, and L_D is the accumulation region width. We note that while changes in ionic concentration are not expected to alter the thermodynamics of existing degradation mechanisms, which are dependent on the voltage at a given interface and not the density of carriers, they can alter equilibrium concentrations and reaction rates (kinetics). It follows that at every bias there is a list of degradation mechanisms that the perovskite can undergo which are dictated by voltage and available chemical species, and a rate for each mechanism that is dictated by concentration. As a result, the considerations that must be taken at a given interface change depending on defect concentrations, contact materials, and applied bias. Worse yet, if these reactions modify the interface, it is dominant degradation pathways may change.

With a better understanding of what degradation mechanisms are for each transport layer/perovskite/transport layer stack, one could and should design interfaces and interlayers to avoid certain reactions. However, to accomplish this, the community must first establish the additional degradation mechanisms enabled by other device layers. Although this will be highly dependent on device architecture and is poorly understood to date, there are several concerns that plague common architectures in literature. These reactions are of the photooxidative, diffusive, and thermally induced nature.

5.2. Photooxidative Reactions

Reactions between a transport layer and atmospheric oxygen or other layers in the device can lead to changes in its oxidation state. Depending on the transport layer, this can cause changes in conductivity, transparency, structure, and/or band alignment with other layers. Although the former two are unlikely to have a major impact on device performance due to the small thickness of transport layers (10–20 nm), the latter can alter the selective properties of the transport layers and defect distribution within the perovskite. While small changes in these parameters may initially have little to no effect on device performance, the reactions and their effects can be perturbative and not self-limiting. This would result in moderate changes that reduce FF, likely by increasing series resistance, decreasing shunt resistance, and/or reducing the built-in field across the perovskite. Furthermore, if these changes become large enough, they could drastically hinder extraction, forcing free carriers to spend significantly more time at the interface where recombination is most prevalent. Depending on the barrier to extraction and defect density at that interface, this could result in losses to V_{oc}, J_{sc}, FF, and/or the diodic behavior of the device.

In addition to oxidizing or reducing the transport layer, these reactions can also lead to the reduction or oxidation of the perovskite. For example, when excited by UV light, metal oxides (TiO_x, SnO_x, NiO_x) are well known to form reactive superoxides that can catalyze the oxidation of most organic materials in contact with them, including perovskites. This has been realized by several groups, including Ito and co-workers, who found that 12 h of UV light exposure entirely converts $MAPbI_3$ on TiO_x to PbI_2.[168] To explain this, they proposed the following reaction

$$2I^- \rightleftharpoons I_2 + 2e^- \tag{20}$$

$$3CH_3NH_3^+ \rightleftharpoons 3CH_3NH_2 + 3H^+ \tag{21}$$

$$I^- + I_2 + 3H^+ + 2e^- \rightleftharpoons 3HI \tag{22}$$

First, TiO_x extracts electrons from iodine, deconstructing methylammonium iodide to form neutral iodine and a methylammonium cation. Then, an equilibrium is formed between the methylammonium cation and its deprotonated form, methylamine. Although the left-hand-side of this equilibrium should be favored due to its high acid dissociation constant (pK_a of 10.8), continual evaporation of methylamine and consumption of protons in the successive reaction cause it to move forward via Le Chatelier's principle.[169] Finally, electrons from the TiO_x are reinjected into the perovskite, allowing the iodine generated in step 1 to bond to the protons generated in step 2 and a negative iodide ion from the perovskite to form hydroiodic acid, which quickly evaporates away. Cumulatively, these reactions break apart methylammonium into gaseous compounds, leaving behind PbI_2 at the interface which hinders charge extraction and therefore reduces J_{sc} and FF.[170] Studies have shown that this can be mitigated by modifying the interface with an inorganic perovskite (CsBr[171]), placing an electron acceptor (C_{60}[172]), blocker (Sb_2S_3[168]), or insulator (AlO_x[173]) between TiO_x and the perovskite, or replacing the TiO_x with a less photocatalytic oxide (SnO_x[170]).

5.3. Diffusive Reactions

Additionally, the ionic nature of perovskites allows ions to easily diffuse into or out of it and react. While reactions of this nature have the potential to degrade any layer, those between the perovskite and top metal contact cause catastrophic device degradation across a variety of metals, cell architectures, and degradation testing parameters due to the propensity of almost all metals to react with halide and/or halogen species. Studies detailing these reactions suggest that they occur through three separate, but connected, mechanisms.

First, numerous stressors including light, temperature, humidity, and electrical bias can create halide vacancy/interstitial pairs and other volatile organohalide species that diffuse through the top transport layer and react with the metal contact, both corroding the metal and causing an organohalide deficiency in the perovskite. For example, Kato et al. demonstrated that dark aging of a FTO/TiO_x/$MAPbI_3$/Spiro-OMeTAD/Ag device in air for three weeks results in the

UNCORRECTED PROOF

© 2020 WILEY-VCH Verlag GmbH & Co. KGaA, Weinheim

Pursuant to the DOE Public Access Plan, this document represents the authors' peer-reviewed, accepted manuscript.
The published version of the article is available from the relevant publisher.

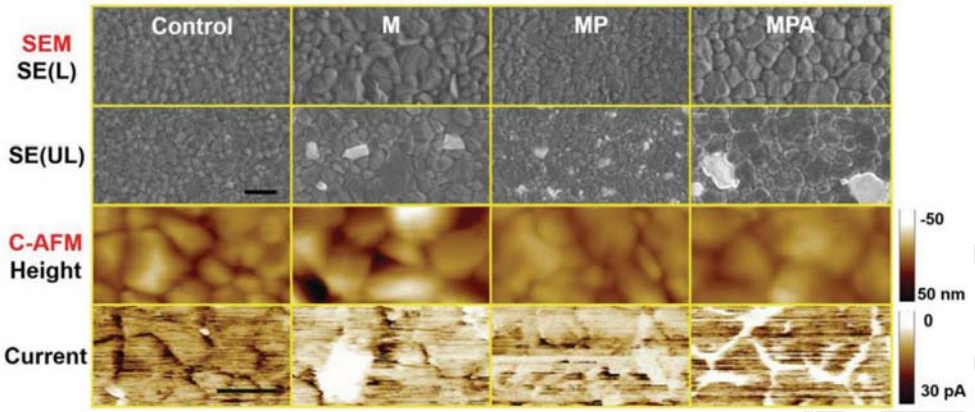

Figure 21. Scanning electron microscope and C-AFM images of $MAPbI_3$ films in FTO/NiO_x/$MAPbI_3$ (control), FTO/NiO_x/$MAPbI_3$ (M), FTO/NiO_x/$MAPbI_3$/PCBM (MP), FTO/NiO_x/$MAPbI_3$/PCBM/Ag (MPA) stacks. M, MP, and MPA are aged at 100 °C for 24h. Reproduced with permission.[175] Copyright 2017, Wiley-VCH.

diffusion of organohalide species to the Ag contact where they convert approximately a fourth of the Ag to AgI, a yellowish wide-bandgap insulating semiconductor that destroys the conductivity of the electrode.[174] Similarly, Li et al. demonstrated that dark aging of a FTO/NiO_x/$MAPbI_3$/PCBM/Ag device in N_2 at 85 °C results in analogous degradation.[175] Moreover, they showed that the presence of Ag creates a sink for the volatilized species, causing accelerated loss of organohalide species at grain domains (as shown by the scanning electron microscope and C-AFM scans in **Figure 21**) that in turn lead to drastically reduced carrier lifetimes and extraction rates.

Second, temperatures in the upper range of standard testing conditions can cause metal to diffuse from the electrode through the top transport layer and into the perovskite, creating species that can hinder charge transport and/or serve as centers for nonradiative recombination. In fact, Domanski et al. demonstrated such diffusion occurs in as little as 15 h for FTO/TiO_x/FAMACsPbIBr/spiro-OMeTAD/Au devices aged in N_2 when temperatures are increased from 20 to 70 °C, as shown by the time-of-flight secondary ion mass spectrometry (ToF-SIMS) in **Figure 22**. Moreover, they reveal that this diffusion of ions is sufficient to lead to a concentration of Au atoms in the perovskite that is only three orders of magnitude less than that of lead (8.9×10^{14} compared to 10^{17} cm^{-2}).[176] Similarly, Boyd et al. demonstrated that Indium doped tin oxide (ITO)/NiO_x/perovskite/C_{60}/SnO_x/ITO/Ag devices with $FA_{0.83}Cs_{0.17}Pb(I_{0.83}Br_{0.17})_3$, $FA_{0.75}Cs_{0.25}Sn_{0.5}Pb_{0.5}I_3$, and $MAPbI_3$ perovskites suffer from the same fate at 85 °C, indicating that the degradation seen in Domanski's study does not appear to be specific to the active layer, transport layer, gold, or n–i–p configuration used.[177] To further probe how universal this degradation may be, Ming et al. studied the ability of common metals to form interstitial defects in $MAPbI_3$, the energy levels of those defects, and their ability to diffuse through the lattice.[178] They found that all metals studied besides Mo_i and W_i readily form defects, that all defects besides Cu_i and Ag_i introduce detrimental midgap states, and that Cu_i^+, Ag_i^+, Au_i^+, Co_i^+, Ni_i^+, and Pd_i^+ should readily diffuse through perovskites while Cr_i^+, $Mo_i^{2/3+}$,

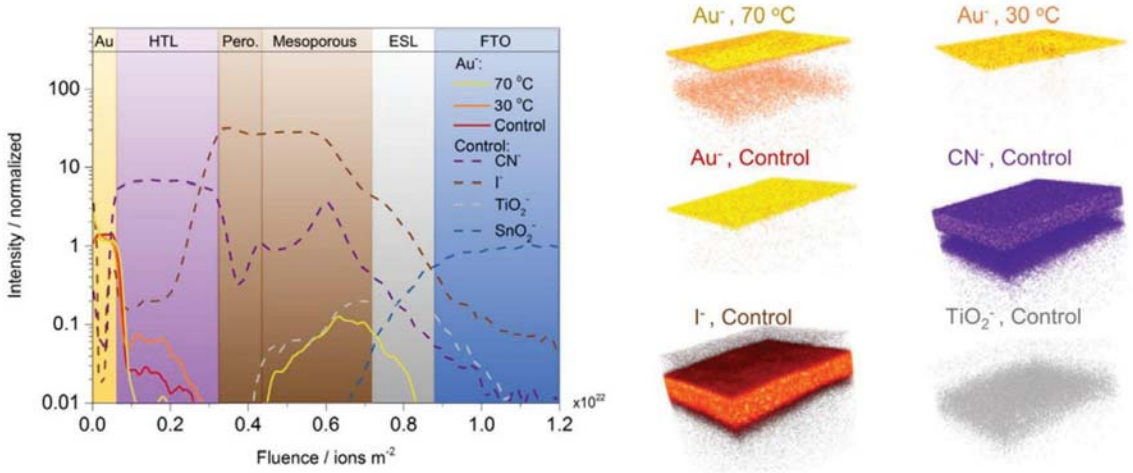

Figure 22. Time-of-flight secondary ion mass spectrometry (TOF-SIMS) depth profile showing diffusion of Au into a FAMACs perovskite after heating at 70 °C in N_2 (left) and corresponding 3D elemental maps for each of the species (right). Reproduced with permission.[176] Copyright 2016, American Chemical Society.

© 2020 WILEY-VCH Verlag GmbH & Co. KGaA, Weinheim

Pursuant to the DOE Public Access Plan, this document represents the authors' peer-reviewed, accepted manuscript. The published version of the article is available from the relevant publisher.

$W_i^{2/3+}$, Co_i^{2+}, Ni_i^{2+}, and Pd_i^{2+} should be largely immobile at room temperature.

Lastly, direct connection between the perovskite and metal contact can lead to the formation of a redox couple between the metal and Pb^{2+} that causes reduction of Pb^{2+} to Pb^0 and accelerated loss of halide species. Zhao et al. have shown that reactions of this nature occur for $MAPbI_3$, $CsPbI_3$, and $CsPbBr_3$ active layers with Ag, Al, Yb, or Cr contacts.[179] Moreover, they demonstrated that the severity of these reactions follows what is expected based on the standard electrochemical potentials of the metals, suggesting that the oxidation of Ag is only enabled by the presence of iodine.

Due to the above reactions catastrophic effect on device performance, significant effort has been made to avoid them. The most obvious method to do so is to utilize alternate contact layers that do not react with halides, such as carbon or transparent conductive oxides (TCOs). However, these materials result in far worse cell performance due to their lower conductivity. Because of these limitations, a variety of barrier layers have been developed to prevent migration of ions between the perovskite and rear metal contact. Cumulatively, these studies have shown that the diffusion of ions, and thus degradation, can be reduced by placing a compact, conformal, and dense material between the top transport layer and metal contact.[177,180–186] However, it is noteworthy this fails to prevent reactions between the top transport layer and perovskite. While reactions of this nature have not been demonstrated to occur under standard operating conditions, heating ITO/NiO_x/MAI and ITO/SnO_x/MAI samples at 120 and 90 °C for 10 min has been demonstrated to generate NiI_2 and SnI_4, respectively.[54] Thus, it is likely that these reactions occur with perovskites and have just not been identified yet due to the severity of reactions between the top transport layer and perovskite.

5.4. Thermally Induced Reactions

Finally, temperatures in the upper range of standard testing conditions (e.g., 85 °C) have the potential to degrade layers within the PSC besides the perovskite. While this is less of a concern for TCOs, metals, and inorganic transport layers which are generally stable to a couple hundred degrees Celsius, organics often possess much lower thermal decomposition temperatures and/or a glass transition temperature where they undergo a transition from a rigid glassy material to a soft material. When this temperature is passed, selective transport properties rapidly change, leading to abrupt deterioration of device performance through losses in J_{sc} and FF. For example, spiro-OMeTAD has a glass transition temperature of 124 °C that reduces significantly when doped with Li-TFSI and 4TBP.[162,187] As a result, devices employing it quickly fail at higher temperatures.[162,170]

Thus, one would expect an increase in temperature below any phase transitions to initiate no new degradation mechanisms while increasing the rate of chemical reactions exponentially and mass transport linearly. However, the effect of temperature on PSC degradation is not so straightforward. This is because, in addition to accelerating various degradation mechanism kinetics, altering the temperature of the perovskite changes strain. In short, with changing temperature, layers in the device want to expand/contract at different rates determined by their coefficient of thermal expansion (CTE). However, since successive layers are bound to each other, not all layers can expand/contract at their desired rate. This mismatch in expansion/contraction leads to strain within one or more of the device layers. While the effect of strain over the range of standard testing conditions appears to be minimal for most layers in the device stack, evidence suggests that the strain resulting from the mismatch in CTE between the perovskite and its substrate impacts the intrinsic stability of the perovskite. More specifically, Zhao et al. have shown that when a perovskite on a ITO/glass substrate is cooled from its processing temperature to room temperature, its desire to shrink more than the substrate induces a tensile strain in the in-plane direction that is compensated for by a contraction in the out-of-plane direction, regardless of the perovskite composition and deposition method utilized.[188] Then, by depositing the perovskite on flexible substrates and bending them concave, to reduce strain, and convex, to increase strain, they show that an increase in strain leads to a reduction in the activation energy for ion migration and accelerated degradation in light, as shown by the images of films and X-ray diffraction (XRD) in **Figure 23**. Finally, they show that due to the origins of this strain, it can be alleviated by either decreasing the mismatch in CTE between the perovskite and substrate or the difference in temperature between fabrication and operation. Others have reported similar results.[189,190]

5.5. State-of-the-Art Device Stability

As discussed in the preceding sections, incorporating the variety of active layers available into the myriad of device architectures utilized allows for the possibility of numerous degradation mechanisms, both at the material and device level. Depending on the specific testing conditions employed, any number of these mechanisms can dominate degradation. As a result, summarizing the countless number of reports on stability is out of the scope of this work (for a discussion on state-of-the-art device stability look here).[191,192] Instead, the goal of this section is to elaborate on how building a mechanistic understanding of degradation allows for the methodical tailoring of active layers, interfaces, and barrier layers to achieve state-of-the-art device stability. To do this, we will first cover the advancements that have led to state-of-the-art operational stability. These advancements iteratively address each of the degradation mechanisms discussed in the preceding sections such that their effect is collectively minimized. However, they may not utilize the best possible solution. As a result, we will follow this discussion with a review of high efficiency devices that have made improvements to one or more of the layers to improve stability.

Due to the volatility of $MAPbI_3$, initial efforts focused on increasing device stability by creating perovskite layers that were more stable to the intrinsic and extrinsic material degradation mechanisms covered in Sections 2 and 3. One of the most notable advancements in this regard came from Saliba et al., who showed that alloying cesium into the A-site of FAMA-based perovskites provided significant improvements to performance, reproducibility, and efficiency.[19] At the optimal concentration,

UNCORRECTED PROOF

© 2020 WILEY-VCH Verlag GmbH & Co. KGaA, Weinheim

Pursuant to the DOE Public Access Plan, this document represents the authors' peer-reviewed, accepted manuscript.
The published version of the article is available from the relevant publisher.

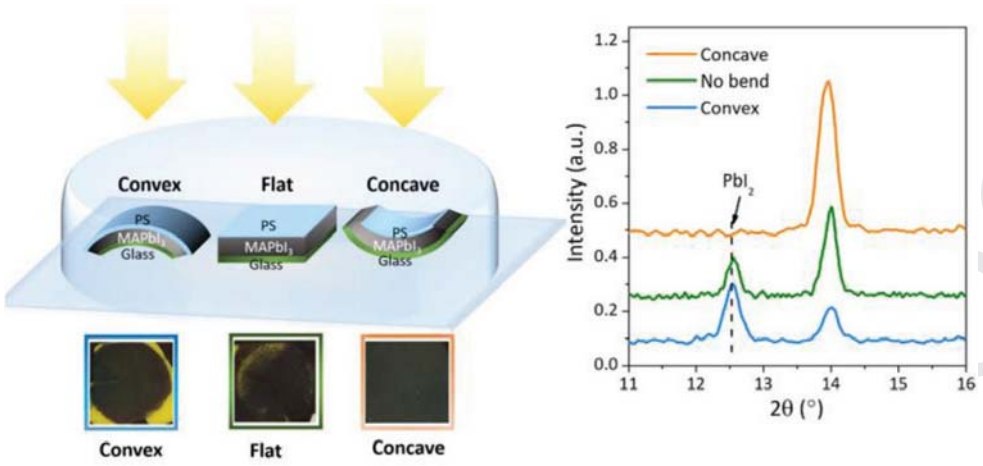

Figure 23. Experimental setup used to induce three different strains in perovskite films (top left), pictures of the films after 500 h illumination (bottom left), and out of plane XRD patterns of the same films (right). Reproduced under the terms of the Creative Commons 4.0 License.[188] Copyright 2017, American Association for the Advancements of Science (AAAS).

the $Cs_{0.05}(MA_{0.17}FA_{0.83})_{0.95}Pb(I_{0.83}Br_{0.17})_3$ films exhibited greater thermal stability to those without cesium, resulting in slower degradation as evidenced by XRD and absorption. Moreover, films with cesium demonstrated remarkably enhanced stability when incorporated into glass/FTO/compact-TiO_x/Li-doped mesoporous TiO_x/perovskite/Spiro-OMeTAD/Au devices; while control devices without cesium quickly decayed from ≈16% to 8% PCE in ≈100 h (in N_2, 25 °C, under illumination, at maximum power point (MPP)), devices employing cesium remained mostly stable after an initial decrease in efficiency from ≈20% to 18%. Despite a remarkable improvement from the control device, these devices still degraded relatively fast due to the device architecture utilized, which failed to address known degradation mechanisms not inherent to the active layer (i.e., those enabled by other layers in the device which were covered earlier in this section). Thus, the stability of these devices can be further enhanced by tailoring interfaces and other layers within the device. For example, in the first demonstration of unencapsulated cells that maintained >90% stability for over 1000 h under operational conditions (light, MPP, ambient), Christians et al. replaced several layers of the commonly used device architecture, Glass/FTO/TiO_x/$(FA_{0.77}MA_{0.16}Cs_{0.05})_{0.97}Pb(I_{0.84}Br_{0.16})_{2.97}$/Spiro-OMeTAD/Au, to enhance stability.[170] First, they removed the standard hygroscopic and pinhole riddled spiro-OMeTAD HTL with mobile LiTFSI dopants in favor of a more chemically inert, conformal, hydrophobic EH44 layer to simultaneously provide a stable interface for extraction and limit moisture ingress. Then, they exchanged the TiO_x ETL for a less photocatalytic SnO_x layer and the back Au contact for a MoO_x/Al contact that had been shown to retard ion migration and associated metal induced degradation. All three of these changes resulted in large improvements to stability, allowing the optimized devices to retain ≈95% of their original efficiency over 1000 h compared to the control devices which degraded to ≈30% of their original efficiency in just 160 h. Results are shown in **Figure 24**. At the time of publication, these results represented a huge breakthrough in stability as they highlighted the ability of interfaces to methodically address degradation mechanisms—namely, those associated with oxygen and moisture ingress, photooxidation, and ionic diffusion. However, despite using the more thermally stable FAMAC-based active layer, these devices still suffered from significant losses in efficiency at higher temperature due to the low glass transition temperature of EH44. In a recent manuscript Schloemer et al. addressed this issue.[162] To do this, they first modified the triarylamine substituents on EH44 to create new molecules and

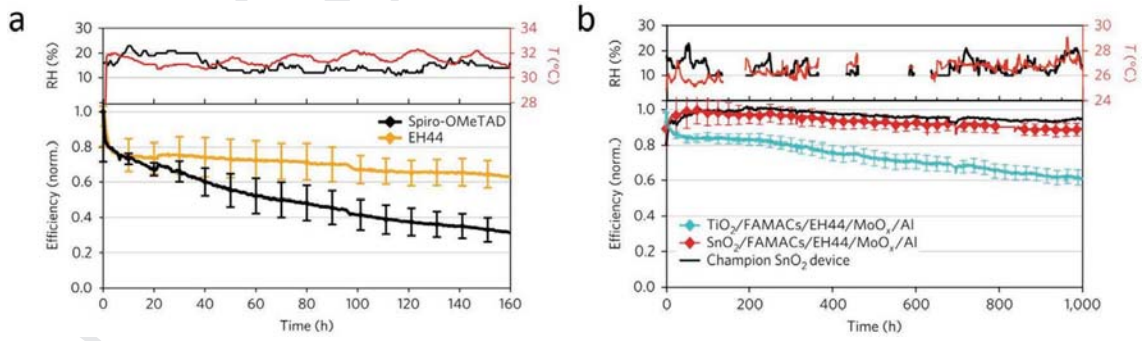

Figure 24. Operational stability of illuminated devices in air at MPP. a) Stability of ITO/TiO_x/FAMACs/HTL/Au devices with spiro-OMeTAD and EH44. b) Stability of ITO/ETL/FAMACs/EH44/MoO_x/Al devices employing TiO_x and SnO_x. Reproduced with permission.[170] Copyright 2018, Nature Publishing Group.

© 2020 WILEY-VCH Verlag GmbH & Co. KGaA, Weinheim

Pursuant to the DOE Public Access Plan, this document represents the authors' peer-reviewed, accepted manuscript. The published version of the article is available from the relevant publisher.

associated dopants. Then, they altered dopant type and concentration for each of the molecules and tested the stability of the optimized HTLs using analogous devices and degradation tests to Christians and co-workers, but at higher temperatures (≈50 °C). Their results show that the newly designed HTLs form substantially more stable devices, retaining 60–70% of their initial PCE over 600 h compared to the control devices which completely degraded in ≈500 h. To the best of our knowledge, these results are the current state-of-the-art in terms of operational stability in ambient conditions, as the modifications made to the device structure collectively address the most severe intrinsic and extrinsic degradation mechanisms at the material and device level. However, due to measurable degradation of device modes, several degradation mechanisms clearly had not been entirely eliminated.

To address these mechanisms, additional improvements must be made in one or more of the layers. The community has done significant work on this front by gauging the stability of devices to some variant of either dark/85 °C/85% RH to improve the robustness of the device to external degradation factors or light in inert atmosphere to enhance the stability of the device under operational conditions assuming perfect encapsulation. Generally, studies of this nature have avoided reinventing the wheel by modifying a particular layer or set of layers within the device while using other components that have shown to be successful. These include: FTO and ITO for the bottom TCO; TiO_x and SnO_x for the bottom ETL; PTAA, NiOx, or Poly-TPD for the bottom HTL; C_{60} derivatives with BCP for the top ETL; spiro-OMeTAD, CuSCN, or P3HT for the top HTL; and some combination of MoO_x or other buffer layers and Al, Ag, or Au for the top contact. Modifications can be broken up into two categories, those that address inherent instabilities of the active layer, and those that address those of the device stack.

Improvements to active layer stability can be achieved through alloying or incorporating additives to reduce defect concentrations and/or coat the surfaces of the perovskite with more chemically stable elements (i.e., hydrophobic fullerene end-capped polyethylene glycol).[129] Alloying, which was described in detail earlier, has resulted in three compositions that are generally considered to be the most stable: $FA_aMA_bCs_{1-a-b}Pb(I_xBr_{1-x})_3$, $FA_aCs_{1-a}Pb(I_xBr_{1-x})_3$, and $FA_aCs_{1-a}Pb_{0.60}Sn_{0.40}I_3$. On the other hand, additives have resulted in hundreds of reports that gauge the effectiveness of their specific additive with the use of a control device. As the mechanistic effect of each of these additives was discussed earlier, the following discussion will focus solely on reporting the stability results of devices that incorporate additives to achieve high efficiency (>20%) and good stability. Tavakoli et al. added the ammonium salt MACl to the perovskite of an FTO/compact-TiO_x/SnO_x/$(FA_{0.85}MA_{0.15})_{0.95}Cs_{0.05}Pb(I_{0.9}Br_{0.1})_3$/spiro-OMeTAD/Au architecture. The 21.6% efficient devices exhibited better stability than the control, maintaining 98% of their original efficiency over 60 days shelf life testing, as opposed to the control which maintained 94%. Additionally, devices were shown to be stable under illumination, retaining 96%, 90%, and 85% of their initial PCE over 500 h of illumination at V_{oc} and 20, 50, and 65 °C, respectively.[77] Li et al. introduced the metal cation NaF into the perovskite of an FTO/SnO_x/$(Cs_{0.05}FA_{0.54}MA_{0.41})Pb(I_{0.98}Br_{0.02})_3$/spiro-OMeTAD/Au device stack.[157] The resulting 21.46% efficient devices retained 90% of their original PCE over 6000 h of shelf-life testing at 25–40 °C and 25–45% RH, 90% over 1000 h at 85 °C, 95% over 1000 h of illumination at V_{oc}, and 90% over 1000 h under illumination at MPP. Control devices were much less stable, decreasing to 50%, 50%, 70%, and just 40% in 600 h under the same conditions. Wang et al. added europium acetylacetonate $Eu(acac)_3$ into the precursor solution of a FAMAC-based perovskite to create Eu^{3+}–Eu^{2+} metal cation redox-pairs.[102] When incorporated into FTO/SnO_x/FAMACsPbIBr/spiro-OMeTAD/Au architectures, the 21.52% efficient devices retained over 90% of their original PCE over 8000 h of shelf-life testing, 90% over 1000 h under illumination at V_{oc}, and 91% over 500 h under illumination at MPP. These devices showed significantly improved stability to the control devices which degraded to just 10% and 50% under the first two conditions, respectively. Zhang et al. investigated the effect of adding the fullerene derivatives α-bis-PCBM and regular PCBM to the antisolvent of an FTO/compact-TiO_x/mesporous-TiO_x/$FA_{0.85}MA_{0.15}Pb(I_{0.85}Br_{0.15})_3$/spiro-OMeTAD/Au device stack.[128] α-bis-PCBM was found to exhibit improved stability to both PCBM and controls not using PCBM, maintaining 90% of their original PCE over 46 days storage in ambient conditions ("room temperature" and 45% RH) and 96% over 600 h of MPP tracking under illumination. Control devices using PCBM degraded to 70% and 50% under the same conditions while control devices using no PCBM degraded to 45% and 0% in just 250 h, respectively. Finally, Bai et al. introduced the ionic liquid $BMIMBF_4$ into the perovskite of an FTO/NiO_x/$(FA_{0.83}MA_{0.17})_{0.95}Cs_{0.05}Pb(I_{0.9}Br_{0.1})_3$/PCBM/BCP/Cr/$Cr_2O_3$/Au architecture, yielding 20% efficient devices that maintained 86% of their original efficiency over 100 h of aging at 40–50% RH/60–65 °C and 95% over 1800 h under illumination at V_{oc} and 70–75 °C.[154] Controls without the IL additive degraded fully in just 100 h and to 60% of their initial PCE under the same conditions. Collectively, these results show that optimization of the defect structure and surfaces in perovskites can lead to further stabilization of the active layer, and thus the device. However, interfaces must be addressed as well.

Several reports have shown that optimizing the transport layers can result in large enhancements to stability. For example, Tan et al. employed a chlorine capping method to TiO_2 to improve perovskite adhesion and suppress the Pb–I antisites that are generally created at the interface in favor of Pb–Cl antisites which have a higher formation energy and shallower transition energies.[193] The resulting 20% efficient ITO/TiO_x/CsFAMAPbIBr/spiro-OMeTAD/Au devices retained 96% of their original PCE over 2000 h of storage in air and 90% over 500 h of UV-free illumination at MPP in N_2, compared to control devices which degraded to ≈40% over 1440 h and 50% over just 2.5 h, respectively. Similarly, Choi et al. modified a SnO_x surface with zwitterion to passivate Pb-I anti-site defects with positively charged atoms in the zwitterion while simultaneously lowering SnO_x's work function and creating a dipole at the interface to improve charge extraction and prohibit the back-transfer of electrons.[194] When coupled with the dopant free HTL asy-PBTBDT, this lead to 20.5% efficient FTO/SnO_x/Zwitterion/$FAMAPbI_{3-x}Br_x$/asy-PBTBDT/Au devices that retained 93% of their initial efficiency over 140 h at 85 °C/85% RH,

© 2020 WILEY-VCH Verlag GmbH & Co. KGaA, Weinheim

Pursuant to the DOE Public Access Plan, this document represents the authors' peer-reviewed, accepted manuscript. The published version of the article is available from the relevant publisher.

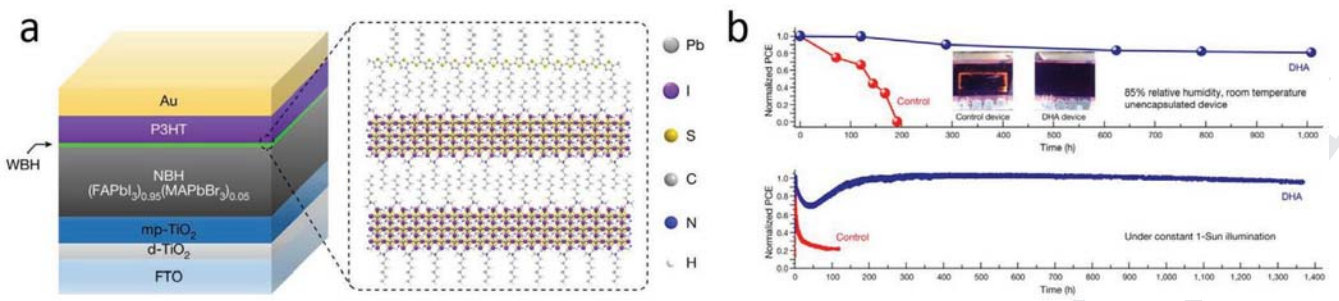

Figure 25. a) Device stack and interactions between wide-bandgap perovskite and P3HT. b) Stability of unencapsulated devices with and without wide-bandgap layer under 85% RH at room temperature (top) and encapsulated devices with and without wide bandgap layer under illumination at MPP in N_2 (bottom). Reproduced with permission.[78] Copyright 2019, Nature Publishing Group.

compared to devices with no zwitterions that retained 82%, and devices with no zwitterions and spiro-OMeTAD as the HTL which retained 70%. In addition to modifications to the ETL, modifications can be made to the HTL to increase stability. For example, Jung et al. incorporated *n*-hexyl trimethyl ammonium bromide into a post treatment for the perovskite of a FTO/compact-TiO_x/mesoporous-TiO_x/$(FAPbI_3)_{.95}(MAPbBr_3)_{.05}$/P3HT/Au device to create a wide-bandgap interlayer between the perovskite and HTL.[78] This wide-bandgap layer was suggested to passivate defects on the surface while simultaneously providing alkyl chains for the P3HT to template off, resulting in orientated P3HT and thus much better mobility due to strong π–π interactions. Devices employing this layer generated substantially higher PCEs of 22.7% rather than 13.8% as well as improved stability, retaining 80% of their initial PCE over 1000 h at 85% RH / room temperature and 95% over 1370 h encapsulated under illumination at MPP in N_2, compared to control devices which degraded to 0% over 200 h and 20% over 100 h, respectively. The device structure, wide-bandgap layer-P3HT interaction, and stability results are shown in **Figure 25**. Cumulatively, these results highlight the importance of modifying charge extracting interfaces on stability.

However, when these charge extracting interfaces are above the perovskite, they must also be stable to the metal interface, provide a barrier to external factors, and block/hinder metal and halide diffusion—something that spiro-OMeTAD does not. To achieve this, Arora et al. employed inorganic CuSCN as the HTL in FTO/TiO_2/$CsFAMAPbI_{3-x}Br_x$/CUSCN/Au devices due to its cheap price, high hole mobility, well-aligned work function, and ability to form a compact uniform and pinhole free layer.[195] When coated with PMAA, these 20.4% devices had far improved stability in dark/air at 85 °C, maintaining 85% of their original PCE over 1000 h compared to the control with Spiro-OMeTAD which degraded to 60%, signifying that they were better at blocking ion diffusion. However, when illuminated and put under bias, devices quickly degraded due to an interaction between the CuSCN and Au. To alleviate this, they employed a reduced graphene oxide layer between the two that blocked the reaction, allowing devices to retain over 95% of their initial PCE over 100 h under illumination at MPP in N_2 at 60 °C, compared to control devices which only retained 90%.

Given the reactivity of the metal contact, others have left the perovskite interfaces alone and instead elected to optimize the top transport layer/metal interface in order to hinder diffusion. For example, Hou et al. employed such a strategy, using a Ta-WO_x interlayer to form a ITO/C_{60}-SAM/SnO_x/PCBM/$FA_{0.83}MA_{0.17}Pb_{1.1}Br_{0.5}I_{2.8}$/PDCBT/Ta-$WO_x$/Au device.[196] In said study, incorporation of the layer was found to dope the top of the HTL, improving electron transfer between it and the metal contact while also providing a barrier for Au diffusion. As a result, the fabricated 21.2% efficient devices exhibited significantly enhanced stability under illumination at V_{oc} in N_2, maintaining 95% of their initial PCE over 1000 h when control devices finished with spiro-OMeTAD/MoO_x/Au and PDCBT/MoO_x/Au degraded to ≈50% in just 200 h. To achieve a similar effect, Wu et al. employed a bismuth interlayer between the BCP and Ag of FTO/Li^+-doped $NiMgO_x$/perovskite/PCBM/BCP/Ag devices with FAMACs- and MA-based perovskites.[183] The bismuth layer was found to drastically improve stability by protecting the diffusion of ions out of and into the perovskite while still maintaining ohmic contact between the PCBM/BCP and Ag layers due to its properly matched work function with Ag (4.25 and 4.3 eV, respectively) and similar conductivity to TCOs. This effect and the resulting stability of devices are shown in **Figure 26**. As can be seen, devices employing the MAFAC-based perovskite retained 95% of their original efficiency over 500 h in the dark at 85 °C in air and 97% under illumination near MPP in N_2 at 45 °C, while devices employing $MAPbI_3$ with a bismuth layer retained 87% and 91% under the same conditions, and control devices employing $MAPbI_3$ without the bismuth interlayer retained 42% and 27%, respectively. Other groups have reported similar results, albeit with lower efficiencies. Boyd et al. reported ITO/NiO_x/$MAPbI_3$/C_{60}/Spun-coat-PCBM/SnO_x/ITO/Ag devices that maintained ≈100% of their original PCE over 1000 h at 85 °C in the dark and N_2,[177] Chen et al. reported ITO/NiO_x/$MAPbI_3$/PCBM/methyl acetylacetonate/Ag devices that retained 87% over 1000 h illumination at V_{oc} in N_2,[184] Bi et al. reported FTO/$NiMgLiO_x$/$MAPbI_3$/graphene doped PCBM/Carbon quantum dots/Ag devices that maintained 88% over 1000 h under illumination at V_{oc} when encapsulated and 98% over 500 h at 85 °C in N_2 when not encapsulated,[185] Chen et al. reported FTO/$NiMgLiO_x$/$MAPbI_3$/PCBM/$TiNbO_x$/Ag devices that maintained 90% over 1000 h illumination at V_{oc} in N_2, Fang et al. reported FTO/$NiMgLiO_x$/$MAPbI_3$/PCBM/cerium oxide/ag devices that maintained 90% over 200 h under illumination at MPP in air and 30% RH,[186] etc. As can be seen, the variety and effectiveness of interfacial layers is broad, but clearly incorporating buffer layers is crucial

© 2020 WILEY-VCH Verlag GmbH & Co. KGaA, Weinheim

Pursuant to the DOE Public Access Plan, this document represents the authors' peer-reviewed, accepted manuscript. The published version of the article is available from the relevant publisher.

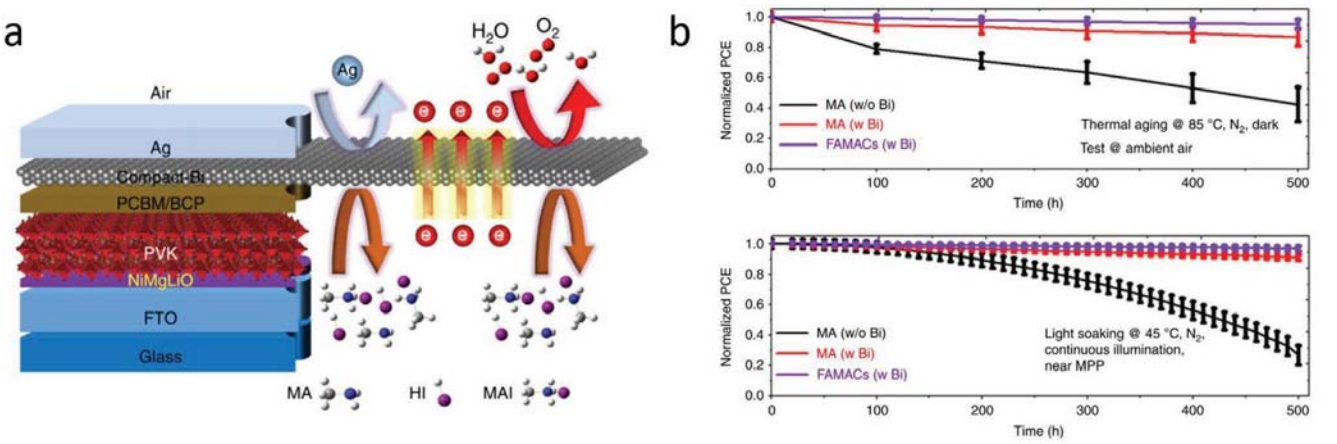

Figure 26. a) Device structure and illustration of the blocking properties of the bismuth interlayer. b) Stability of devices at 85 °C in N_2 and dark (top) and under illumination near MPP at 45 °C in N_2 (bottom). Reproduced under the terms of the Creative Commons 4.0 License.[183] Copyright 2019, Nature Publishing Group,

for long-term PSC stability. While the above discussion is just a small fragment of the devices reported in literature, they highlight that the communities mechanistic understanding of degradation is starting to lead to improvements that have the potential to result in stable and efficient devices.

6. Beyond Devices

6.1. From Device to Module

Once stable and efficient device architectures are identified, the community must overcome the final pillar for commercialization: stability at scale. Moving from the previously discussed research-scale devices to large area modules creates several additional materials and processing challenges to be overcome. The first complication is that while small-area devices can be easily fabricated using spin coating, the technique does not scale to large areas. Thus, recipes must be moved to deposition methods that are appropriate for large area, such as slot-die coating, blade coating, gravure printing, screen printing, and spray coating.[74] However, many procedures for spin coating do not easily translate their good performance to these processes because of wetting issues and "anti-solvent" crystallization treatments that are challenging to implement on a large scale due to different drying dynamics. Consequently, new inks must be developed that are conducive to these large-area deposition methods. Once developed, these inks must be applied uniformly at scale while avoiding macroscopic defects, such as pinholes, that can diminish the performance of the entire module and facilitate degradation. Dealing with this defect propagation will be a challenge, even if vapor phase deposition processes are employed.[197]

Assuming large area and uniform coating of all layers in the device stack is achieved, the next hurdle to overcome is the high series resistance that results from the high sheet resistance TCO in a meter-wide cell. The most common way to do this at the module level is to divide the film into many narrow (≈5 mm wide) cells by using three sets of parallel scribe lines that cause the top low-sheet resistance metal contact of one cell to connect to the bottom contact of the adjacent cell, adjoining cells in series. This transforms the cell shape to have negligible series resistance from the TCO due to the short distance the current must travel to the low resistance back contact. While these scribes are an elegant way to connect individual cells in series, they have both explicit and implicit consequences to the performance and stability of the resulting module.[74] First, the area taken by the interconnect no longer generates power, causing the active area of the module to be less than the module area, reducing total anticipated power production. To minimize this effect, scribes are placed as close together as possible. Second, the P2 scribe exposes the perovskite such that the top (metal) contact directly touches the perovskite absorber, and thus introduces a new interface that can precipitate deleterious reaction pathways if not controlled. Third, the P3 scribe leaves an opening in the material and may alter layers within the device (i.e., laser scribing creates a heat effected zone which can volatilize species[198] while mechanical scribing may result in tearing of one or more layers).[199] As appropriately designed contacts serve as an effective encapsulate for the PSC absorber, these regions open an avenue from the environment to the exposed absorber as well as other interfaces unless additional measures are taken. A schematic of the P1, P2, and P3 scribes and consequences are illustrated in **Figure 27**. It is noteworthy that in addition to these well-known mechanisms, the ionic diffusion in PSCs could cause details of the module current pathway and device layout to create additional issues within the module that are distinct from cells. Taken together, these additional scribe-induced interfaces and pathways, if not controlled, are expected to enable degradation. Indeed, many modules have degradation that initiates at the interconnect and spreads,[200] as will be discussed in the next subsection. As a result, these degradation pathways must be addressed.

Once addressed, the next set of challenges, or in this case opportunities, comes from packaging the module. For packaging, three classes of materials must be considered: front/back-sheets, edge-seals, and encapsulants. A more in-depth discussion on packaging requirements can be found here.[201]

© 2020 WILEY-VCH Verlag GmbH & Co. KGaA, Weinheim

UNCORRECTED PROOF

Pursuant to the DOE Public Access Plan, this document represents the authors' peer-reviewed, accepted manuscript. The published version of the article is available from the relevant publisher.

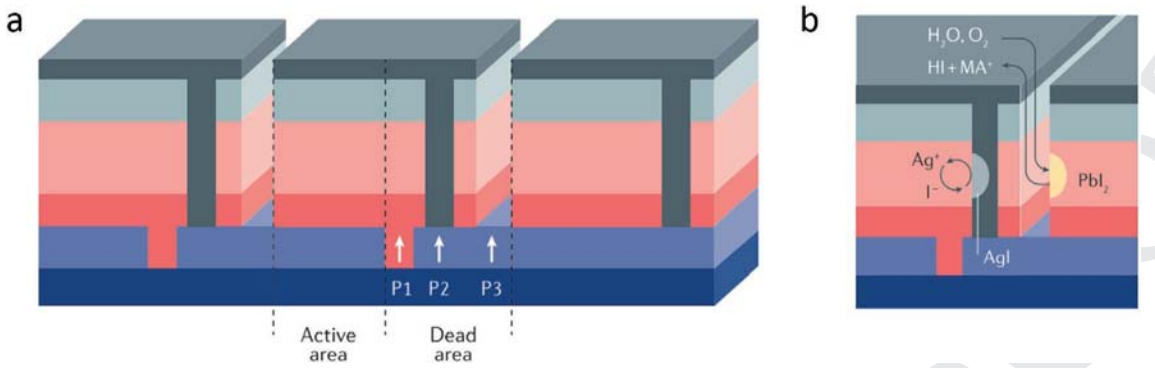

Figure 27. Perovskite module. a) Standard module layout displaying the P1, P2, and P3 scribe lines and resulting dead area as well as the substrate in dark blue, bottom contact in light blue, bottom transport layer in red, perovskite in pink, top transport layer in light grey, and top contact in dark grey. b) Additional degradation mechanisms that result from the scribes with a Ag based electrode. Reproduced with permission.[74] Copyright 2018, Nature Publishing Group.

Typical front/back-sheets include glass, flexible barriers, and breathable back-sheets. Si and polycrystalline thin films have taken somewhat divergent approaches to packaging. While all packages prevent liquid water ingress, moisture permeable back-sheets allow encapsulated Si modules to equilibrate with the ambient environment. On the other hand, thin-film modules rely on glass or high moisture barriers and edge-seals to prevent moisture ingress. While there is no substitute for hardening cell architectures to extrinsic stresses like moisture, barriers will likely be required, although to what level is still unknown.

The most commonly used edge-seal material, desiccant-filled poly isobutylene (PIB) requires an edge perimeter of ≈1 cm to keep out moisture in the most humid environments for 25 years.[202] Generally, this thixotropic material is processed at ≈140 °C to allow it to soften and flow, however, pressure/time can be substituted for temperature to reduce thermal budget. While existing photovoltaic players handle it in "tape" form with well-defined thickness, heated drums of PIB can also dispense it as a viscous liquid. Besides PIB, laser-welded glass frit is the most likely alternate edge-seal candidate, although it is still more of an experimental rather than commercially deployed option, with its advantages being true hermiticity and challenges processing and potential fragility.

"Encapsulant" means something different for the cell and module communities. The cell community use it to mean "moisture barrier," whereas the module community uses it to describe (permeable) materials that literally encase the cell. The most common module-level encapsulants are ethylene-vinyl acetate (EVA), polyolefins, silicones, and ionomers (e.g., Surlyn), although cell-level studies have also experimented with a variety overcoats including epoxies (photocurable, thermal, and multipart),[203,204] poly-methylmethacrylate,[205] polyurethane,[206] fluoropolymer,[207] and inorganic barrier layers.[208] Si and polycrystalline thin films usually use EVA or polyolefins—processed at ≈140 °C—which not all perovskite architectures can withstand. In addition to temperature, chemical byproducts/interactions can be a concern. While a limited number of studies have been published comparing encapsulants, a low elastic modulus has been identified as one desirable property such that encapsulated cells do not delaminate/fracture upon thermal cycling, making EVA and some polyolefins plausible candidates.[209] Choosing inert/noninteracting materials is another consideration that might be relaxed with certain overcoats. There have been multiple proposals to generate overcoats from ALD,[208,210] plasma,[211–213] and solution processes.[205] With good barrier properties, these also have the potential to relax cost constraints on front/back-sheets—some enable cells to withstand liquid water for minutes to hours. While limiting moisture and oxygen is important for other technologies, for perovskites there may be an additional/parallel requirement to keep constituents like halides or organic cations inside.

Packaging and their failures may be of general interest to many, but they are often outside the bailiwick of academic and early stage industry entrants. Moreover, packaging adds complexity to device fabrication, especially if a package is designed to isolate the cell from a particular known or hypothesized degradation mechanism. Thus, if PSCs require novel or unproven packaging, it can be difficult to ascertain where failures originate. This can cause tests to be dominated by details of the package, including interactions between the cell and the package and the ability of the package to protect the device from external factors, rather than degradation mechanisms inherent to the architecture.[204,214] However, these tests are critical to assessing real-world degradation as the natural environment is complex with multiple stresses occurring simultaneously and/or sequentially, which has the potential to elucidate mechanisms that might be missed or underestimated otherwise.

Finally, transitioning from individual unpackaged cells to the module level induces some operation challenges such as partial shading, mechanical stresses, and potential induced degradation due to high system voltages. Partial shading can result in hot-spot formation when a shaded cell is forced to pass the current from illuminated series-connected cells. To pass this current, the shaded cell must go into reverse breakdown, which leads to significant dissipation and heating. While non-MPP conditions can harm perovskite cells, preliminary investigations indicate losses from partial shading may be partially recoverable.[215] Next, mechanical stresses due to hail, CTE mismatches between layers, and mechanical loading have been shown to cause delamination in other technologies and will likely be a problem for perovskites due to their weak cohesion

UNCORRECTED PROOF

© 2020 WILEY-VCH Verlag GmbH & Co. KGaA, Weinheim

Pursuant to the DOE Public Access Plan, this document represents the authors' peer-reviewed, accepted manuscript.
The published version of the article is available from the relevant publisher.

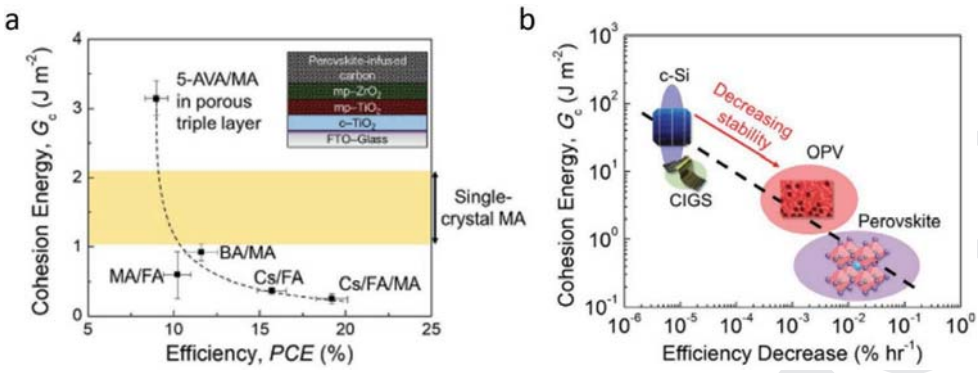

Figure 28. a) Cohesion energy of common perovskite A-site combinations as a function of PCE. b) Cohesion energy of various photovoltaic technologies versus stability. Reproduced with permission.[216] Copyright 2018, Wiley-VCH.

energy; this has led to concern that cells/modules may require careful design to survive these stresses (**Figure 28**).[216,217] Third, potential induced degradation (PID) can result from encapsulants, system technology, and grounding due to the high voltages that serially connected modules reach.[218] However, it is presently unknown how susceptible perovskites will be to PID.

6.2. State-of-the-Art Modules

While much of the perovskite community has started to shift focus from optimizing device efficiency to stability, only a handful of research groups notably led by large established electronics companies have begun developing modules due the relatively nascent nature of the perovskite technology and the increase in technical sophistication associated with the module fabrication process. As the perovskite field begins to focus on larger scale fabrication and integrating small lab-scale device improvements into the module-space, three key areas must be addressed simultaneously. Namely, reducing the losses in PCE that arise from interconnecting cells and converting established spin-coating recipes to scalable deposition methods; increasing module area while maintaining uniform, defect-free films; and characterizing, understanding, and improving module stability. However, gauging the importance of developments across modules is complicated by how processes at lab-scale are translated to large volume production. This can lead to the conflation of instabilities that arise from process imperfections with those that are more intrinsic but may not be primary drivers of degradation at the cell level. The following section aims to summarize several of the more noteworthy publications pertaining to modules, first reviewing state-of-the-art module efficiencies and then moving on to stability.

The efficiency of perovskite modules is substantially lower than that of research-scale devices. While the current record for single junction cells is 25.2%,[2] the most efficient module of area greater than 200 cm^2 is just 16.1%.[219] As detailed above, this loss in efficiency of roughly 36% from device to module is partially due to the increased number of interconnects. However, quantifying these inherent engineering losses relative to other losses from defects or process inhomogeneity that result from scaling to a larger area is difficult. One approach to decoupling these factors is to examine the change in module efficiency as a function of area and compare these losses to those expected from the increase in series resistance. For example, Agresti et al. report efficiency drops from 15.3% to 13.4% when scaling the active area from 82 to 108 cm^2,[220] and microquanta report drops from 17.25%[221] to 14.25%[222] when scaling from 17 to 200 cm^2. Thus, smaller area modules can be expected to have greater efficiency. However, even at relatively small scales, there is still an efficiency loss of roughly 31.5% from the record lab-scale device efficiency to microquanta's record minimodule efficiency. This is much higher than the efficiency losses that other photovoltaic technologies have observed when moving from device to module.[74] As a result, additional loss mechanisms must be at play that act to reduce efficiencies at a rate greater than simply scaling area. Indeed, if one restricts record devices to those which are produced with scalable inks and methods, it can be seen that small area cells of 0.12 cm^2, large area cells of 1.2 cm^2, and modules consisting of four ≈2.25 cm^2 cells perform at relatively similar PCEs of 18.5%,[223] 17.3%,[223] and 17.9%[224] when adjusted by active area. This suggests that naïve application of ink and process technology without regard for the differences in coating techniques produces inhomogeneity or other types of anisotropy which have consequences to performance. Consequently, fabricating high efficiency modules will require significant advancements in ink formulations and processing.

While many research groups do not have the capability to fabricate large scale modules (>200 cm^2), advancements in ink formulations can be made using a benchtop sized blade coater. Moreover, altering inks is likely to change the details of micro- and macro-scale defects, and thus degradation rates. As a result, we believe that comparing the small amount of stability results available among modules of varying size, coating methods, substrates, perovskite compositions, and degradation testing parameters is complex and likely couples multiple variables. Instead, we will focus on characterizing the additional degradation mechanisms that module level processing and production introduce, while assuming the transition from spin-coating to scalable deposition methods is surmountable. These then primarily come from the P2 and P3 scribe lines used to serially connect sub-cells, which create vertically penetrating interfaces that directly expose perovskite to metal and ambient conditions. While the P3 scribe line serves only to break conductivity in the top metal contact from cell to cell and can thus be filled with a

UNCORRECTED PROOF

© 2020 WILEY-VCH Verlag GmbH & Co. KGaA, Weinheim

Pursuant to the DOE Public Access Plan, this document represents the authors' peer-reviewed, accepted manuscript. The published version of the article is available from the relevant publisher.

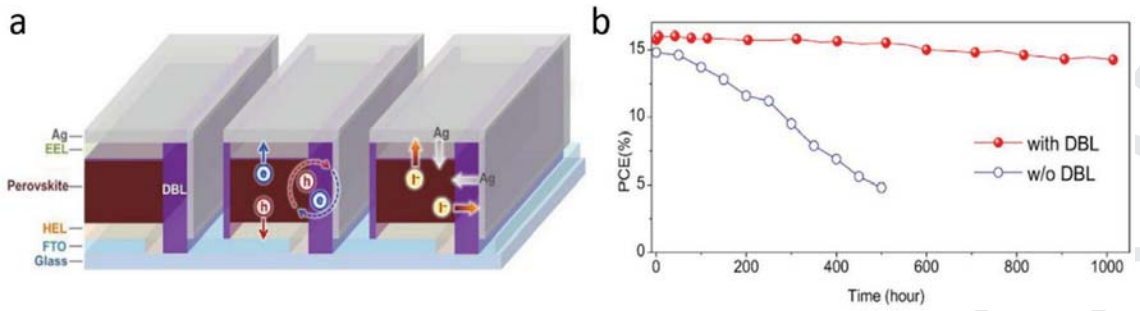

Figure 29. a) Module design employing a diffusion blocking layer. b) Stability of module at 85 °C/85% RH with and without the diffusion blocking layer. Reproduced with permission.[225] Copyright 2019, Elsevier Publishing.

range of insulating materials to prevent atmospheric degradation, the P2 scribe line represents a unique challenge due to its requirement to be conductive yet stable to the perovskite-metal reactions discussed earlier.[200]

One strategy to accomplish this is to use diffusion barrier layers (DBLs) to reduce iodide diffusion into the contact. The effectiveness of several of these layers at blocking ionic diffusion and slowing module degradation was investigated by Bi et al.[225] In short, they used ToF-SIMS, XPS, and scanning electron microscopy with energy dispersive X-rays to calculate the blocking properties of 0D Al_2O_3 nanoparticles, 1D polydimethylsiloxane (PDMS), and 2D graphitic carbon nitride (g-C_3N_4) DBLs in thermally aged Ag/DBL/$MAPbI_3$ stacks. Their results show that while all DBLs resulted in 10^3–10^7 times lower diffusion coefficients, the 2D material had the best blocking properties due to its ability to form a compact, pinhole free layer with channels smaller than the diameter of iodide ions. Then, they investigated the effect of the layer on module stability and efficiency when incorporated at the perovskite/top transport layer and P2 scribe/metal interconnect interfaces as shown in **Figure 29**. Impressively, their results show that doing so both increases the module efficiency from 14.1% to 15.6%, due to the defect passivation of the 2D layer, and stability, due to reduced ionic diffusion. This led to the realization of encapsulated modules that maintained 95% of their original PCE over 1000 h of aging at 85 °C/85% R.H. in dark and 91% at 60 °C/ambient conditions in 1 sun UV-filtered illumination at MPP (Figure 29). These results represent a significant improvement over the control device, which decreased to roughly 40% of its original efficiency over just 500 h in both conditions. Another study by Agresti et al.[220] followed an analogous approach, utilizing functionalized MoS_2 between the HTL and perovskite (but not in the P2 scribe) to prevent ion diffusion. Similarly, they found that doing so resulted in slightly higher PCE and stability, allowing their modified modules to retain 75% of their initial PCE over 1000 h at 65 °C in the dark as opposed to the control, which degraded to less than 50%.

Besides using barrier layers, other potential passivation strategies have been explored. For example, Hong et al. demonstrated that instead of using the P2 trench as the electrical connection between adjacent cells, a forward bias of 3 volts could be applied to the interconnect region to force metal ions (Au or Cu) to migrate between the two electrodes, connecting the cells.[226] However, while this resulted in modules that were shelf-life stable for 400 h in a N_2 environment, exposing them to 85 °C/85% RH or 1-sun illumination at V_{oc} resulted in a quick decay in performance to ≈70% of their original PCE in just 185 h. Another potential solution is to do away with the metal contact in favor of electrodes that are less likely to react. Grancini et al.[227] investigated this approach, fabricating encapsulated HTM-free devices on mesoporous TiO_2 and ZrO_2 with carbon-based electrodes that demonstrated no loss in efficiency over 10 000 h of UV-filtered AM1.5 g illumination at V_{oc} and 55 °C (**Figure 30**).

It should be noted these architectures are distinct from others reported by the community due to the carbon-based

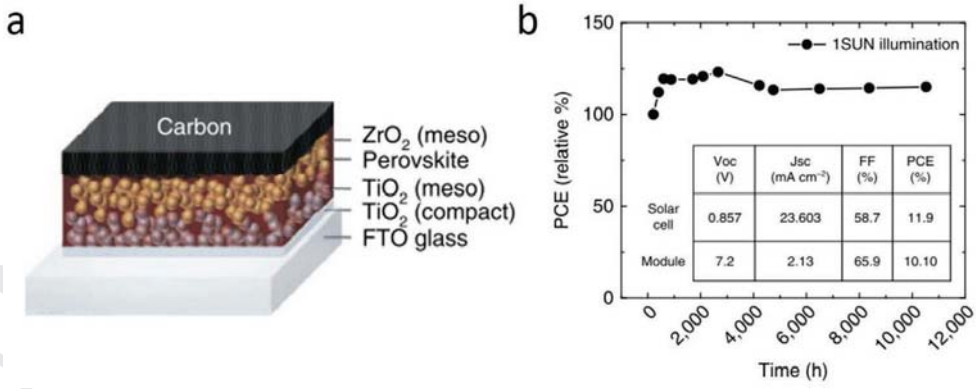

Figure 30. Module design employing a TiO_2/ZrO_2 scaffold (left) and corresponding stability under illumination at 55 °C in short circuit conditions (right). Reproduced under the terms of the Creative Commons 4.0 License.[227] Copyright 2017, Springer Nature.

© 2020 WILEY-VCH Verlag GmbH & Co. KGaA, Weinheim

Pursuant to the DOE Public Access Plan, this document represents the authors' peer-reviewed, accepted manuscript. The published version of the article is available from the relevant publisher.

electrode and mesoscale porous structure into which the perovskite is infiltrated. This unique architecture appears to provide both a kinetic barrier to mass transport and robust interfaces which are electronically favorable. In fact, most outdoor module stability studies reported thus far are based on this design. For example, Hu et al. reported a similar 10.4% efficient 49 cm^2 printable module that showed no degradation over 1000 h under AM1.5 g illumination, 1 month outdoors, or 1 year in the dark;[228] Priyadarshi et al. reported a similar structured 11% efficient module that demonstrated 2000 h ambient stability;[229] and Li et al. reported similarly structured cells that were stable in hot desert climate.[230] While these results are promising, the stability of these devices at conditions where current flows were not reported and thus are still under question. Moreover, it should be noted that these modules have substantially lower PCE than standard modules—likely due to the alternate contact layers and high series resistance from eliminating the metal contact. As a result, there is a need for more modules, particularly those of higher efficiency, to be tested outdoors.

Additionally, more work must be done to investigate how outdoor conditions affect performance. To the best of our knowledge, there are only a handful of reports on this so far. Gehlhaar et al. monitored various properties of perovskite modules outdoors.[231] Using this, they generated a model suggesting perovskite modules might reach temperatures just over 90 °C in cases of extreme ambient temperature (>40 °C) and high solar irradiance. Schwenzer et al. obtained an outdoor temperature profile, examined the effect of load conditions on cells aged indoors under an inert atmosphere with these profiles, and compared the resulting data to devices aged at a constant 25 °C.[232,233] They observed that pronounced degradation occurred from temperature cycling at reverse bias, with a lessening of the effect as the bias approached open-circuit conditions. Khenkin et al. examined the effects of diurnal cycling,[234] while Tress et al. went even further to simulate real-world conditions over the course of a year with irradiance, temperature, and wind speed data to study the energy production of perovskites under simulated real-world operating conditions rather than constant illumination.[235] Results from the latter work show several interesting trends: 1) PSCs exhibit a low decrease in efficiency with elevated temperature and low light intensity, and 2) PSCs show a recovery in parameters overnight, suggesting some of the degradation from constant illumination can be reversible. These unique results highlight the importance of more outdoor tests but are not in themselves insightful regarding degradation mechanisms.

In addition to getting more outdoor data, the community must also standardize indoor tests so that comparisons across literature reports can be undertaken. While many groups may not have the ability to MPP-track modules, conducting stability tests at V_{oc}, J_{sc}, and anywhere in between can be achieved by not connecting the anode and cathode, connecting them with a conductive medium, and connecting them with a resistor. Tests of this nature would go a long way toward understanding the degradation induced by interconnects and how they differ from devices. This gets us to our next, and final, point: the need to develop and use proper testing protocols and degradation screening tests.

6.3. Proper Testing Protocols

A degradation screening test should target a particular degradation pathway that will exist in fielded cells, modules, and/or systems. Ideally, such tests could provide perfect prediction of operational lifetime. However, such insight requires a complete picture of the degradation mechanisms and how they couple to specific degradation modes (e.g., V_{oc} or J_{sc} loss). Unfortunately, the perovskite community does not yet have complete grasp on the degradation mechanisms available to the myriad of specific device structures, nor is it clear how particular modes and relevant mechanisms might be altered by modifications to one of the layers. Thus, it is of utmost importance to develop a set of protocols to be able to compare degradation across perovskite devices and modules.[159,236] Thankfully, there are numerous protocols that have already been developed for other photovoltaic device technologies. The most relevant for the perovskite photovoltaic community to understand are those from the International Electrotechnical Commission (IEC) and ISOS. However, it is important to realize that the two are at opposite ends of the spectrum with respect to the stages of protocol development. The IEC protocols are standards that have been through an arduous process and agreed upon by working groups of international representatives, with fine-tuning taking place over time. The ones that are most relevant to enabling PSC development are IEC 60904 (photovoltaic characterization—including IV, reference cells and spectrum, simulators, mismatch calculation),[237] 61730 (safety),[238] and 61215 (qualification).[239] On the other hand, the ISOS protocols are merely consensus recommended practices (not standards) to provide a framework for aging and reporting early-stage results to enable labs to more readily compare results.

The origins of the IEC 61215 qualification tests are grounded in a methodical correlation between fielded failures and lab tests. Much of the early work is based on parallel work that happened as part of the Flat Plate Solar Array (FSA) Project, sometimes referred to as the JPL Block Buys, and the European Solar Test Installation (ESTI) under the Joint Research Center (JRC) of the European Commission.[240] The JPL Block Buys generated a set of protocols that commercial modules would pass before field tests. Postmortem analysis was done on failed modules, which led to modification of existing protocols and introduction of new protocols. Five block buys occurred between 1975 and 1981, with protocols evolving from a thermal cycle test and moderate damp heat test (68 h, 70 °C, 90% R.H.) to introduce hot spot, mechanical loading, hail tests, high pot, and humidity freeze by the fifth block buy. These modifications allowed for far lower rates of failure; one study claimed that the preblock V failure rate was 88.6%, whereas the postblock V rate was <1.3%.[241]

It is critical to understand what the IEC 61215 qualification tests are and are not. They aim to minimize well-understood infant mortality failure modes. Many of these are related to packaging and can be thought of as more module-scale problems that are shared across technologies. Furthermore, most do not step outside of the bounds of conceivable field conditions. Hail and mechanical load tests probe the mechanical integrity of the package under harsh, but realistic conditions. Freeze–thaw and humidity-freeze tests excite debonding and

UNCORRECTED PROOF

© 2020 WILEY-VCH Verlag GmbH & Co. KGaA, Weinheim

Pursuant to the DOE Public Access Plan, this document represents the authors' peer-reviewed, accepted manuscript.
The published version of the article is available from the relevant publisher.

delamination, again by introducing worst case realistic mechanical stresses. The wet leakage current test and insulation test are both safety tests of the package. The hot-spot endurance test specifically probes how cells interact with one another under worst-case shading conditions. The often-feared damp heat test is intended to reveal susceptibility to corrosion, but by stepping outside the bounds of conditions that might realistically be experienced in terrestrial applications. While modules may be warrantied for 25 years, passing the IEC qualification tests in no way should be interpreted as a service life prediction. The tests do not provide quantitative acceleration factors, provide a failure rate, or predict a mean time between failure. The IEC tests, in fact, are only required to be performed on a group of ten panels when a sizable module manufacturer produces millions each year. The applicability of these standards is then not clear to undertaking lab scale development. Even in the context of developing a robust deployable technology, their relevance might be viewed with a degree of skepticism. However, these standards cannot be defenestrated, because at the point where perovskite modules role off production lines at GW scales, standards of these types will need to have been developed and applied with the expectation that there will be at least a minimum core that is very similar to existing standards.

On the other hand, the ISOS protocols target earlier stage research with the attempt to provide guidance to the international community such that data can be more readily compared between groups. These were originally deemed necessary because early stability work in the OPV community was being performed at many conditions (temperature, humidity, irradiance, load, etc.), which made it challenging to compare results between labs. After three meetings, general consensus practices for dark, light-soak, temperature cycle, and outdoor aging were recommended.[5] Each had three levels of increasing "aggression" as well as increased requirements for equipment, control, and monitoring. For instance, the lowest level of dark testing was a "shelf-life" test in which samples could be stored in the dark in a lab drawer and measured periodically on a schedule, without further control of aging conditions. The next level up introduced either 65 or 85 °C, with the highest level a damp-heat test using 85% R.H. in addition to heat. Recently, this framework has been amended.[242] The update formalized a controlled ambient condition for each class of test that had become popular. It also specified some previously considered but infrequently used protocols for light cycle and voltage bias tests. Lastly, it established a much more detailed reporting framework to facilitate scraping data for machine learning efforts.

Ultimately, the ISOS protocols focus on facilitating the community in hardening cells to the most important stressors. They are not, however, prescriptive as to how to understand a mechanism. High quality stability studies should seek to take a step past merely making a processing, material, or architecture change and include some more detailed level of analysis/characterization to identify a mechanism (e.g., deterioration of the active layer leading to decreased quasi Fermi level splitting) rather than merely a mode (e.g., V_{oc} loss). With carefully designed studies, using the ISOS protocol framework, quantitative acceleration factors might be established. For example, establishing the activation energy of a process through temperature dependence (Arrhenius behavior) is well-known to the community, but for the reasons above may not be straightforward for perovskites. Additionally, multi-stress models (e.g., Eyring) can consider how other common stresses such as heat, light, humidity, mechanical stress, and electric field may be coupled to excite a pathway. While these stresses may be applied at values that exceed what a fielded system will experience, care should be taken not to generate new mechanisms that will not occur in standard operation; an example of this is increasing temperature past a phase transition. It is also critical to note that stresses can be nonlinear with regards to degradation mechanisms. However, while controlled laboratory tests are critical in moving the field forward in addressing the most obvious degradation pathways, it will be important to follow the example that previously commercialized photovoltaic technologies set in getting more devices outdoors to generate confidence that no critical degradation pathways are being overlooked.

Acknowledgements

S.P.D. would like to thank Dennis Schroeder and Talysa Klein for help with the TOC image. This work was authored by the National Renewable Energy Laboratory, operated by Alliance for Sustainable Energy, LLC, for the U.S. Department of Energy (DOE) under Contract No. DE-AC36-08GO28308. This material is based upon work supported by the U.S. Department of Energy's Office of Energy Efficiency and Renewable Energy (EERE) under the Solar Energy Technologies Office (SETO) project "De-risking Halide Perovskite Solar Cells" program (DE-FOA-0000990). The views expressed in the article do not necessarily represent the views of the DOE or the U.S. Government. The U.S. Government retains and the publisher, by accepting the article for publication, acknowledges that the U.S. Government retains a nonexclusive, paid-up, irrevocable, worldwide license to publish or reproduce the published form of this work, or allow others to do so, for U.S. Government purposes.

Conflict of Interest

The authors declare no conflict of interest.

Keywords

defect, degradation, device, module, perovskite, review, stability

Received: December 10, 2019
Revised: January 23, 2020
Published online:

[1] A. Kojima, K. Teshima, Y. Shirai, T. Miyasaka, *J. Am. Chem. Soc.* **2009**, *131*, 6050.
[2] NREL, **2019**, Rev. 07.
[3] J. J. Berry, J. Van De Lagemaat, M. M. Al-Jassim, S. Kurtz, Y. Yan, K. Zhu, *ACS Energy Lett.* **2017**, *2*, 2540.
[4] J. A. Christians, S. N. Habisreutinger, J. J. Berry, J. M. Luther, *ACS Energy Lett.* **2018**, *3*, 2136.
[5] M. O. Reese, S. A. Gevorgyan, M. Jørgensen, E. Bundgaard, S. R. Kurtz, D. S. Ginley, D. C. Olson, M. T. Lloyd, P. Morvillo, E. A. Katz, A. Elschner, O. Haillant, T. R. Currier, V. Shrotriya, M. Hermenau, M. Riede, K. R. Kirov, G. Trimmel, T. Rath,

© 2020 WILEY-VCH Verlag GmbH & Co. KGaA, Weinheim

UNCORRECTED PROOF

Pursuant to the DOE Public Access Plan, this document represents the authors' peer-reviewed, accepted manuscript. The published version of the article is available from the relevant publisher.

O. Inganäs, F. Zhang, M. Andersson, K. Tvingstedt, M. Lira-Cantu, D. Laird, C. McGuiness, S. Gowrisanker, M. Pannone, M. Xiao, J. Hauch, R. Steim, D. M. Delongchamp, R. Rösch, H. Hoppe, N. Espinosa, A. Urbina, G. Yaman-Uzunoglu, J. B. Bonekamp, A. J. J. M. Van Breemen, C. Girotto, E. Voroshazi, F. C. Krebs, *Sol. Energy Mater. Sol. Cells* **2011**, *95*, 1253.

[6] Z. Li, M. Yang, J. S. Park, S. H. Wei, J. J. Berry, K. Zhu, *Chem. Mater.* **2016**, *28*, 284.

[7] W. J. Yin, T. Shi, Y. Yan, *Appl. Phys. Lett.* **2014**, *104*, 063903.

[8] C. J. Bartel, C. Sutton, B. R. Goldsmith, R. Ouyang, C. B. Musgrave, L. M. Ghiringhelli, M. Scheffler, *Sci. Adv.* **2019**, *5*, eaav0693.

[9] A. Poglitsch, D. Weber, *J. Chem. Phys.* **1987**, *87*, 6373.

[10] C. Quarti, E. Mosconi, J. M. Ball, V. D'Innocenzo, C. Tao, S. Pathak, H. J. Snaith, A. Petrozza, F. De Angelis, *Energy Environ. Sci.* **2016**, *9*, 155.

[11] F. Lehmann, A. Franz, D. M. Többens, S. Levcenco, T. Unold, A. Taubert, S. Schorr, *RSC Adv.* **2019**, *9*, 11151.

[12] T. Chen, B. J. Foley, C. Park, C. M. Brown, L. W. Harriger, J. Lee, J. Ruff, M. Yoon, J. J. Choi, S. H. Lee, *Sci. Adv.* **2016**, *2*, 1601650.

[13] F. Cordero, F. Craciun, F. Trequattrini, A. Generosi, B. Paci, A. M. Paoletti, G. Pennesi, *J. Phys. Chem. Lett.* **2019**, *10*, 2463.

[14] R. J. Sutton, M. R. Filip, A. A. Haghighirad, N. Sakai, B. Wenger, F. Giustino, H. J. Snaith, *ACS Energy Lett.* **2018**, *3*, 1787.

[15] B. Wang, N. Novendra, A. Navrotsky, *J. Am. Chem. Soc.* **2019**, *141*, 14501.

[16] E. C. Schueller, G. Laurita, D. H. Fabini, C. C. Stoumpos, M. G. Kanatzidis, R. Seshadri, *Inorg. Chem.* **2018**, *57*, 695.

[17] C. C. Stoumpos, C. D. Malliakas, M. G. Kanatzidis, *Inorg. Chem.* **2013**, *52*, 9019.

[18] E. S. Parrott, R. L. Milot, T. Stergiopoulos, H. J. Snaith, M. B. Johnston, L. M. Herz, *J. Phys. Chem. Lett.* **2016**, *7*, 1321.

[19] M. Saliba, T. Matsui, J. Y. Seo, K. Domanski, J. P. Correa-Baena, M. K. Nazeeruddin, S. M. Zakeeruddin, W. Tress, A. Abate, A. Hagfeldt, M. Grätzel, *Energy Environ. Sci.* **2016**, *9*, 1989.

[20] M. Saliba, T. Matsui, K. Domanski, J. Y. Seo, A. Ummadisingu, S. M. Zakeeruddin, J. P. Correa-Baena, W. R. Tress, A. Abate, A. Hagfeldt, M. Grätzel, *Science* **2016**, *354*, 206.

[21] L. T. Schelhas, Z. Li, J. A. Christians, A. Goyal, P. Kairys, S. P. Harvey, D. H. Kim, K. H. Stone, J. M. Luther, K. Zhu, V. Stevanovic, J. J. Berry, *Energy Environ. Sci.* **2019**, *12*, 1341.

[22] E. T. Hoke, D. J. Slotcavage, E. R. Dohner, A. R. Bowring, H. I. Karunadasa, M. D. McGehee, *Chem. Sci.* **2015**, *6*, 613.

[23] C. G. Bischak, C. L. Hetherington, H. Wu, S. Aloni, D. F. Ogletree, D. T. Limmer, N. S. Ginsberg, *Nano Lett.* **2017**, *17*, 1028.

[24] D. J. Slotcavage, H. I. Karunadasa, M. D. McGehee, *ACS Energy Lett.* **2016**, *1*, 1199.

[25] K. X. Steirer, P. Schulz, G. Teeter, V. Stevanovic, M. Yang, K. Zhu, J. J. Berry, *ACS Energy Lett.* **2016**, *1*, 360.

[26] J. Kang, L. W. Wang, *J. Phys. Chem. Lett.* **2017**, *8*, 489.

[27] P. Xu, S. Chen, H. J. Xiang, X. G. Gong, S. H. Wei, *Chem. Mater.* **2014**, *26*, 6068.

[28] A. Zunger, *Theoretical Design and Discovery of the Most-Promising, Previously Overlooked Hybrid Perovskite Compounds*, **2012**.

[29] D. Shi, V. Adinolfi, R. Comin, M. Yuan, E. Alarousu, A. Buin, Y. Chen, S. Hoogland, A. Rothenberger, K. Katsiev, Y. Losovyj, X. Zhang, P. A. Dowben, O. F. Mohammed, E. H. Sargent, O. M. Bakr, *Science* **2015**, *347*, 519.

[30] Y. Huang, W. J. Yin, Y. He, *J. Phys. Chem. C* **2018**, *122*, 1345.

[31] T. Shi, H. S. Zhang, W. Meng, Q. Teng, M. Liu, X. Yang, Y. Yan, H. L. Yip, Y. J. Zhao, *J. Mater. Chem. A* **2017**, *5*, 15124.

[32] N. Liu, C. Y. Yam, *Phys. Chem. Chem. Phys.* **2018**, *20*, 6800.

[33] D. A. Egger, A. Bera, D. Cahen, G. Hodes, T. Kirchartz, L. Kronik, R. Lovrincic, A. M. Rappe, D. R. Reichman, O. Yaffe, *Adv. Mater.* **2018**, *30*, 1800691.

[34] P. Schulz, D. Cahen, A. Kahn, *Chem. Rev.* **2019**, *119*, 3349.

[35] Y. C. Zhao, W. K. Zhou, X. Zhou, K. H. Liu, D. P. Yu, Q. Zhao, *Light: Sci. Appl.* **2017**, *6*, 16243.

[36] G. Y. Kim, A. Senocrate, T. Y. Yang, G. Gregori, M. Grätzel, J. Maier, *Nat. Mater.* **2018**, *17*, 445.

[37] E. Mosconi, D. Meggiolaro, H. J. Snaith, S. D. Stranks, F. De Angelis, *Energy Environ. Sci.* **2016**, *9*, 3180.

[38] N. Aristidou, C. Eames, I. Sanchez-Molina, X. Bu, J. Kosco, M. Saiful Islam, S. A. Haque, *Nat. Commun.* **2017**, *8*, 15218.

[39] N. Aristidou, I. Sanchez-Molina, T. Chotchuangchutchaval, M. Brown, L. Martinez, T. Rath, S. A. Haque, *Angew. Chem.* **2015**, *127*, 8326.

[40] F. T. F. O'Mahony, Y. H. Lee, C. Jellett, S. Dmitrov, D. T. J. Bryant, J. R. Durrant, B. C. O'Regan, M. Graetzel, M. K. Nazeeruddin, S. A. Haque, *J. Mater. Chem. A* **2015**, *3*, 7219.

[41] D. Bryant, N. Aristidou, S. Pont, I. Sanchez-Molina, T. Chotchuna ngatchaval, S. Wheeler, J. R. Durrant, S. A. Haque, *Energy Environ. Sci.* **2016**, *9*, 1655.

[42] B. Conings, J. Drijkoningen, N. Gauquelin, A. Babayigit, J. D'Haen, L. D'Olieslaeger, A. Ethirajan, J. Verbeeck, J. Manca, E. Mosconi, F. De Angelis, H. G. Boyen, *Adv. Energy Mater.* **2015**, *5*, 1500477.

[43] A. Dualeh, P. Gao, S. Il Seok, M. K. Nazeeruddin, M. Grätzel, *Chem. Mater.* **2014**, *26*, 6160.

[44] M. Sawicka, P. Storoniak, P. Skurski, J. Blazejowski, J. Rak, *Chem. Phys.* **2006**, *324*, 425.

[45] D. P. Nenon, J. A. Christians, L. M. Wheeler, J. L. Blackburn, E. M. Sanehira, B. Dou, M. L. Olsen, K. Zhu, J. J. Berry, J. M. Luther, *Energy Environ. Sci.* **2016**, *9*, 2072.

[46] E. J. Juarez-Perez, Z. Hawash, S. R. Raga, L. K. Ono, Y. Qi, *Energy Environ. Sci.* **2016**, *9*, 3406.

[47] A. E. Williams, P. J. Holliman, M. J. Carnie, M. L. Davies, D. A. Worsley, T. M. Watson, *J. Mater. Chem. A* **2014**, *2*, 19338.

[48] N. K. Kim, Y. H. Min, S. Noh, E. Cho, G. Jeong, M. Joo, S. W. Ahn, J. S. Lee, S. Kim, K. Ihm, H. Ahn, Y. Kang, H. S. Lee, D. Kim, *Sci. Rep.* **2017**, *7*, 4645.

[49] E. J. Juarez-Perez, L. K. Ono, M. Maeda, Y. Jiang, Z. Hawash, Y. Qi, *J. Mater. Chem. A* **2018**, *6*, 9604.

[50] A. Latini, G. Gigli, A. Ciccioli, *Sustainable Energy Fuels* **2017**, *1*, 1351.

[51] S. R. Raga, L. K. Ono, Y. Qi, *J. Mater. Chem. A* **2016**, *4*, 2494.

[52] S. Pang, Y. Zhou, Z. Wang, M. Yang, A. R. Krause, Z. Zhou, K. Zhu, N. P. Padture, G. Cui, *J. Am. Chem. Soc.* **2016**, *138*, 750.

[53] S. P. Dunfield, D. T. Moore, T. R. Klein, D. M. Fabian, J. A. Christians, A. G. Dixon, B. Dou, S. Ardo, M. C. Beard, S. E. Shaheen, J. J. Berry, M. F. A. M. Van Hest, *ACS Energy Lett.* **2018**, *3*, 1192.

[54] W. A. Dunlap-Shohl, T. Li, D. B. Mitzi, *ACS Appl. Energy Mater.* **2019**, *2*, 5083.

[55] A. M. Askar, G. M. Bernard, B. Wiltshire, K. Shankar, V. K. Michaelis, *J. Phys. Chem. C* **2017**, *121*, 1013.

[56] A. M. A. Leguy, Y. Hu, M. Campoy-Quiles, M. I. Alonso, O. J. Weber, P. Azarhoosh, M. Van Schilfgaarde, M. T. Weller, T. Bein, J. Nelson, P. Docampo, P. R. F. Barnes, *Chem. Mater.* **2015**, *27*, 3397.

[57] A. Kakekhani, R. N. Katti, A. M. Rappe, *APL Mater.* **2019**, *7*, 041112.

[58] Z. Wang, Z. Shi, T. Li, Y. Chen, W. Huang, *Angew. Chem., Int. Ed.* **2017**, *56*, 1190.

[59] W. Tan, A. R. Bowring, A. C. Meng, M. D. McGehee, P. C. McIntyre, *ACS Appl. Mater. Interfaces* **2018**, *10*, 5485.

[60] Y. Zong, Z. Zhou, M. Chen, N. P. Padture, Y. Zhou, *Adv. Energy Mater.* **2018**, *8*, 1800997.

[61] Y. Bai, Y. Lin, L. Ren, X. Shi, E. Strounina, Y. Deng, Q. Wang, Y. Fang, X. Zheng, Y. Lin, Z. G. Chen, Y. Du, L. Wang, J. Huang, *ACS Energy Lett.* **2019**, *4*, 1231.

UNCORRECTED PROOF

 © 2020 WILEY-VCH Verlag GmbH & Co. KGaA, Weinheim

Pursuant to the DOE Public Access Plan, this document represents the authors' peer-reviewed, accepted manuscript. The published version of the article is available from the relevant publisher.

[62] S. Yang, S. Chen, E. Mosconi, Y. Fang, X. Xiao, C. Wang, Y. Zhou, Z. Yu, J. Zhao, Y. Gao, F. De Angelis, J. Huang, *Science* **2019**, *365*, 473.
[63] J. H. Noh, S. H. Im, J. H. Heo, T. N. Mandal, S. Il Seok, *Nano Lett.* **2013**, *13*, 1764.
[64] Z. Liu, L. Qiu, E. J. Juarez-Perez, Z. Hawash, T. Kim, Y. Jiang, Z. Wu, S. R. Raga, L. K. Ono, S. (F) Liu, Y. Qi, *Nat. Commun.* **2018**, *9*, 3880.
[65] F. El-Mellouhi, A. Marzouk, E. T. Bentria, S. N. Rashkeev, S. Kais, F. H. Alharbi, *ChemSusChem* **2016**, *9*, 2648.
[66] R. Prasanna, A. Gold-Parker, T. Leijtens, B. Conings, A. Babayigit, H. G. Boyen, M. F. Toney, M. D. McGehee, *J. Am. Chem. Soc.* **2017**, *139*, 11117.
[67] T. Leijtens, R. Prasanna, A. Gold-Parker, M. F. Toney, M. D. McGehee, *ACS Energy Lett.* **2017**, *2*, 2159.
[68] J. S. Yun, J. Kim, T. Young, R. J. Patterson, D. Kim, J. Seidel, S. Lim, M. A. Green, S. Huang, A. Ho-Baillie, *Adv. Funct. Mater.* **2018**, *28*, 1705363.
[69] Z. Fan, H. Xiao, Y. Wang, Z. Zhao, Z. Lin, H. C. Cheng, S. J. Lee, G. Wang, Z. Feng, W. A. Goddard, Y. Huang, X. Duan, *Joule* **2017**, *1*, 548.
[70] F. Zhang, K. Zhu, *Adv. Energy Mater.* **2019**, *2019*, 1902579.
[71] H. Min, M. Kim, S. U. Lee, H. Kim, G. Kim, K. Choi, J. H. Lee, S. Il Seok, *Science* **2019**, *366*, 749.
[72] B. Chen, P. N. Rudd, S. Yang, Y. Yuan, J. Huang, *Chem. Soc. Rev.* **2019**, *48*, 3842.
[73] D. Y. Son, J. W. Lee, Y. J. Choi, I. H. Jang, S. Lee, P. J. Yoo, H. Shin, N. Ahn, M. Choi, D. Kim, N. G. Park, *Nat. Energy* **2016**, *1*, 16081.
[74] Z. Li, T. R. Klein, D. H. Kim, M. Yang, J. J. Berry, M. F. A. M. Van Hest, K. Zhu, *Nat. Rev. Mater.* **2018**, *3*, 18017.
[75] Y. Zhao, K. Zhu, *J. Phys. Chem. C* **2014**, *118*, 9412.
[76] W. Nie, H. Tsai, R. Asadpour, J. C. Blancon, A. J. Neukirch, G. Gupta, J. J. Crochet, M. Chhowalla, S. Tretiak, M. A. Alam, H. L. Wang, A. D. Mohite, *Science* **2015**, *347*, 522.
[77] M. M. Tavakoli, M. Saliba, P. Yadav, P. Holzhey, A. Hagfeldt, S. M. Zakeeruddin, M. Grätzel, *Adv. Energy Mater.* **2019**, *9*, 1802646.
[78] E. H. Jung, N. J. Jeon, E. Y. Park, C. S. Moon, T. J. Shin, T. Y. Yang, J. H. Noh, J. Seo, *Nature* **2019**, *567*, 511.
[79] N. J. Jeon, H. Na, E. H. Jung, T. Y. Yang, Y. G. Lee, G. Kim, H. W. Shin, S. Il Seok, J. Lee, J. Seo, *Nat. Energy* **2018**, *3*, 682.
[80] Q. Jiang, Z. Chu, P. Wang, X. Yang, H. Liu, Y. Wang, Z. Yin, J. Wu, X. Zhang, J. You, *Adv. Mater.* **2017**, *29*, 1703852.
[81] H. C. Liao, P. Guo, C. P. Hsu, M. Lin, B. Wang, L. Zeng, W. Huang, C. M. M. Soe, W. F. Su, M. J. Bedzyk, M. R. Wasielewski, A. Facchetti, R. P. H. Chang, M. G. Kanatzidis, T. J. Marks, *Adv. Energy Mater.* **2017**, *7*, 1.
[82] H. Lai, B. Kan, T. Liu, N. Zheng, Z. Xie, T. Zhou, X. Wan, X. Zhang, Y. Liu, Y. Chen, *J. Am. Chem. Soc.* **2018**, *140*, 11639.
[83] M. Yang, D. H. Kim, Y. Yu, Z. Li, O. G. Reid, Z. Song, D. Zhao, C. Wang, L. Li, Y. Meng, T. Guo, Y. Yan, K. Zhu, *Mater. Today Energy* **2018**, *7*, 232.
[84] C. Zuo, L. Ding, *Nanoscale* **2014**, *6*, 9935.
[85] Y. Rong, X. Hou, Y. Hu, A. Mei, L. Liu, P. Wang, H. Han, *Nat. Commun.* **2017**, *8*, 14555.
[86] T. Oku, Y. Ohishi, N. Ueoka, *RSC Adv.* **2018**, *8*, 10389.
[87] W. Fu, J. Wang, L. Zuo, K. Gao, F. Liu, D. S. Ginger, A. K. Y. Jen, *ACS Energy Lett.* **2018**, *3*, 2086.
[88] J. Liu, Q. Han, Y. Bai, K. Z. Du, T. Li, D. Ji, Y. Zhou, C. Cao, D. Shin, J. Ding, A. D. Franklin, J. T. Glass, J. Hu, M. J. Therien, D. B. Mitzi, *Energy Environ. Sci.* **2017**, *10*, 2365.
[89] J. Tong, Z. Song, D. H. Kim, X. Chen, C. Chen, A. F. Palmstrom, P. F. Ndione, M. O. Reese, S. P. Dunfield, O. G. Reid, J. Liu, F. Zhang, S. P. Harvey, Z. Li, S. T. Christensen, G. Teeter, D. Zhao, M. M. Al-Jassim, M. F. A. M. Van Hest, M. C. Beard, S. E. Shaheen, J. J. Berry, Y. Yan, K. Zhu, *Science* **2019**, *364*, 475.
[90] N. D. Pham, V. T. Tiong, D. Yao, W. Martens, A. Guerrero, J. Bisquert, H. Wang, *Nano Energy* **2017**, *41*, 476.
[91] H. Dong, Z. Wu, J. Xi, X. Xu, L. Zuo, T. Lei, X. Zhao, L. Zhang, X. Hou, A. K. Y. Jen, *Adv. Funct. Mater.* **2018**, *28*, 1704836.
[92] S. Yang, W. Liu, L. Zuo, X. Zhang, T. Ye, J. Chen, C. Z. Li, G. Wu, H. Chen, *J. Mater. Chem. A* **2016**, *4*, 9430.
[93] Y. Xiao, L. Yang, G. Han, Y. Li, M. Li, H. Li, *Org. Electron.* **2019**, *65*, 201.
[94] X. Yan, S. Hu, Y. Zhang, H. Li, C. Sheng, *Sol. Energy Mater. Sol. Cells* **2019**, *191*, 283.
[95] Y. Xia, C. Ran, Y. Chen, Q. Li, N. Jiang, C. Li, Y. Pan, T. Li, J. P. Wang, W. Huang, *J. Mater. Chem. A* **2017**, *5*, 3193.
[96] X. Zheng, B. Chen, J. Dai, Y. Fang, Y. Bai, Y. Lin, H. Wei, X. C. Zeng, J. Huang, *Nat. Energy* **2017**, *2*, 9.
[97] X. Li, M. Ibrahim Dar, C. Yi, J. Luo, M. Tschumi, S. M. Zakeeruddin, M. K. Nazeeruddin, H. Han, M. Grätzel, *Nat. Chem.* **2015**, *7*, 703.
[98] Q. Chen, H. Zhou, T. Bin Song, S. Luo, Z. Hong, H. S. Duan, L. Dou, Y. Liu, Y. Yang, *Nano Lett.* **2014**, *14*, 4158.
[99] Y. C. Kim, N. J. Jeon, J. H. Noh, W. S. Yang, J. Seo, J. S. Yun, A. Ho-Baillie, S. Huang, M. A. Green, J. Seidel, T. K. Ahn, S. Il Seok, *Adv. Energy Mater.* **2016**, *6*, 1.
[100] W. Ke, C. Xiao, C. Wang, B. Saparov, H. S. Duan, D. Zhao, Z. Xiao, P. Schulz, S. P. Harvey, W. Liao, W. Meng, Y. Yu, A. J. Cimaroli, C. S. Jiang, K. Zhu, M. Al-Jassim, G. Fang, D. B. Mitzi, Y. Yan, *Adv. Mater.* **2016**, *28*, 5214.
[101] M. Abdi-Jalebi, Z. Andaji-Garmaroudi, S. Cacovich, C. Stavrakas, B. Philippe, J. M. Richter, M. Alsari, E. P. Booker, E. M. Hutter, A. J. Pearson, S. Lilliu, T. J. Savenije, H. Rensmo, G. Divitini, C. Ducati, R. H. Friend, S. D. Stranks, *Nature* **2018**, *555*, 497.
[102] L. Wang, H. Zhou, J. Hu, B. Huang, M. Sun, B. Dong, G. Zheng, Y. Huang, Y. Chen, L. Li, Z. Xu, N. Li, Z. Liu, Q. Chen, L. D. Sun, C. H. Yan, *Science* **2019**, *363*, 265.
[103] C. Xiao, F. Zhang, Z. Li, C. Jiang, K. Zhu, M. Al-jassim, C. Xiao, F. Zhang, Z. Li, S. P. Harvey, X. Chen, K. Wang, *Matter* **2019**, 1.
[104] M. Abdi-Jalebi, M. I. Dar, A. Sadhanala, S. P. Senanayak, M. Franckevičius, N. Arora, Y. Hu, M. K. Nazeeruddin, S. M. Zakeeruddin, M. Grätzel, R. H. Friend, *Adv. Energy Mater.* **2016**, *6*, 1502472.
[105] C. Chang, X. Zou, J. Cheng, Y. Yang, Y. Yao, T. Ling, H. Ren, Z. Xiao, *Adv. Mater. Sci. Eng.* **2019**, *2019*, 1.
[106] M. Abdi-Jalebi, M. Pazoki, B. Philippe, M. I. Dar, M. Alsari, A. Sadhanala, G. Divitini, R. Imani, S. Lilliu, J. Kullgren, H. Rensmo, M. Grätzel, R. H. Friend, *ACS Nano* **2018**, *12*, 7301.
[107] J. P. Correa-Baena, Y. Luo, T. M. Brenner, J. Snaider, S. Sun, X. Li, M. A. Jensen, N. T. P. Hartono, L. Nienhaus, S. Wieghold, J. R. Poindexter, S. Wang, Y. S. Meng, T. Wang, B. Lai, M. V. Holt, Z. Cai, M. G. Bawendi, L. Huang, T. Buonassisi, D. P. Fenning, *Science* **2019**, *363*, 627.
[108] M. Zhang, J. S. Yun, Q. Ma, J. Zheng, C. F. J. Lau, X. Deng, J. Kim, D. Kim, J. Seidel, M. A. Green, S. Huang, A. W. Y. Ho-Baillie, *ACS Energy Lett.* **2017**, *2*, 438.
[109] Y. Shirahata, T. Oku, *Mater. Res. Express* **2018**, *5*, 055504.
[110] S. Ye, H. Rao, Z. Zhao, L. Zhang, H. Bao, W. Sun, Y. Li, F. Gu, J. Wang, Z. Liu, Z. Bian, C. Huang, *J. Am. Chem. Soc.* **2017**, *139*, 7504.
[111] K. L. Wang, R. Wang, Z. K. Wang, M. Li, Y. Zhang, H. Ma, L. S. Liao, Y. Yang, *Nano Lett.* **2019**, *19*, 5176.
[112] J. Jin, H. Li, C. Chen, B. Zhang, L. Xu, B. Dong, H. Song, Q. Dai, *ACS Appl. Mater. Interfaces* **2017**, *9*, 42875.
[113] A. Kooijman, L. A. Muscarella, R. M. Williams, *Appl. Sci.* **2019**, *9*, 1678.
[114] F. Yang, M. A. Kamarudin, G. Kapil, D. Hirotani, P. Zhang, C. H. Ng, T. Ma, S. Hayase, *ACS Appl. Mater. Interfaces* **2018**, *10*, 24543.

UNCORRECTED PROOF

 © 2020 WILEY-VCH Verlag GmbH & Co. KGaA, Weinheim

Pursuant to the DOE Public Access Plan, this document represents the authors' peer-reviewed, accepted manuscript.
The published version of the article is available from the relevant publisher.

[115] C. Lu, J. Zhang, D. Hou, X. Gan, H. Sun, Z. Zeng, R. Chen, H. Tian, Q. Xiong, Y. Zhang, Y. Li, Y. Zhu, *Appl. Phys. Lett.* **2018**, *112*, 1.
[116] M. C. Wu, T. H. Lin, S. H. Chan, W. F. Su, *J. Taiwan Inst. Chem. Eng.* **2017**, *80*, 695.
[117] X. Gong, L. Guan, H. Pan, Q. Sun, X. Zhao, H. Li, H. Pan, Y. Shen, Y. Shao, L. Sun, Z. Cui, L. Ding, M. Wang, *Adv. Funct. Mater.* **2018**, *28*, 1804286.
[118] E. P. Yao, P. Sun, W. Huang, E. P. Yao, Y. Yang, M. Wang, *Nano Energy* **2017**, *36*, 213.
[119] W. S. Subhani, K. Wang, M. Du, S. F. Liu, *Nano Energy* **2019**, *61*, 165.
[120] S. H. Chan, M. C. Wu, K. M. Lee, W. C. Chen, T. H. Lin, W. F. Su, *J. Mater. Chem. A* **2017**, *5*, 18044.
[121] J. R. Poindexter, R. L. Z. Hoye, L. Nienhaus, R. C. Kurchin, A. E. Morishige, E. E. Looney, A. Osherov, J. P. Correa-Baena, B. Lai, V. Bulović, V. Stevanović, M. G. Bawendi, T. Buonassisi, *ACS Nano* **2017**, *11*, 7101.
[122] C. Chen, D. Liu, B. Zhang, W. Bi, H. Li, J. Jin, X. Chen, L. Xu, H. Song, Q. Dai, *Adv. Energy Mater.* **2018**, *8*, 1.
[123] E. Mosconi, B. Merabet, D. Meggiolaro, A. Zaoui, F. De Angelis, *J. Phys. Chem. C* **2018**, *122*, 14107.
[124] G. Han, H. D. Hadi, A. Bruno, S. A. Kulkarni, T. M. Koh, L. H. Wong, C. Soci, N. Mathews, S. Zhang, S. G. Mhaisalkar, *J. Phys. Chem. C* **2018**, *122*, 13884.
[125] C. Liu, W. Li, H. Li, C. Zhang, J. Fan, Y. Mai, *Nanoscale* **2017**, *9*, 13967.
[126] J. Xu, A. Buin, A. H. Ip, W. Li, O. Voznyy, R. Comin, M. Yuan, S. Jeon, Z. Ning, J. J. McDowell, P. Kanjanaboos, J. P. Sun, X. Lan, L. N. Quan, D. H. Kim, I. G. Hill, P. Maksymovych, E. H. Sargent, *Nat. Commun.* **2015**, *6*, 7081.
[127] C. H. Chiang, C. G. Wu, *Nat. Photonics* **2016**, *10*, 196.
[128] F. Zhang, W. Shi, J. Luo, N. Pellet, C. Yi, X. Li, X. Zhao, T. J. S. Dennis, X. Li, S. Wang, Y. Xiao, S. M. Zakeeruddin, D. Bi, M. Grätzel, *Adv. Mater.* **2017**, *29*, 1606806.
[129] Q. Fu, S. Xiao, X. Tang, Y. Chen, T. Hu, *ACS Appl. Mater. Interfaces* **2019**, *11*, 24782.
[130] J. W. Lee, Z. Dai, C. Lee, H. M. Lee, T. H. Han, N. De Marco, O. Lin, C. S. Choi, B. Dunn, J. Koh, D. Di Carlo, J. H. Ko, H. D. Maynard, Y. Yang, *J. Am. Chem. Soc.* **2018**, *140*, 6317.
[131] N. J. Jeon, J. H. Noh, Y. C. Kim, W. S. Yang, S. Ryu, S. Il Seok, *Nat. Mater.* **2014**, *13*, 897.
[132] D. Bi, C. Yi, J. Luo, J. D. Décoppet, F. Zhang, S. M. Zakeeruddin, X. Li, A. Hagfeldt, M. Grätzel, *Nat. Energy* **2016**, *1*, 16142.
[133] R. Wang, J. Xue, L. Meng, J. W. Lee, Z. Zhao, P. Sun, L. Cai, T. Huang, Z. Wang, Z. K. Wang, Y. Duan, J. L. Yang, S. Tan, Y. Yuan, Y. Huang, Y. Yang, *Joule* **2019**, *3*, 1464.
[134] I. Wharf, T. Gramstad, R. Makhija, M. Onyszchuk, *Can. J. Chem.* **1976**, *54*, 3430.
[135] N. K. Noel, A. Abate, S. D. Stranks, E. S. Parrott, V. M. Burlakov, A. Goriely, H. J. Snaith, *ACS Nano* **2014**, *8*, 9815.
[136] T. Y. Wen, S. Yang, P. F. Liu, L. J. Tang, H. W. Qiao, X. Chen, X. H. Yang, Y. Hou, H. G. Yang, *Adv. Energy Mater.* **2018**, *8*, 1703143.
[137] Q. Zeng, X. Zhang, X. Feng, S. Lu, Z. Chen, X. Yong, S. A. T. Redfern, H. Wei, H. Wang, H. Shen, W. Zhang, W. Zheng, H. Zhang, J. S. Tse, B. Yang, *Adv. Mater.* **2018**, *30*, 1705393.
[138] L. Meng, C. Sun, R. Wang, W. Huang, Z. Zhao, P. Sun, T. Huang, J. Xue, J. W. Lee, C. Zhu, Y. Huang, Y. Li, Y. Yang, *J. Am. Chem. Soc.* **2018**, *140*, 17255.
[139] C. Fei, B. Li, R. Zhang, H. Fu, J. Tian, G. Cao, *Adv. Energy Mater.* **2017**, *7*, 1602017.
[140] L. Gao, S. Huang, L. Chen, X. Li, B. Ding, S. Huang, G. Yang, *Sol. RRL* **2018**, *2*, 1800088.
[141] S. G. Ko, G. Il Ryu, B. Kim, G. J. Cha, J. H. Ri, G. S. Sonu, U. C. Kim, *Sol. Energy Mater. Sol. Cells* **2019**, *196*, 105.
[142] T. Wu, Y. Wang, X. Li, Y. Wu, X. Meng, D. Cui, X. Yang, L. Han, *Adv. Energy Mater.* **2019**, *9*, 1803766.
[143] M. Qin, J. Cao, T. Zhang, J. Mai, T. K. Lau, S. Zhou, Y. Zhou, J. Wang, Y. J. Hsu, N. Zhao, J. Xu, X. Zhan, X. Lu, *Adv. Energy Mater.* **2018**, *8*, 1703399.
[144] Y. H. Wu, X. Q. Shi, X. H. Ding, Y. K. Ren, T. Hayat, A. Alsaedi, Y. Ding, P. Xu, S. Y. Dai, *ACS Appl. Mater. Interfaces* **2018**, *10*, 3602.
[145] X. Liu, J. Wu, Y. Yang, T. Wu, Q. Guo, *J. Power Sources* **2018**, *399*, 144.
[146] W. Q. Wu, Z. Yang, P. N. Rudd, Y. Shao, X. Dai, H. Wei, J. Zhao, Y. Fang, Q. Wang, Y. Liu, Y. Deng, X. Xiao, Y. Feng, J. Huang, *Sci. Adv.* **2019**, *5*, eaav8925.
[147] J. W. Lee, Z. Dai, T. H. Han, C. Choi, S. Y. Chang, S. J. Lee, N. De Marco, H. Zhao, P. Sun, Y. Huang, Y. Yang, *Nat. Commun.* **2018**, *9*, 3021.
[148] T. Niu, J. Lu, M. C. Tang, D. Barrit, D. M. Smilgies, Z. Yang, J. Li, Y. Fan, T. Luo, I. McCulloch, A. Amassian, S. Liu, K. Zhao, *Energy Environ. Sci.* **2018**, *11*, 3358.
[149] M. Shahiduzzaman, K. Yamamoto, Y. Furumoto, T. Kuwabara, K. Takahashi, T. Taima, *RSC Adv.* **2015**, *5*, 77495.
[150] J. Y. Seo, T. Matsui, J. Luo, J. P. Correa-Baena, F. Giordano, M. Saliba, K. Schenk, A. Ummadisingu, K. Domanski, M. Hadadian, A. Hagfeldt, S. M. Zakeeruddin, U. Steiner, M. Grätzel, A. Abate, *Adv. Energy Mater.* **2016**, *6*, 1600767.
[151] M. Salado, F. J. Ramos, V. M. Manzanares, P. Gao, M. K. Nazeeruddin, P. J. Dyson, S. Ahmad, *ChemSusChem* **2016**, *9*, 2708.
[152] M. Salado, M. A. Fernández, J. P. Holgado, S. Kazim, M. K. Nazeeruddin, P. J. Dyson, S. Ahmad, *ChemSusChem* **2017**, *10*, 3846.
[153] S. Wang, Z. Li, Y. Zhang, X. Liu, J. Han, X. Li, Z. Liu, S. (F) Liu, W. C. H. Choy, *Adv. Funct. Mater.* **2019**, *29*, 1.
[154] S. Bai, P. Da, C. Li, Z. Wang, Z. Yuan, F. Fu, M. Kawecki, X. Liu, N. Sakai, J. T. W. Wang, S. Huettner, S. Buecheler, M. Fahlman, F. Gao, H. J. Snaith, *Nature* **2019**, *571*, 245.
[155] M. Sun, F. Zhang, H. Liu, X. Li, Y. Xiao, S. Wang, *J. Mater. Chem. A* **2017**, *5*, 13448.
[156] F. Zhang, D. Bi, N. Pellet, C. Xiao, Z. Li, J. J. Berry, S. M. Zakeeruddin, K. Zhu, M. Grätzel, *Energy Environ. Sci.* **2018**, *11*, 3480.
[157] N. Li, S. Tao, Y. Chen, X. Niu, C. K. Onwudinanti, C. Hu, Z. Qiu, Z. Xu, G. Zheng, L. Wang, Y. Zhang, L. Li, H. Liu, Y. Lun, J. Hong, X. Wang, Y. Liu, H. Xie, Y. Gao, Y. Bai, S. Yang, G. Brocks, Q. Chen, H. Zhou, *Nat. Energy* **2019**, *4*, 408.
[158] H. Zhu, F. Zhang, Y. Xiao, S. Wang, X. Li, *J. Mater. Chem. A* **2018**, *6*, 4971.
[159] H. J. Snaith, P. Hacke, *Nat. Energy* **2018**, *3*, 459.
[160] R. A. Belisle, P. Jain, R. Prasanna, T. Leijtens, M. D. McGehee, *ACS Energy Lett.* **2016**, *1*, 556.
[161] L. Bertoluzzi, C. C. Boyd, N. Rolston, J. Xu, R. Prasanna, B. C. O'Regan, M. D. McGehee, *Joule* **2019**, *4*, 1.
[162] T. H. Schloemer, T. S. Gehan, J. A. Christians, D. G. Mitchell, A. Dixon, Z. Li, K. Zhu, J. J. Berry, J. M. Luther, A. Sellinger, *ACS Energy Lett.* **2019**, *4*, 473.
[163] I. L. Braly, R. J. Stoddard, A. Rajagopal, A. K. Y. Jen, H. W. Hillhouse, *J. Phys. Chem. Lett.* **2018**, *9*, 3779.
[164] E. M. Miller, Y. Zhao, C. C. Mercado, S. K. Saha, J. M. Luther, K. Zhu, V. Stevanović, C. L. Perkins, J. Van De Lagemaat, *Phys. Chem. Chem. Phys.* **2014**, *16*, 22122.
[165] A. M. Tirmzi, J. A. Christians, R. P. Dwyer, D. T. Moore, J. A. Marohn, *J. Phys. Chem. C* **2019**, *123*, 3402.
[166] Y. Du, C. Xin, W. Huang, B. Shi, Y. Ding, C. Wei, Y. Zhao, Y. Li, X. Zhang, *ACS Sustainable Chem. Eng.* **2018**, *6*, 16806.
[167] N. K. Noel, S. N. Habisreutinger, A. Pellaroque, F. Pulvirenti, B. Wenger, F. Zhang, Y. H. Lin, O. G. Reid, J. Leisen, Y. Zhang,

UNCORRECTED PROOF

© 2020 WILEY-VCH Verlag GmbH & Co. KGaA, Weinheim

Pursuant to the DOE Public Access Plan, this document represents the authors' peer-reviewed, accepted manuscript. The published version of the article is available from the relevant publisher.

S. Barlow, S. R. Marder, A. Kahn, H. J. Snaith, C. B. Arnold, B. P. Rand, *Energy Environ. Sci.* **2019**, *12*, 3063.
[168] S. Ito, S. Tanaka, K. Manabe, H. Nishino, *J. Phys. Chem. C* **2014**, *118*, 16995.
[169] H. L. Le Chatelier, *C. R.* **1884**, *99*, 786.
[170] J. A. Christians, P. Schulz, J. S. Tinkham, T. H. Schloemer, S. P. Harvey, B. J. Tremolet De Villers, A. Sellinger, J. J. Berry, J. M. Luther, *Nat. Energy* **2018**, *3*, 68.
[171] W. Li, W. Zhang, S. Van Reenen, R. J. Sutton, J. Fan, A. A. Haghighirad, M. B. Johnston, L. Wang, H. J. Snaith, *Energy Environ. Sci.* **2016**, *9*, 490.
[172] C. Liu, M. Cai, Y. Yang, Z. Arain, Y. Ding, X. Shi, P. Shi, S. Ma, T. Hayat, A. Alsaedi, J. Wu, S. Dai, G. Cao, *J. Mater. Chem. A* **2019**, *7*, 11086.
[173] T. Leijtens, G. E. Eperon, S. Pathak, A. Abate, M. M. Lee, H. J. Snaith, *Nat. Commun.* **2013**, *4*, 2885.
[174] Y. Kato, L. K. Ono, M. V. Lee, S. Wang, S. R. Raga, Y. Qi, *Adv. Mater. Interfaces* **2015**, *2*, 1500195.
[175] J. Li, Q. Dong, N. Li, L. Wang, *Adv. Energy Mater.* **2017**, *7*, 1602922.
[176] K. Domanski, J. P. Correa-Baena, N. Mine, M. K. Nazeeruddin, A. Abate, M. Saliba, W. Tress, A. Hagfeldt, M. Grätzel, *ACS Nano* **2016**, *10*, 6306.
[177] C. C. Boyd, R. Cheacharoen, K. A. Bush, R. Prasanna, T. Leijtens, M. D. McGehee, *ACS Energy Lett.* **2018**, *3*, 1772.
[178] W. Ming, D. Yang, T. Li, L. Zhang, M. H. Du, *Adv. Sci.* **2018**, *5*, 1700662.
[179] L. Zhao, R. A. Kerner, Z. Xiao, Y. L. Lin, K. M. Lee, J. Schwartz, B. P. Rand, *ACS Energy Lett.* **2016**, *1*, 595.
[180] K. A. Bush, A. F. Palmstrom, Z. J. Yu, M. Boccard, R. Cheacharoen, J. P. Mailoa, D. P. McMeekin, R. L. Z. Hoye, C. D. Bailie, T. Leijtens, I. M. Peters, M. C. Minichetti, N. Rolston, R. Prasanna, S. Sofia, D. Harwood, W. Ma, F. Moghadam, H. J. Snaith, T. Buonassisi, Z. C. Holman, S. F. Bent, M. D. McGehee, *Nat. Energy* **2017**, *2*, 17009.
[181] J. A. Raiford, C. C. Boyd, A. F. Palmstrom, E. J. Wolf, B. A. Fearon, J. J. Berry, M. D. McGehee, S. F. Bent, *Adv. Energy Mater.* **2019**, *9*, 1902353.
[182] A. F. Palmstrom, G. E. Eperon, T. Leijtens, R. Prasanna, S. N. Habisreutinger, W. Nemeth, E. A. Gaulding, S. P. Dunfield, M. Reese, S. Nanayakkara, T. Moot, J. Werner, J. Liu, B. To, S. T. Christensen, M. D. McGehee, M. F. A. M. van Hest, J. M. Luther, J. J. Berry, D. T. Moore, *Joule* **2019**, *3*, 2193.
[183] S. Wu, R. Chen, S. Zhang, B. H. Babu, Y. Yue, H. Zhu, Z. Yang, C. Chen, W. Chen, Y. Huang, S. Fang, T. Liu, L. Han, W. Chen, *Nat. Commun.* **2019**, *10*, 1161.
[184] W. Chen, L. Xu, X. Feng, J. Jie, Z. He, *Adv. Mater.* **2017**, *29*, 1603923.
[185] E. Bi, H. Chen, F. Xie, Y. Wu, W. Chen, Y. Su, A. Islam, M. Grätzel, X. Yang, L. Han, *Nat. Commun.* **2017**, *8*, 1.
[186] R. Fang, S. Wu, W. Chen, W. Chen, Z. Liu, S. Zhang, R. Chen, Y. Yue, L. Deng, Y. B. Cheng, L. Han, *ACS Nano* **2018**, *12*, 2403.
[187] T. Malinauskas, D. Tomkute-Luksiene, R. Sens, M. Daskeviciene, R. Send, H. Wonneberger, V. Jankauskas, I. Bruder, V. Getautis, *ACS Appl. Mater. Interfaces* **2015**, *7*, 11107.
[188] J. Zhao, Y. Deng, H. Wei, X. Zheng, Z. Yu, Y. Shao, J. E. Shield, J. Huang, *Sci. Adv.* **2017**, *3*, eaao5616.
[189] N. Rolston, K. A. Bush, A. D. Printz, A. Gold-Parker, Y. Ding, M. F. Toney, M. D. McGehee, R. H. Dauskardt, *Adv. Energy Mater.* **2018**, *8*, 1802139.
[190] K. A. Bush, N. Rolston, A. Gold-Parker, S. Manzoor, J. Hausele, Z. J. Yu, J. A. Raiford, R. Cheacharoen, Z. C. Holman, M. F. Toney, R. H. Dauskardt, M. D. McGehee, *ACS Energy Lett.* **2018**, *3*, 1225.
[191] Z. Zhao, F. Gu, H. Rao, S. Ye, Z. Liu, Z. Bian, C. Huang, *Adv. Energy Mater.* **2019**, *9*, 1.
[192] R. Wang, M. Mujahid, Y. Duan, Z. K. Wang, J. Xue, Y. Yang, *Adv. Funct. Mater.* **2019**, *29*, 1808843.
[193] H. Tan, A. Jain, O. Voznyy, X. Lan, F. P. G. De Arquer, J. Z. Fan, R. Quintero-Bermudez, M. Yuan, B. Zhang, Y. Zhao, F. Fan, P. Li, L. N. Quan, Y. Zhao, Z. H. Lu, Z. Yang, S. Hoogland, E. H. Sargent, *Science* **2017**, *355*, 722.
[194] K. Choi, J. Lee, H. Il Kim, C. W. Park, G. W. Kim, H. Choi, S. Park, S. A. Park, T. Park, *Energy Environ. Sci.* **2018**, *11*, 3238.
[195] N. Arora, M. I. Dar, A. Hinderhofer, N. Pellet, F. Schreiber, S. M. Zakeeruddin, M. Grätzel, *Science* **2017**, *358*, 768.
[196] Y. Hou, X. Du, S. Scheiner, D. P. McMeekin, Z. Wang, N. Li, M. S. Killian, H. Chen, M. Richter, I. Levchuk, N. Schrenker, E. Spiecker, T. Stubhan, N. A. Luechinger, A. Hirsch, P. Schmuki, H. P. Steinrück, R. H. Fink, M. Halik, H. J. Snaith, C. J. Brabec, *Science* **2017**, *358*, 1192.
[197] R. C. Shallcross, S. Olthof, K. Meerholz, N. R. Armstrong, *ACS Appl. Mater. Interfaces* **2019**, *11*, 32500.
[198] M. Rekow, R. Murison, T. Panarello, C. Dinkel, S. Nikumb, J. Pern, L. Mansfield, in *25th European Photovoltaic Solar Energy Conference and Exhibition (25th EU PVSEC), WCPEC-5*, **2010**, pp. 6–10. Q11
[199] F. J. Pern, F. Yan, L. Mansfield, S. Glynn, M. Rekow, R. Murison, in *Conf. Record of the IEEE Photovoltaic Specialist Conf.*, IEEE, **2011**, p. 002792. Q12
[200] J. A. Christians, F. Zhang, R. C. Bramante, M. O. Reese, T. H. Schloemer, A. Sellinger, M. F. A. M. Van Hest, K. Zhu, J. J. Berry, J. M. Luther, *ACS Energy Lett.* **2018**, *3*, 2502.
[201] M. O. Reese, S. Glynn, M. D. Kempe, D. L. McGott, M. S. Dabney, T. M. Barnes, S. Booth, D. Feldman, N. M. Haegel, *Nat. Energy* **2018**, *3*, 1002.
[202] M. D. Kempe, A. A. Dameron, M. O. Reese, *Prog. Photovoltaics* **2014**, *22*, 1159.
[203] T. Leijtens, G. E. Eperon, N. K. Noel, S. N. Habisreutinger, A. Petrozza, H. J. Snaith, *Adv. Energy Mater.* **2015**, *5*, 1500963.
[204] Q. Dong, F. Liu, K. Wong, W. Tam, A. B. Djuris, A. Ng, C. Surya, K. Chan, A. Man, C. Ng, *ChemSusChem* **2016**, *9*, 2597.
[205] S. N. Habisreutinger, T. Leijtens, G. E. Eperon, S. D. Stranks, R. J. Nicholas, H. J. Snaith, *Nano Lett.* **2014**, *14*, 5561.
[206] Z. Fu, M. Xu, Y. Sheng, Z. Yan, J. Meng, C. Tong, D. Li, Z. Wan, Y. Ming, A. Mei, Y. Hu, Y. Rong, H. Han, *Adv. Funct. Mater.* **2019**, *29*, 1809129.
[207] F. Bella, G. Griffini, J. P. Correa-Baena, G. Saracco, M. Grätzel, A. Hagfeldt, S. Turri, C. Gerbaldi, *Science* **2016**, *354*, 203.
[208] D. Koushik, W. J. H. Verhees, Y. Kuang, S. Veenstra, D. Zhang, M. A. Verheijen, M. Creatore, R. E. I. Schropp, *Energy Environ. Sci.* **2017**, *10*, 91.
[209] R. Cheacharoen, C. C. Boyd, G. F. Burkhard, T. Leijtens, J. A. Raiford, K. A. Bush, S. F. Bent, M. D. McGehee, *Sustainable Energy Fuels* **2018**, *2*, 2398.
[210] Y. Lv, P. Xu, G. Ren, F. Chen, H. Nan, R. Liu, D. Wang, X. Tan, X. Liu, H. Zhang, Z. K. Chen, *ACS Appl. Mater. Interfaces* **2018**, *10*, 23928.
[211] C. Wu, K. Wang, X. Feng, Y. Jiang, D. Yang, Y. Hou, Y. Yan, M. Sanghadasa, S. Priya, *Nano Lett.* **2019**, *19*, 1251.
[212] N. Rolston, A. D. Printz, F. Hilt, M. Q. Hovish, K. Brüning, C. J. Tassone, R. H. Dauskardt, *J. Mater. Chem. A* **2017**, *5*, 22975.
[213] J. Idígoras, F. J. Aparicio, L. Contreras-Bernal, S. Ramos-Terrón, M. Alcaire, J. R. Sánchez-Valencia, A. Borras, Á. Barranco, J. A. Anta, *ACS Appl. Mater. Interfaces* **2018**, *10*, 11587.
[214] V. Stoichkov, N. Bristow, J. Troughton, F. De Rossi, T. M. Watson, J. Kettle, *Sol. Energy* **2018**, *170*, 549.
[215] A. R. Bowring, L. Bertoluzzi, B. C. O'Regan, M. D. McGehee, *Adv. Energy Mater.* **2018**, *8*, 1702365.
[216] N. Rolston, A. D. Printz, J. M. Tracy, H. C. Weerasinghe, D. Vak, L. J. Haur, A. Priyadarshi, N. Mathews, D. J. Slotcavage, M. D. McGehee, R. E. Kalan, K. Zielinski, R. L. Grimm, H. Tsai,

UNCORRECTED PROOF

 © 2020 WILEY-VCH Verlag GmbH & Co. KGaA, Weinheim

Pursuant to the DOE Public Access Plan, this document represents the authors' peer-reviewed, accepted manuscript.
The published version of the article is available from the relevant publisher.

W. Nie, A. D. Mohite, S. Gholipour, M. Saliba, M. Grätzel, R. H. Dauskardt, *Adv. Energy Mater.* **2018**, *8*, 1702116.
[217] N. Rolston, B. L. Watson, C. D. Bailie, M. D. McGehee, J. P. Bastos, R. Gehlhaar, J. E. Kim, D. Vak, A. T. Mallajosyula, G. Gupta, A. D. Mohite, R. H. Dauskardt, *Extrem. Mech. Lett.* **2016**, *9*, 353.
[218] W. Luo, Y. S. Khoo, P. Hacke, V. Naumann, D. Lausch, S. P. Harvey, J. P. Singh, J. Chai, Y. Wang, A. G. Aberle, S. Ramakrishna, *Energy Environ. Sci.* **2017**, *10*, 43.
[219] NREL, National Renewable Energy Laboratory, **2019**, p. 52.
[220] A. Agresti, S. Pescetelli, A. L. Palma, B. Martín-García, L. Najafi, S. Bellani, I. Moreels, M. Prato, F. Bonaccorso, A. Di Carlo, *ACS Energy Lett.* **2019**, *4*, 1862.
[221] M. A. Green, Y. Hishikawa, E. D. Dunlop, D. H. Levi, J. Hohl-Ebinger, M. Yoshita, A. W. Y. Ho-Baillie, *Prog. Photovoltaics* **2019**, *27*, 3.
[222] Microquanta, Microquanta Semiconductor, http://www.microquanta.com/newsinfo/06F899BB54AE99B2/ (accessed: 2019).
[223] M. Yang, Z. Li, M. O. Reese, O. G. Reid, D. H. Kim, S. Siol, T. R. Klein, Y. Yan, J. J. Berry, M. F. A. M. Van Hest, K. Zhu, *Nat. Energy* **2017**, *2*, 17038.
[224] M. Yang, D. H. Kim, T. R. Klein, Z. Li, M. O. Reese, B. J. Tremolet De Villers, J. J. Berry, M. F. A. M. Van Hest, K. Zhu, *ACS Energy Lett.* **2018**, *3*, 322.
[225] E. Bi, W. Tang, H. Chen, Y. Wang, J. Barbaud, T. Wu, W. Kong, P. Tu, H. Zhu, X. Zeng, J. He, S. ichi Kan, X. Yang, M. Grätzel, L. Han, *Joule* **2019**, *3*, 2748.
[226] S. Hong, J. Lee, H. Kang, G. Kim, S. Kee, J. H. Lee, S. Jung, B. Park, S. Kim, H. Back, K. Yu, K. Lee, *Sci. Adv.* **2018**, *4*, eaat3604.
[227] G. Grancini, C. Roldán-Carmona, I. Zimmermann, E. Mosconi, X. Lee, D. Martineau, S. Narbey, F. Oswald, F. De Angelis, M. Graetzel, M. K. Nazeeruddin, *Nat. Commun.* **2017**, *8*, 15684.
[228] Y. Hu, S. Si, A. Mei, Y. Rong, H. Liu, X. Li, H. Han, *Sol. RRL* **2017**, *1*, 1600019.
[229] A. Priyadarshi, L. J. Haur, P. Murray, D. Fu, S. Kulkarni, G. Xing, T. C. Sum, N. Mathews, S. G. Mhaisalkar, *Energy Environ. Sci.* **2016**, *9*, 3687.
[230] X. Li, M. Tschumi, H. Han, S. S. Babkair, R. A. Alzubaydi, A. A. Ansari, S. S. Habib, M. K. Nazeeruddin, S. M. Zakeeruddin, M. Grätzel, *Energy Technol.* **2015**, *3*, 551.
[231] R. Gehlhaar, T. Merckx, W. Qiu, T. Aernouts, *Glob. Challenges* **2018**, *2*, 1800008.
[232] J. A. Schwenzer, L. Rakocevic, R. Gehlhaar, T. Abzieher, S. Gharibzadeh, S. Moghadamzadeh, A. Quintilla, B. S. Richards, U. Lemmer, U. W. Paetzold, *ACS Appl. Mater. Interfaces* **2018**, *10*, 16390.
[233] J. A. Schwenzer, L. Rakocevic, T. Abzieher, D. Rueda-Delgad, R. Gehlhaar, B. S. Richards, U. Lemmer, U. W. Paetzold, in *2018 IEEE 7th World Conf. Photovoltaic Energy Conversion (WCPEC 2018)—A Joint Conf. 45th IEEE PVSC, 28th PVSEC 34th EU PVSEC*, IEEE, **2018**, p. 2816.
[234] M. V. Khenkin, K. M. Anoop, I. Visoly-Fisher, Y. Galagan, F. Di Giacomo, B. R. Patil, G. Sherafatipour, V. Turkovic, H. G. Rubahn, M. Madsen, T. Merckx, G. Uytterhoeven, J. P. A. Bastos, T. Aernouts, F. Brunetti, M. Lira-Cantu, E. A. Katz, *Energy Environ. Sci.* **2018**, *11*, 739.
[235] W. Tress, K. Domanski, B. Carlsen, A. Agarwalla, E. A. Alharbi, M. Graetzel, A. Hagfeldt, *Nat. Energy* **2019**, *4*, 568.
[236] P. Holzhey, M. Saliba, *J. Mater. Chem. A* **2018**, *6*, 21794.
[237] IEC, *IEC 60904 Ed. 2.0 Photovoltaic Devices*, IEC Central Office, Geneva, Switzerland **2006**.
[238] IEC, *IEC 61730 Photovoltaic (PV) Module Safety Qualification*, IEC Central Office, Geneva, Switzerland **2015**.
[239] IEC, *IEC 61215: Terrestrial Photovoltaic (PV) Modules—Design Qualification and Type Approval*, IEC Central Office, Geneva, Switzerland **2005**.
[240] C. R. Osterwald, T. J. McMahon, *Prog. Photovoltaics* **2009**, *17*, 11.
[241] A. L. Rosenthal, M. G. Thomas, S. J. Durand, in *Conf. Record of IEEE Photovoltaic Specialist Conf.*, IEEE, **1993**, p. 1289.
[242] M. V Khenkin, E. A. Katz, A. Abate, G. Bardizza, J. J. Berry, C. Brabec, F. Brunetti, V. Bulović, Q. Burlingame, A. Di Carlo, M. Matheron, M. Mcgehee, R. Meitzner, M. K. Nazeeruddin, *Nat. Energy* **2020**, *5*, 35.

UNCORRECTED PROOF

© 2020 WILEY-VCH Verlag GmbH & Co. KGaA, Weinheim

Pursuant to the DOE Public Access Plan, this document represents the authors' peer-reviewed, accepted manuscript. The published version of the article is available from the relevant publisher.